THÈSE DE DOCTORAT DE

L'UNIVERSITE D'ANGERS
COMUE **U**NIVERSITE **B**RETAGNE **L**OIRE

Ecole Doctorale N°601
Mathématique et Sciences et Technologies de l'Information et de la Communication
Spécialité : Traitement du signal et des images

Par

Mohamad EL SAYED HUSSEIN JOMAA

Signal processing of electroencephalograms with 256 sensors in epileptic children

Thèse présentée et soutenue à ANGERS, le 03/12/2019
Laboratoire Angevin de Recherche en Ingénierie des Systèmes
Thèse N° :

Rapporteurs avant soutenance :

Christian-G. BÉNAR, DR2 Inserm, Institut de Neurosciences des systèmes-INS, Aix Marseille Université/Inserm

François JOUEN, Directeur d'études, École Pratique des Hautes Études

Composition du jury :

Président :

Examinateurs : Régine LE BOUQUIN-JEANNÈS, Professeur des Universités, Université de Rennes 1

Xavier DE TIÈGE, Professeur, Université Libre de Bruxelles

Dir. de thèse : Anne HUMEAU-HEURTIER, Professeur des Universités, Université d'Angers

Co-dir. de thèse : Patrick VAN BOGAERT, Professeur des Universités-Praticien Hospitalier, Centre Hospitalier Universitaire d'Angers

RÉSUMÉ

Le traitement des signaux d'électroencéphalographie (EEG) est d'un intérêt majeur dans les domaines médicaux. Dans cette thèse, nos travaux portent sur l'étude des signaux EEG de sujets épileptiques. Plus plus précisément, nous proposons d'étudier l'irrégularité de signaux EEG acquis chez des enfants épileptiques. L'épilepsie est l'une des affections neurologiques chroniques les plus courantes chez l'enfant et touche 0,5% à 1% des enfants [1]. L'étude de l'épilepsie d'un point de vue électro-neurophysiologique aiderait à mieux comprendre le trouble et permettrait de progresser plus rapidement dans la recherche de traitements. Notre objectif principal dans cette thèse est de proposer des approches de traitement du signal basées sur l'entropie qui aideraient dans ces étapes.

Cette thèse a été partiellement financée par le projet DESIRE. DESIRE est un projet financé par le 7e PC (convention de subvention n ° 602531), impliquant 25 partenaires dans 11 pays.

DESIRE se concentre sur les troubles épileptogènes du développement ou les encéphalopathies épileptiques et développementales (EED), c'est à dire des épilepsies précoces dont l'origine est étroitement liée aux processus de développement du cerveau et pour lesquelles l'activité épileptique elle-même. Les malformations du développement cortical (MCD), qu'elles soient macroscopiques ou subtiles, sont l'une des principales causes de l'EED. Les troubles mentaux se manifestent souvent par des encéphalopathies épileptiques (EE), c'est-à-dire des conditions dans lesquelles l'activité épileptique elle-même peut contribuer à de graves troubles cognitifs et comportementaux. Un traitement efficace de l'épilepsie permettra donc de limiter les séquelles cognitives et comportementales de ces patients. Les EED sont les épilepsies pédiatriques pharmaco-résistantes les plus fréquentes, avec une perspective à vie d'invalidité et de qualité de vie réduite.

DESIRE a pour objectifs spécifiques de faire progresser l'état de l'art en ce qui concerne :

— les causes génétiques et épigénétiques et les mécanismes pathogènes (MP) de l'EED, en particulier le les malformations du développement cortical associées à

l'épilepsie , pour élucider les réseaux moléculaires et les complexes protéiques perturbés et rechercher des bases communes pour ces troubles apparemment hétérogènes.

— les outils de diagnostic, biomarqueurs et protocoles de traitement, et les protocoles à travers l'étude d'une cohorte unique d'enfants bien caractérisée et bien caractérisée afin de fournir un diagnostic standardisé pour la stratification des patients et la recherche en Europe.

— le traitement de l'EDD à l'aide de protocoles cliniques multidisciplinaires randomisés et mise à l'essai de stratégies précliniques dans des modèles expérimentaux afin de prendre en compte de nouvelles stratégies préventives.

Dans cette thèse, nous avons développé une nouvelle approche d'entropie basée sur l'entropie à permutation multi-échelle dans l'optique de l'appliquer à l'analyse de l'EEG de repos de patients avec EED avant et après mise en place d'un traitement anti-épileptique et de corréler les données EEG avec la condition clinique des patients. La base de l'entropie multi-échelle est la procédure suivante

$$y_j^{(\tau)} = \frac{1}{\tau} \sum_{i=(j-1)\tau+1}^{j\tau} x_i. \tag{1}$$

$\{x_i\}$ est est la série chronologique originale. $\mathbf{y}^{(\tau)}$ est alors le sous-échantillonnage de $\{x_i\}$ par le facteur τ qui est l'échelle de temps. $\mathbf{y}^{(\tau)}$ est alors appelée série chronologique à gros grains. Ensuite, l'entropie de permutation [11] de chaque série chronologique à gros grains est calculée comme suit

$$PE_x^d = -\sum_{i=1}^{d!} p(\pi_i) \ln(p(\pi_i)), \tag{2}$$

où

$$p(\pi_i) = \frac{\#\{t | t \leq N-d, type(\mathbf{x}_t^d) = \pi_i\}}{N-d+1}, \tag{3}$$

où π est appelé un motif et correspond à un certain ordre de permutation des éléments du sous-vecteur de longueur d. $p(\pi_i)$ est la fréquence relative du motif. L'équation 3 signifie le nombre de tous les vecteurs $\mathbf{x}_t^{d,l}$ sur tout t qui, lorsqu'ils sont triés, ont le même ordre que π_i ; le tout est divisé par le nombre total de vecteurs $\mathbf{x}_t^{d,l}$ ($\#$ désigne la cardinalité). La nouvelle méthode que nous avons introduite s'appelle "multivariate Improved Weighted Multi-scale Permutation Entropy" (mvIWMPE). Appliquée sur des

signaux multivariés synthétiques et comparée à d'autres méthodes multivariées reposant sur l'entropie de permutation, nous montrons que notre méthode permet de mieux différencier les signaux comparativement aux résultats donnés par l'entropie de permutation multivariée multi-échelle (mvMPE) ou ceux donnés par l'entropie de permutation pondérée multivariée multi-échelle (mvMWPE). L'avantage de notre méthode par rapport à la "multivariate improved multi-scale permutation entropy (mvIMPE)" réside dans l'introduction du facteur de pondération qui inclut dans les calculs les amplitudes des échantillons de signal. Nous avons finalement appliqué cette méthode sur de vrais signaux EEG d'enfants en bonne santé afin de bien différencier deux états, les yeux ouverts et les yeux fermés.

Nous avons développé une autre approche d'entropie multivariée basée sur la "Sample Entropy" [99]. La "Sample Entropy" est calculée comme suit

$$SampEn = -\ln \frac{B_{m+1}(r)}{B_m(r)}. \tag{4}$$

$B_m(r)$ (respectivement $B_{m+1}(r)$) est la fréquence à laquelle le sous-vecteur de longueurs m (respectivement $m+1$) présente des similitudes dans une plage de tolérance r. Cette approche développée a été comparée à l'approche existante [4] [5] en appliquant les deux méthodes sur des signaux synthétiques comportant un nombre variable de canaux. Il a été remarqué que les deux méthodes donnent des résultats similaires lorsqu'elles sont appliquées sur un petit nombre de canaux (2 ou 3), mais notre méthode donne de meilleurs résultats lorsque le nombre de canaux est supérieur. Nous avons également appliqué notre méthode sur des signaux EEG de patients épileptiques à deux moments de leur traitement. Les résultats ont été mis en correspondance avec le diagnostic clinique réalisé à l'hôpital pour déterminer si la santé des patients s'améliorait.

Une troisième mesure de complexité a été développée sur la base d'une approche temps-fréquence variable. Cette mesure a également été appliquée sur des signaux synthétiques, puis sur des signaux EEG réels provenant des mêmes patients épileptiques que ceux utilisés dans l'étude d'entropie multivariée basée sur la "Sample Entropy". En extrayant plusieurs caractéristiques des résultats et en les comparant à différents moments du traitement, les résultats correspondent à ce qui avait été trouvé lors du diagnostic clinique à l'hôpital.

Enfin, nous avons introduit une nouvelle approche de connectivité basée sur

mvlWMPE et MI dans le but de tester l'hypothèse que cette méthode peut être adaptée à l'étude de la connectivité fonctionnelle cérébrale :

$$I(\mathbf{x}, \mathbf{y}) = H(\mathbf{x}) + H(\mathbf{y}) - H(\mathbf{x}, \mathbf{y}), \tag{5}$$

où $I(\mathbf{x}, \mathbf{y})$ est l'information mutuelle entre deux signaux ou séries temporelles $\mathbf{x}$ et $\mathbf{y}$. $H(\mathbf{x})$ et $H(\mathbf{y})$ sont les entropies des signaux $\mathbf{x}$ et $\mathbf{y}$ respectivement et $H(\mathbf{x}, \mathbf{y})$ est l'entropie bivariée des deux signaux $\mathbf{x}$ et $\mathbf{y}$. Nous avons d'abord testé la capacité de cette méthode à extraire des réseaux dont les nœuds significatifs correspondent aux réseaux à état de repos (RSN) connus extraits à l'aide de l'imagerie par résonance magnétique fonctionnelle (IRMf). Pour cette raison, nous avons appliqué la méthode aux signaux corticaux calculés à partir des signaux EEG d'enfants en bonne santé. Après avoir extrait les réseaux, nous avons extrait les mesures de réseau de nœuds et de réseaux globaux et testé leurs valeurs afin d'identifier les nœuds significatifs. Les méthodes ont permis de trouver des nœuds statistiquement significatifs qui avaient déjà été trouvés dans les études RSN IRMf. Nous avons ensuite étudié l'influence de la variabilité inter-sujets sur la méthode. Nous avons donc appliqué la méthode aux mêmes enfants en bonne santé, mais cette fois dans l'intérêt de comparer les valeurs des mesures de réseau extraites d'un sujet à l'autre. Les résultats montrent des variabilités significatives inter-sujets. Notre méthode ne permettra donc pas de comparer les résultats des sujets entre eux. Suite à cela, nous avons étudié la variabilité intra-sujet de notre méthode. Nous avons donc effectué une comparaison similaire en utilisant des mesures de réseau, mais cette fois en comparant les valeurs d'un même sujet. Les résultats n'ont pas montré de variabilité intra-sujet significative. Cela signifie que nous pouvons utiliser cette méthode pour étudier un sujet donné à des moments différents. Nous avons alors analysé les états des patients épileptiques à différents moments de leur traitement. Les résultats obtenus sont en cohérence avec le diagnostic clinique réalisé à l'hôpital.

Ce manuscrit est divisé en 3 chapitres. Dans le premier chapitre, une revue de la littérature sur différents concepts utilisés dans cette thèse est d'abord proposée. Nous présentons ainsi des méthodes d'entropie qui ont été développées précédemment et qui sont en quelque sorte liées au travail développé dans cette thèse. Ensuite, nous proposons une brève revue du système d'acquisition et des signaux EEG ainsi que la neurophysiologie associée. Après cela, nous décrivons l'épilepsie infantile. Enfin, nous

présentons le concept général de connectivité fonctionnelle, l'importance de l'étude de l'épilepsie et un bref résumé des différentes méthodes basées sur l'EEG/ la magnetoencéphalographie (MEG) pour calculer la connectivité fonctionnelle.

Au chapitre 2, nous présentons trois nouvelles méthodes basées sur l'entropie que nous avons développées ; mvIWMPE, une nouvelle approche multivariée de la "Sample Entropy" et une nouvelle mesure de complexité temps-fréquence en temps variable. Nous appliquons les méthodes développées sur des signaux synthétiques et sur des signaux EEG haute densité provenant d'enfants sains et épileptiques.

Dans le troisième chapitre, nous adaptons la mvIWMPE développée avec l'information mutuelle afin de proposer une nouvelle méthode de connectivité fonctionnelle basée sur l'EEG. Nous appliquons cette méthode sur des données acquises chez des enfants en bonne santé et chez des enfants atteints de différents types d'épilepsie infantile dans le but d'étudier la méthode et d'évaluer sa capacité à détecter des altérations du réseau au cours des différentes phases de l'épilepsie.

Enfin, nous terminons ce manuscrit par une conclusion générale du travail et des perspectives.

ACKNOWLEDGEMENT

First of all, I would like to thank my supervisors, Prof. Anne Humeau-Heurtier and Prof. Patrick Van Bogaert, for guiding me throughout my journey in the thesis. Much appreciation is not enough to express my gratitude for their patience and support. Not only they were my mentors in work, they were careful to make me feel home in Angers and settle down very fast at the beginning of my stay in Angers. I was very lucky to have both them as my supervisors.

Second, I would like to thank Dr. Marcelo Alejandro Colominas. Being his colleague helped me a lot in acquiring experience that he didn't hesitate to share.

I would also like to thank Prof. Jean-Marc Girault and Prof. Sylvie Nguyen The Tich for assisting as my thesis following committee. Their suggestions and comments were valuable.

Last but not least, I would like to thank my family and my lovely wife. They were the supports from behind the scenes. They believed in my potential kept their moral support coming.

TABLE OF CONTENTS

INTRODUCTION

The processing of electroencephalography (EEG) signals is of major interest for the medical fields. In this thesis, our main focus was irregularity and complexity measures of the signals. We aim to study the EEG signals of children with childhood epilepsy. Epilepsy is one of the most common chronic neurologic conditions in children and affects 0.5% to 1% of the children [1]. Studying the in-depth aspects of epilepsy from an electro-neurophysiological point of view would help better understand the disorder and takes steps closer towards finding cures. Our main point in this thesis is to propose entropy-based signal processing approaches that would help in those steps.

DESIRE Project

This thesis was partly funded by the DESIRE project. DESIRE is an FP7 funded project (Grant Agreement no : 602531), involving 25 partners in 11 countries, with eight third parties, a total of 2166 person months, with more than 250 researchers involved and 19 clinical centres involved in the clinical trial. It is co-ordinated by Prof. Renzo Guerrini, Dipartimento di Neuroscienze, Area del Farmaco e Salute del Bambino (NEUROFARBA) Universita degli Studi di Firenze, Italy.

Scope of DESIRE

DESIRE focuses on epileptogenic developmental disorders EDD, i.e. early onset epilepsies whose origin is closely related to developmental brain processes. A major cause of EDD are malformations of cortical development (MCD), either macroscopic or subtle. EDD are often manifested as epileptic encephalopathies (EE), i.e. conditions in which epileptic activity itself may contribute to severe cognitive and behavioral impairments. EDD are the most frequent drug-resistant pediatric epilepsies carrying a lifelong perspective of disability and reduced quality of life.

Objectives of DESIRE

Specific objectives of DESIRE are to advance the state of the art with respect to :

— the genetic and epigenetic causes and pathogenic mechanisms (PM) of EDD, particularly epileptogenic MCD, to elucidate molecular networks and disrupted protein complexes and search for common bases for these apparently heterogeneous disorders.

— the diagnostic tools (biomarkers) and protocols through the study of a unique and well-characterized cohort of children to provide standardized diagnosis for patient stratification and research across Europe.

— treatment of EDD using randomized, multidisciplinary clinical protocols and testing preclinical strategies in experimental models to also address novel preventative strategies.

Thesis Objectives

The first main objective of the thesis is to propose a state of the art on the methods that quantify the irregularity of time series. Then we adapt and develop new methods based on entropy measures to study EEG signals in general.

The second main objective throughout this thesis is to create our database of EEG recordings of children with epilepsy and healthy children. We then use this database and apply our entropy methods on EEG recorded in epileptic children and in healthy subjects and to compare their results.

Finally the last main objective of this thesis is to develop a new functional connectivity method, based on developed entropy measures in order to apply it on the signals of the recorded database. By comparing the results of the epileptic children with those of the healthy children, we hypothesize that it could help to understand the network alterations that are caused by the epileptic disorder itself, and the origin of some cognitive deficits. This might help in better handling the disorder and hopefully in treatment.

Organisation

This manuscript is divided into 3 chapters. In the first chapter, a literature review of the state of the art is proposed. The covered topics include entropy methods that were

previously developed and are somehow related to the work in this thesis. Then we write a brief review of the EEG machine and the neurophysiology behind the EEG signals. After that we describe and summarize the definition of childhood epilepsy and some types of childhood epilepsies. Finally, we present the general concept of functional connectivity, why it is necessary to study epilepsy, and a brief summary of the different EEG/MEG-based methods to calculate functional connectivity.

In chapter 2, we introduce three novel entropy-based methods that we developed ; multivariate improved weighted multi-scale permutation entropy (mvIWMPE), a new multivariate approach of sample entropy, and a new time-varying time–frequency complexity measure. We apply the developed methods on synthetic signals and on real high density EEG signals from children (healthy and epileptic children).

In the third chapter, we adapt the developed mvIWMPE with mutual information (MI) in order to develop a new EEG-based functional connectivity method. We apply this method on healthy children along with children with different types of childhood epilepsies. The aim is to study the method and evaluate its ability to detect network alterations among different stages of epilepsy.

Finally, we end this manuscript with a general conclusion of the work and some perspectives.

CHAPITRE 1

STATE OF THE ART

1.1 Entropy in Signal Processing

1.1.1 Introduction

There are several methods to quantify the irregularity of signals and systems. One of the commonly used methods is using entropy measures [71]. The concept of entropy originally derived from thermodynamics where it was used to describe the state of a fluid system and the probability of its molecule's distribution. In ordered systems (crystals) the molecules are fixed in place and have low possibility of motion and getting out of order, thus having low entropy. As the system moves to a more disordered state (melting of ice crystals) the molecules get more freedom to move, thus increasing the probability of disorder. This results in the increase of the fluid system entropy.

This concept of entropy was adapted by Shannon [104] for information theory to measure the information in a signal. Nowadays, entropy, when used in information theory and signal processing, is used to measure or quantify the unpredictability, irregularity or complexity of a signal. Many entropy measures, based on Shannon's entropy, were developed and are to be discussed in Sec. 1.1 of Chapter 1, starting with Shannon's entropy.

1.1.2 Shannon's Entropy

As mentioned above, the concept of information entropy was introduced by Claude Shannon in 1948 [104]. Shannon defined the entropy of a discrete random variable X with values $\{x_1, x_2, \ldots, x_N\}$ and a probability distribution $P(X)$ as :

$$H(X) = -\sum_{i=1}^{n} P(x_i) \log_b P(x_i), \tag{1.1}$$

where b is the base of the logarithm. In the case that $P(x_i) = 0$ for a certain i, then $P(x_i) \log P(x_i) = 0$.

To further explain the use of Shannon entropy let us consider the example of a coin toss. The coin toss has only two outcomes $X = \{A, B\}$. Initially, we will consider the two outcomes equiprobable ($P(A) = P(B) = \frac{1}{2}$). With the logarithm of base 2, the

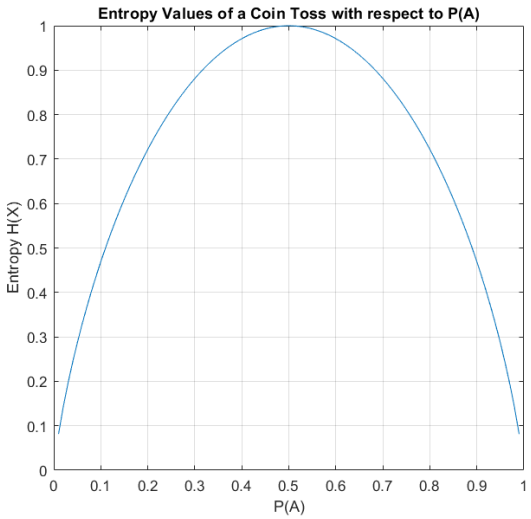

FIGURE 1.1 – The Shannon entropy values of a coin toss with respect to the probability of the fist outcome A. The figure would be the same for the second outcome B as $P(A) + P(B) = 1$

entropy of the outcome of the coin toss would be :

$$H(X) = -\sum_{i=1}^{2} P(\frac{1}{2}) \log_2 \frac{1}{2} = 1. \tag{1.2}$$

This is the case of the most uncertainty where the entropy is at its highest value. However, if we consider the outcomes to have different probabilities, such as $P(A) = 0.7$ and $P(B) = 0.3$, then the value of entropy would be $H(X) = 0.8816$ which implies less uncertainty than the equiprobable case.

Shannon entropy always gives the highest value for uniform distributions of X. Fig. 1.1 shows the entropy of X with respect to $P(A)$. Note that the entropy is maximal for $P(A) = 0.5$ (uniform distribution of X).

1.1.3 Approximate Entropy

Approximate entropy ($ApEn$) was introduced by Pincus *et al* in 1991 [96] to calculate the uncertainty or unpredictability of the fluctuations of a time series.

Consider a time series $X = \{x_1, x_2, x_3, \ldots, x_N\}$ with N points. For a fixed integer m extract the vectors $\mathbf{u}_1, \mathbf{u}_2, \ldots, \mathbf{u}_{N-m+1}$ where $\mathbf{u}_i = [x_i, x_{i+1}, \ldots, x_{i+m-1}]$. For every i find $C_i^m(r)$, the number of vectors $\mathbf{u}_j$ $(1 \leq j \leq N-m+1)$ that satisfy the condition $d[\mathbf{u}_i, \mathbf{u}_j] \leq$

r. r is a predefined real number that is considered as a threshold, $d[\mathbf{u}_i, \mathbf{u}_j]$ is the distance between $\mathbf{u}_i$ and $\mathbf{u}_j$ and is calculated as $\max_m |x_{i+k} - x_{j+k}| : 0 \leq k \leq m-1$, where x_i is a scalar component of $\mathbf{u}_i$ and x_j is that of $\mathbf{u}_j$. It is worth noting here that $d[\mathbf{u}_i, \mathbf{u}_j]$ is considered for the condition of $i = j$ and thus meaning that self-comparisons are being considered. Then, define

$$\Phi^m(r) = \frac{\sum_{i=1}^{N-m+1} \log C_i^m(r)}{N-m+1}. \tag{1.3}$$

Finally, $ApEn$ is calculated as

$$ApEn(m, r) = \Phi^m(r) - \Phi^{m+1}(r), \tag{1.4}$$

where $\Phi^{m+1}(r)$ is calculated as $\Phi^m(r)$ but for $m+1$ instead of m.

1.1.4 Sample Entropy

Sample entropy (SampEn) was first introduced by Richman and Moorman in 2000 [99]. It is the negative logarithm of the conditional probability that a time series of length N, showing similarity within a tolerance r for length m, will also show similarity within a tolerance r for length $m+1$, without considering self-matches. To calculate SampEn of a time series $\{x_1, \ldots, x_i, \ldots, x_N\}$ of length N, first the delay vectors (DV) should be generated. For a given embedding dimension m the DVs will be $\mathbf{u}_i = [x_i, x_{i+1}, \ldots, x_{i+(m-1)}]$ where $i = 1, 2, \ldots, N-(m-1)$. For a given threshold or tolerance r, calculate all the possible distances between pairs of DVs ($\mathbf{u}_i$ and $\mathbf{u}_j$ with $i \neq j$) and count the number of pairs that have a distance less than the tolerance r. Any type of distance could be used here, but the most commonly used is the Chebyshev distance. $B_m(r)$ will denote the frequency of occurrence. Then, extend the embedding dimension from m to $m+1$ and generate the new DVs. For those new DVs, recalculate the distances between all possible pairs and count those with distances less than r and denote their frequency of occurrence by $B_{m+1}(r)$. SampEn will then be

$$SampEn = -\ln \frac{B_{m+1}(r)}{B_m(r)}. \tag{1.5}$$

The values of the parameters are commonly used as $m = 2$ or $m = 3$ and $r = 0.15\times$(standard deviation of normalized signal) to $r = 0.25\times$(standard deviation of nor-

malized signal) [99].

The lower the value of SampEn, the more regular the series is, thus more predictable it is.

1.1.5 Fuzzy Entropy

Fuzzy entropy (FuzzyEn) was introduced by Chen *et al* in 2007 [26][27].

Consider a time series $\{x_i\}_{i=1,\dots,N}$ with N time points. Similar to Sample entropy (sec. 1.1.4), the DV should first be generated based on the given embedding dimension m. DVs will be $\mathbf{u}_i = [x_i, x_{i+1}, \dots, x_{i+(m-1)}] - \tilde{x}(i)$ where $i = 1, 2, \dots, N-(m-1)$. Here $\tilde{x}(i)$ is the mean of the vector $[x_i, x_{i+1}, \dots, x_{i+(m-1)}]$. We then calculate all the possible distances d_m^{ij} between pairs of DVs ($\mathbf{u}_i$ and $\mathbf{u}_j$ with $i \neq j$). As in Sample entropy (sec. 1.1.4), any type of distance can be used, but mainly the Chebyshev distance is the most common in application. Then based on the parameter r, the degree of similarity $D_m^{ij}(r)$ between every pair of DVs is

$$D_m^{ij}(r) = \mu(d_m^{ij}, r). \tag{1.6}$$

Here, $\mu(d_m^{ij}, r)$ is the fuzzy function. Any function that satisfies the following properties can be considered as a fuzzy function :

— being continuous so that the similarity does not change abruptly

— being convex so that self similarity is convex.

In [26], $\exp^{\frac{-(d_m^{ij})^n}{r}}$ was considered as the fuzzy function with r determining the width of the exponential function and n being an additional parameter to determine its gradient.

Averaging all the obtained degrees of similarity for each vector $\mathbf{u}_i$ we obtain $\phi_m^r(i)$. Then

$$\Phi_m^r = \frac{\sum_{i=1}^{N-m} \phi_m^r(i)}{N-m}. \tag{1.7}$$

The same steps should be repeated for an embedding dimension of $m+1$ to obtain finally

$$\Phi_{m+1}^r = \frac{\sum_{i=1}^{N-m} \phi_{m+1}^r(i)}{N-m}. \tag{1.8}$$

Finally we can define FuzzyEn as

$$FuzzyEn(m, r) = -\ln \frac{\Phi_{m+1}^r}{\Phi_m^r}. \tag{1.9}$$

1.1.6 Permutation Entropy

Permutation entropy was introduced by Bandt and Pompe in 2002 [11].

Consider a time series $\{x_i\}_{i=1,...,N}$ with N time points. For each time point a vector containing d points is constructed such that $\mathbf{x}_t^{d,l} = \{x_t, x_{t+l}, ..., x_{t+(d-2)l}, x_{t+(d-1)l}\}$ where d is the embedding dimension and l is the time delay.

Each element of the vector $\mathbf{x}_t^{d,l}$ is associated to a number from 1 to d and then ordered in increasing order to become $\{x_{t+(j_1-1)l}, x_{t+(j_2-1)l}, ..., x_{t+(j_{d-1}-1)l}, x_{t+(j_d-1)l}\}$ with $x_{t+(j_n-1)l} \leq x_{t+(j_{n+1}-1)l}$. Since the vectors have d points there will be $d!$ possible orders, π, named motifs. The relative frequency of each motif, π_i, is calculated as follows

$$p(\pi_i) = \frac{\#\{t|t \leq N-d, type(\mathbf{x}_t^{d,l}) = \pi_i\}}{N-d+1}, \tag{1.10}$$

which means the number of all vectors $\mathbf{x}_t^{d,l}$ across all t that, when ordered, have the same type as π_i, divided by the total number of vectors $\mathbf{x}_t^{d,l}$ ($\#$ means number of elements in a set or cardinality). Note that the condition $(d+1)! \leq N$ should be satisfied to get valid entropy results. PE is then calculated as [11]

$$PE_x^{d,l} = -\sum_{i=1}^{d!} p(\pi_i) \ln(p(\pi_i)), \tag{1.11}$$

where $0 \ln(0) = 0$ is set as a convention. This algorithm is based on the original concept of entropy, Shannon Entropy [104], having the same equation.

The higher the value of d, the more data is being sorted and the number of motifs increase in a factorial manner. This could lead to more precise results but it will also lead to longer calculation times and would require longer signals. Thus, in order to compensate between the amount of data to be sorted and the calculation time, $d = 3$ is commonly used [11][8]. The value of l is commonly used as 1 [11] as the general case is the intention to study every consecutive time point of the time series without skipping points.

The entropy value is maximum when the time series is totally uncorrelated. In this case, the value of entropy is $\ln(d!)$. This is when the time series is the most irregular. On the other hand, the value of entropy reaches the minimum when the time series is monotonic. The corresponding value is $\ln(1) = 0$. As expected, this is when the time series is the least irregular.

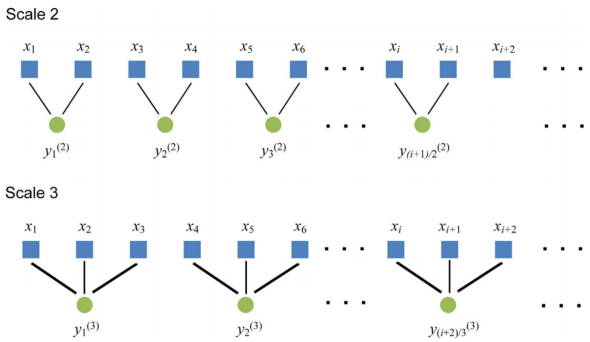

FIGURE 1.2 – A representation of the common coarse-graining procedure that is applied in all multi-scale approaches in this thesis. Scales 2 and 3 are represented. $\mathbf{X} = \{x_i\}$ is the original signal and $\mathbf{Y}^{(\tau)} = \{y_i^{(\tau)}\}$ is the coarse-grained signal. Figure from [8].

1.1.7 Multi-scale Sample Entropy

The concept of multi-scale entropy was first introduced and applied on sample entropy (SampEn) by Costa *et al* [34][35].

The first step to calculate the multi-scale sample entropy (MSE) is to extract a set of coarse-grained signals of the original signal for different time scales. We will refer to time scales as τ. Consider a time series $\{x_i\}_{i=1,\dots,N}$ with N time points. The coarse-grained time series as a function of τ would be $\{y^{(\tau)}\}$, where

$$y_j^{(\tau)} = \frac{1}{\tau} \sum_{i=(j-1)\tau+1}^{j\tau} x_i. \tag{1.12}$$

$y^{(\tau)}$ is then the downsampling of $\{x_i\}$ by the factor of τ. Figure 1.2 represents the coarse-graining procedure for scales $\tau = 2$ and $\tau = 3$.

For every value of τ, SampEn of every $\{y^{(\tau)}\}$ is calculated as mentioned in section 1.1.4 and thus resulting in $MSE(\tau)$ as a function of time scale τ.

1.1.8 Multi-scale Permutation Entropy

Multi-scale permutation entropy (MPE), introduced by Morabito *et al* in 2012, is similar to permutation entropy but includes an additional step : the coarse-graining process [90].

Consider a time series $\{x_i\}_{i=1,\dots,N}$ with N time points. Similar to section 1.1.7 the

coarse-grained time series will be as follows

$$y_j^{(\tau)} = \frac{1}{\tau} \sum_{i=(j-1)\tau+1}^{j\tau} x_i, \tag{1.13}$$

where $1 \leq j \leq \lfloor \frac{N}{\tau} \rfloor$. τ stands for time scale and could range from 1 to $\lfloor \frac{N}{(d+1)!} \rfloor$. For each time scale τ, PE of the coarse-grained time series is calculated as mentioned in section 1.1.6 ending with $MPE_\tau^{d,l}$. By this way we obtain the value of permutation entropy as a function of time scale.

1.1.9 Improved Multi-scale Permutation Entropy

Improved multi-scale permutation entropy (IMPE) was introduced by Azami and Escudero [8] to overcome some problems of MPE. These problems are :

— the non-symmetry of the coarse-grained time series

— the variability of the MPE results in large time scales.

IMPE is calculated in two steps [8] :

1. For each time scale τ, τ different coarse-grained time series are extracted from the original time series. The procedure is as follows

$$y_j^{c,\tau} = \frac{1}{\tau} \sum_{i=(j-1)\tau+c}^{j\tau+c-1} x_i, \tag{1.14}$$

   where $1 \leq j \leq \lfloor \frac{N}{\tau} \rfloor$ and $1 \leq c \leq \tau$. Figure 1.3 represents the new coarse-graining approach proposed for calculating IMPE of a time series.

2. For each c, PE of $y^{c,\tau}$ is calculated such that we obtain $PE_{c,\tau}^{d,l}$. Then IMPE of a certain time scale, τ, would be the average of all the values of $PE_{c,\tau}^{d,l}$ across all c

$$IMPE_{(\tau)}^{d,l} = \frac{1}{\tau} \sum_{c=1}^{\tau} PE_{c,\tau}^{d,l}. \tag{1.15}$$

1.1.10 Multivariate Multi-scale Sample Entropy

Multivariate Multi-scale Sample Entropy (mvMSE) was introduced by Ahmed *et al* [4][5]. Two multivariate extensions of the SampEn were proposed, the naive me-

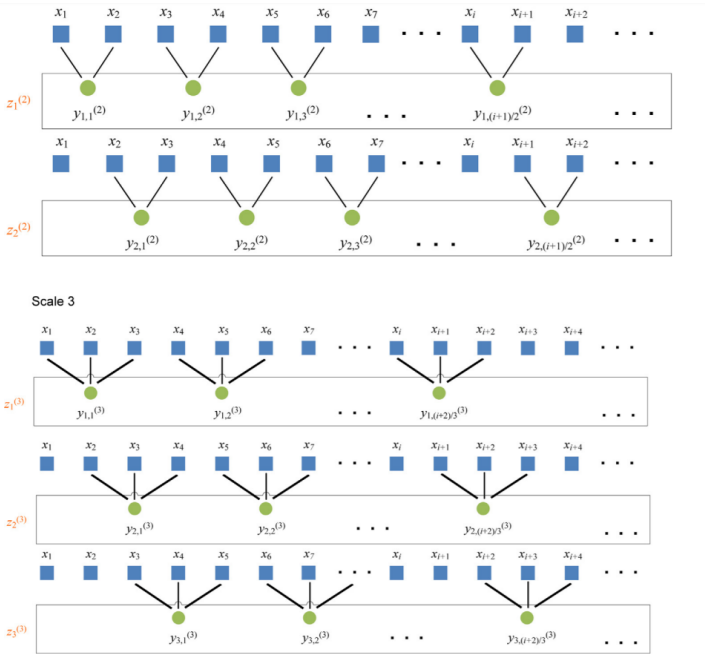

FIGURE 1.3 – A representation of the improved coarse-graining procedure used in [8] for IMPE. Scales 2 and 3 are represented. Figure from [8].

thod [4] and the full method [5], with the full method being commonly used since it outperforms the naive one [4].

Suppose $\{x_{1,k}, \ldots, x_{i,k}, \ldots, x_{N,k}\}$ is a multivariate time series where $1 \leq k \leq K$ is the index of the variate and N is the length of the time series. As in Sec. 1.1.7, the first step to calculate mvMSE is to extract a set of coarse-grained signals of the original signal for different time scales (τ).This is done as follows

$$y_{j,k}^{(\tau)} = \frac{1}{\tau} \sum_{i=(j-1)\tau+1}^{j\tau} x_{i,k}. \tag{1.16}$$

The second step would be to generate the un-extended DVs : $\mathbf{Y}_{\mathbf{M}}^{(\tau)}(i) = [y_{i,1}^{(\tau)}, \ldots, y_{i+(m_1-1),1}^{(\tau)}, y_{i,2}^{(\tau)}, \ldots, y_{i+(m_2-1),2}^{(\tau)}, \ldots, y_{i,K}^{(\tau)}, \ldots, y_{i+(m_K-1),K}^{(\tau)}]$, where $i = 1, 2, \ldots, N - \max\{\mathbf{M}\}$ and $\mathbf{M} = [m_1, m_2, \ldots, m_K]$ is the multivariate embedding dimension vector. Calculate the distances between all the possible pairs of DVs ($\mathbf{Y}_{\mathbf{M}}^{(\tau)}(i)$ and $\mathbf{Y}_{\mathbf{M}}^{(\tau)}(j)$ with $i \neq j$) and find $A_{\mathbf{M}}^{(\tau)}(r)$, the number of distances that are less than a defined tolerance or threshold value r, and the frequency of occurrence of that would be denoted by $B_{\mathbf{M}}^{(\tau)}(r)$,

where

$$B_{\mathbf{M}}^{(\tau)}(r) = \frac{A_{\mathbf{M}}^{(\tau)}(r)}{\frac{(N-\max\{\mathbf{M}\})(N-\max\{\mathbf{M}\}-1)}{2}}. \tag{1.17}$$

To extend the embedding dimension vector $\mathbf{M}$ to $\mathbf{M}+1$ in the full method, K DV subspaces are generated where in each subspace the embedding dimension of only one variate, k, is extended from m_k to $m_k + 1$. This way the extended DV subspace for k would be $\mathbf{Y}_{\mathbf{M}+1}^{(\tau)}(i) = [y_{i,1}^{(\tau)}, \ldots, y_{i+(m_1-1),1}^{(\tau)}, \ldots, y_{i,k}^{(\tau)}, \ldots, y_{i+(m_k-1),k}^{(\tau)}, y_{i+(m_k),k}^{(\tau)} \ldots, y_{i,K}^{(\tau)}, \ldots, y_{i+(m_K-1,K)}^{(\tau)}]$ (note that the dimension of only m_k is increased by 1). The pair-wise distances are calculated between all the DVs across all the K subspaces and the number of pairs with distances less than the threshold r is $A_{\mathbf{M}+1}^{(\tau)}(r)$. The frequency of occurrence for that would be denoted by $B_{\mathbf{M}+1}^{(\tau)}(r)$ as

$$B_{\mathbf{M}+1}^{(\tau)}(r) = \frac{A_{\mathbf{M}+1}^{(\tau)}(r)}{K \times \frac{(N-\max\{\mathbf{M}\})(N-\max\{\mathbf{M}\}-1)}{2}} \tag{1.18}$$

This way, the multivariate multi-scale sample entropy as a function of τ is

$$mvMSE^{(\tau)} = -\ln \frac{B_{\mathbf{M}+1}^{(\tau)}(r)}{B_{\mathbf{M}}^{(\tau)}(r)}. \tag{1.19}$$

1.1.11 Multivariate Multi-scale Permutation Entropy

Consider a multivariate time series $\{x_{1,k}, \ldots, x_{i,k}, \ldots, x_{N,k}\}$ with N time points, K channels and k representing the channel number ($1 \leq k \leq K$). Similar to MPE (section 1.1.8), coarse-grained multivariate time series for all time scales (τ) should be extracted as follows

$$y_{j,k}^{(\tau)} = \frac{1}{\tau} \sum_{i=(j-1)\tau+1}^{j\tau} x_{i,k}. \tag{1.20}$$

For each time scale, τ, the vectors $\mathbf{y}_{i,k}^{(\tau),d,l} = \{y_{i,k}^{(\tau)}, y_{i+1,k}^{(\tau)}, ..., y_{i+(d-2)l,k}^{(\tau)}, y_{i+(d-1)l,k}^{(\tau)}\}$ are extracted for every channel. The elements of $\mathbf{y}_{i,k}^{(\tau),d,l}$ are ordered and compared with the $d!$ possible orders or motifs, $\pi_m^{(\tau)}$. The relative frequency of the permutation in each channel is calculated as follows [90]

$$p(\pi_{j,k}^{(\tau)}) = \frac{\#\{t|t \leq N-d, type(\mathbf{y}_{t,k}^{(\tau),d,l}) = \pi_{j,k}^{(\tau)}\}}{(N-d+1)K}. \tag{1.21}$$

Note that the relative frequency is divided here by the number of channels, K, to maintain $\sum_{k=1}^{K}\sum_{j=1}^{d!} p(\pi_{j,k}^{(\tau)}) = 1$.

Then the marginal relative frequency of the motifs is calculated

$$p(\pi_j^{(\tau)}) = \sum_{k=1}^{k} p(\pi_{j,k}^{(\tau)}). \tag{1.22}$$

So the multivariate multi-scale permutation entropy (mvMPE) is calculated [90]

$$mvMPE_{(\tau)}^{d,l} = -\sum_{i=1}^{d!} p(\pi_i^{(\tau)}) \ln(p(\pi_i^{(\tau)})) \tag{1.23}$$

as a function of time scale τ.

1.1.12 Multivariate Multi-scale Weighted Permutation Entropy

Multivariate multi-scale weighted permutation entropy (mvMWPE) [42] is based on the algorithm of the weighted permutation entropy that was introduced by Fadlallah *et al* [47]. This algorithm has the advantage of including the weight of the amplitudes for each permutation.

The steps to calculate mvMWPE are similar to those mentioned in section 1.1.11. The coarse-grained time series of the multivariate time series ($\{x_{1,k}, \ldots, x_{i,k}, \ldots, x_{N,k}\}$ with N time points, K channels and k representing the channel number ($1 \leq k \leq K$)) is calculated for a certain scale factor, τ.

$$y_{j,k}^{(\tau)} = \frac{1}{\tau} \sum_{i=(j-1)\tau+1}^{j\tau} x_{i,k}. \tag{1.24}$$

Then the vectors $\mathbf{y}_{i,k}^{(\tau),d,l} = \{y_{i,k}^{(\tau)}, y_{i+1,k}^{(\tau)}, ..., y_{i+(d-2)l,k}^{(\tau)}, y_{i+(d-1)l,k}^{(\tau)}\}$ are extracted for every channel. The elements of these vectors are ordered and compared with the $d!$ possible motifs, $\pi_m^{(\tau)}$. The absolute frequency of each motif of every channel is then [42]

$$p(\pi_{j,k}^{(\tau)}) = \sum_{j=1}^{N-d} 1_{v:type(v)=\pi_{j,k}^{(\tau)}}(\mathbf{y}_{t,k}^{(\tau),d,l}) w_j^{(\tau)}, \tag{1.25}$$

where $1_{A(v)}$ is an indicator function of the set A and is defined as $1_{A(v)} = 0$ if $v \notin A$ and $1_{A(v)} = 1$ if $v \in A$. $w_j^{(\tau)}$ is the weighted value of the vector $\mathbf{y}_{t,k}^{(\tau),d,l}$, and is commonly

taken as the variance of $\mathbf{y}_{t,k}^{(\tau),d,l}$.

This would result in a matrix $K \times d!$, where K is the number of channels. The relative frequency, $p_r(\pi_{j,k}^{(\tau)})$ of each motif will be the absolute frequency, $p(\pi_{j,k}^{(\tau)})$ divided by the sum of the matrix. Then the marginal frequency is [42]

$$p(\pi_j^{(\tau)}) = \sum_{k=1}^{K} p_r(\pi_{j,k}^{(\tau)}). \tag{1.26}$$

Finally mvMWPE is calculated [42]

$$mvMWPE_{(\tau)}^{d,l} = -\sum_{j=1}^{d!} p(\pi_j^{(\tau)}) \ln(p(\pi_j^{(\tau)})) \tag{1.27}$$

as a function of time scale τ.

1.1.13 Multicomponent Signals and Time-Frequency Entropies

Our article "Time-varying Time-Frequency Complexity Measures for Epileptic EEG Data Analysis" by Colominas, El Sayed Hussein Jomaa *et al* [31], described multicomponent signals as follows :

The multicomponent signals, which are made of a superposition of a small number of components modulated both in amplitude and frequency (AM-FM), are a versatile way to model phenomena such as audio signals [86], biomedical signals [124], or economic temporal series [131].

For a signal with K component we have

$$x(t) = \sum_{k=1}^{K} x_k(t) = \sum_{k=1}^{K} a_k(t) \cos(2\pi\phi_k(t)), \tag{1.28}$$

with $a_k(t)$, $\phi_k'(t) > 0 \forall t$ and ϕ' is the derivative of ϕ. In this case, the temporal variations of $a_k(t)$ and $\phi_k'(t)$ are much smaller than those of $\phi_k(t)$, which adds new constraints : $|a_k'(t)|$,$|\phi_k''(t)| < \epsilon\phi_k'(t)$, for a small $\epsilon > 0$. The signals modeled as in equation 1.28 have a special structure in a time-frequency plane : every component occupies a "ribbon" around its instantaneous frequency $\phi_k'(t)$. The more components we have, the more ribbons and the larger the occupancy of the plane we will get.

If we analyze the signal of equation 1.28 with the short time Fourier transform

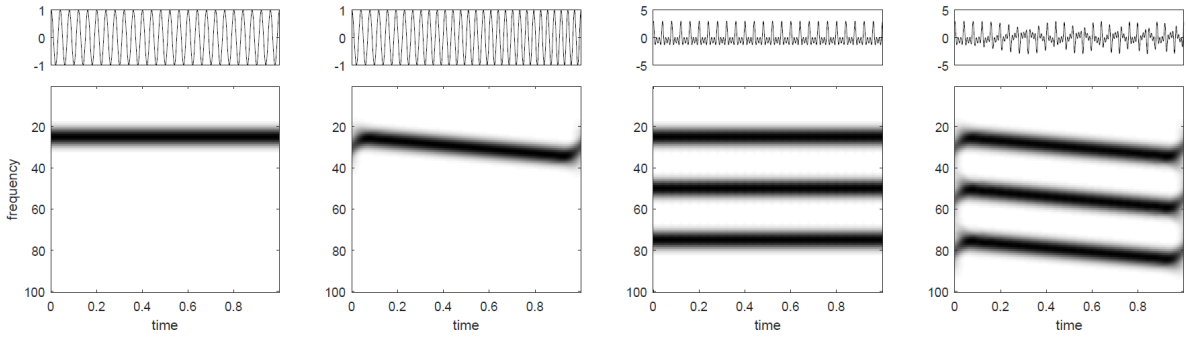

FIGURE 1.4 – AM-FM signals of different complexities and their spectrograms. Left : pure tone as in $x_1(t) = \cos(2\pi f_0 t)$ with $f_0 = 25$. Middle left : chirp signal as in $x_2(t) = \cos(2\pi f_0 t + \pi k t^2)$, with $f_0 = 25$ and $k = 10$. Middle right : summation of three pure tones as in x_1, with $f_{0,1} = 25$, $f_{0,2} = 50$, and $f_{0,3} = 75$. Right : three chirps. In all four cases, the signals are defined for $0 \leq t \leq T = 1$ and were generated with a sampling frequency of $f_s = 1000$. The spectrograms were obtained with a Hann window of 200 samples, and for $0 \leq f \leq 100$. Figure from [31].

(STFT)

$$F_x^g(t,f) = \int x(u) g(u-t) \exp^{-i2\pi f(u-t)} du, \tag{1.29}$$

where $g(t)$ is an even real compact-supported window with supp$\{G(f)\} \subseteq [-B, +B]$, then its spectrogram is

$$S_x^g(t,f) = |F_x^g(t,f)| \equiv \sum_{k=1}^{K} a_k^2(t) |G(f - \phi_k'(t))|^2, \tag{1.30}$$

provided $\phi_{k+1}'(t) - \phi_k'(t) > 2B$, $\forall k$. For the sake of simplicity, and due to its symmetry for real signals, we consider only positive frequencies for the spectrogram.

Time-Frequency Complexity

A widespread manner to measure the information and complexity of the time-frequency plane comes from the analogy between signal energy densities and probability densities [12]. In this analogy, the instantaneous energy $|x(t)|^2$ and the spectral energy $|X(f)|^2$ act as unidimensional densities of the energy of the signal in time and frequency respectively, while the time-frequency representation (TFR) of the signal would behave as a bidimensional energy density in time-frequency. However, to

consider TFR $R_x(t,f)$ as a true density, it should satisfy the marginal properties

$$\int R_x(t,f)df = |x(t)|^2, \int R_x(t,f)dt = |X(f)|^2, \tag{1.31}$$

the energy conservation property

$$\int\int R_x(t,f)dtdf = \int |X(f)|^2 df = \int |x(t)|^2 dt, \tag{1.32}$$

and the non-negativity property

$$Rx(t,f) \geq 0. \tag{1.33}$$

If a given TFR satisfies requirement (1.31), it automatically satisfies requirement (1.32), but the converse is not true [30]. Unfortunately, most TFRs do not satisfy the three requirements simultaneously. The bilinear distributions that are manifestly positive and satisfy the marginal properties do not exist [30]. Wigner-Ville distribution satisfies the marginals but takes negative values, as well as all fixed-kernel Cohen's class TFRs that satisfy requirement (1.31) [12]. The spectrogram, on the other hand, satisfies the positivity property, but it does not do so with the marginals (although it satisfies the energy conservation property) [30] [51]. The negativity of the Wigner-Ville distribution prevented the authors in [12] to use a classical Shannon entropy [104] of the TFR. Instead, they opted for a Rényi entropy [98], which appararently solves the non-positivity issue by taking the logarithm outside of the integral :

$$H_R^\alpha(R_x) = \frac{1}{1-\alpha}\log_2 \int\int \tilde{R_x}^\alpha(t,f)dtdf. \tag{1.34}$$

However, because of the negative values of the Wigner-Ville distribution, it is still possible for (1.33) to not exist, since $\int\int R_x^\alpha(t,f)dtdf < 0$ could happen for odd α. This is a bad result since odd orders $\alpha > 1$ make this entropy asymptotically invariant to the well-known cross-terms of the Wigner-Ville distribution.

All this drives us not to use the Wigner-Ville distribution and we will opt for the spectrogram instead. Although it does not satisfy the marginal properties (1.31), it was already successfully used in the context of time-frequency complexity measures in [74] and [103].

A different way to measure the complexity of the time-frequency plane comes from the singular value decomposition (SVD) entropy, first introduced in [6], and used in the context of time-frequency representations in [19]. The SVD of the time-frequency

	$x_1(t)$	$x_2(t)$	$x_3(t)$	$x_4(t)$
Rényi	13.336	13.378	14.921	14.965
NoC	1	1.029	3	3.093
SVD	0.0027	1.796	0.0361	1.946

TABLE 1.1 – Rényi entropy, number of components (NoC) based on Rényi entropy, and SVD entropy of the signals shown in figure 1.4 for $\alpha = 2$.

representation expands it as

$$R_x(t,f) = \sum_{n=1}^{\inf} \sigma_n u_n(t) v_n(f), \tag{1.35}$$

by solving a system of two coupled integral equations [30] [106]. A Shannon entropy is applied on the singular values σ_n's, after normalization :

$$H_V(R_x) = -\sum_n \frac{\sigma_n}{\sum_n \sigma_n} \log_2(\frac{\sigma_n}{\sum_n \sigma_n}). \tag{1.36}$$

Table 1.1 shows the values of Rényi entropy, SVD entropy, and the number of components based on Rényi entropy of the signals shown in figure 1.4 for $\alpha = 2$. Number of components is [103] [107]

$$N_x^\alpha = 2^{H_R^\alpha(S_x) - \breve{H}_R^\alpha}, \tag{1.37}$$

where S_x is the spectrogram of the signal x and $\breve{H}_R^\alpha$ is the Rényi entropy of a pure tone. While the Rényi entropy cannot distinguish between $x_1(t)$ and $x_2(t)$, the SVD entropy is able to do so. The counting property of the Rényi entropy is well illustrated, as well as the "immunity" of the SVD entropy to the number of components.

1.2 Electroencephalography : Principle and Instrumentation

1.2.1 Cellular Neurophysiology

The ability to generate electrical activity is a very common property of living tissues. Some examples of this are the electrical activity of the heart and its recording of electrocardiogram (ECG) and the electrical activity of muscles and its recording of the electromyogram (EMG). For this it is not surprising to know that the brain does also generate electrical activity.

In 1929, Hans Berger was the first to record electrical activity of the human brain and give it the name we know today, "electroencephalography" (EEG). His findings were confirmed 5 years later by Adrian and Matthews after they repeated Berger's experiment. Berger later published 14 articles on the electrical activity of the human brain, explaining the concept of EEG and the significance of several recordings.

In the following subsections, we will explain the neurophysiological principle of EEG and the instrumentation of the recording system itself.

1.2.2 Neurophysiology

Neurons generate time-varying electrical currents when activated. These are ionic currents generated at the level of cellular membranes. We can distinguish two main forms of neuronal activation [105] : the fast depolarization of the neuronal membranes that results in the action potential caused by sodium and potassium voltage-dependent ionic conductances g_{Na} and $g_{K(DR)}$ respectively, and the more prolonged change of membrane potential due to synaptic activation caused by several neurotransmitter systems.

The action potential consists of a rapid change of membrane potential, such that the intracellular potential jumps suddenly from negative to positive, and quickly, in 1 or 2 milliseconds, returns to the resting intracellular negativity (figure 1.5). Through this mechanism, the nerve impulse propagates the nerve axon and dendrite without losing amplitude (figure 1.6).

Concerning the slower postsynaptic propagation, they are of two main types [105], excitatory post synaptic potentials (EPSPs) and inhibitory post synaptic potentials

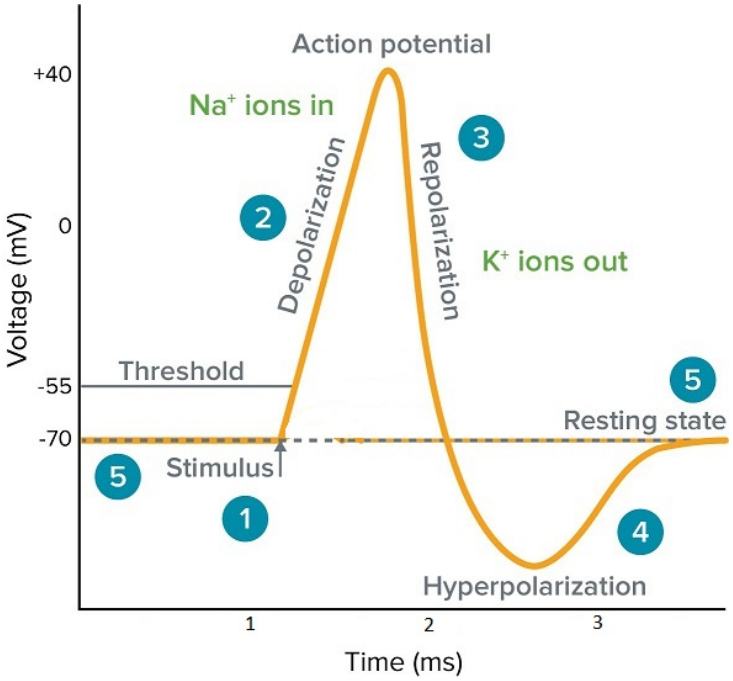

FIGURE 1.5 – The electrical potential difference between intracellular and extracellular mediums of the nerve cell during an action potential [122].

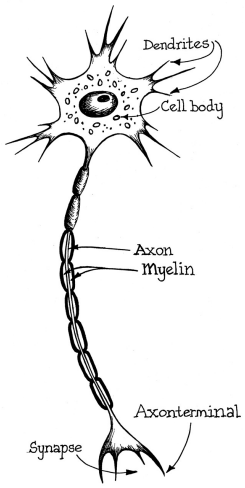

FIGURE 1.6 – A schematic diagram of a neuron showing the main components labelled [97].

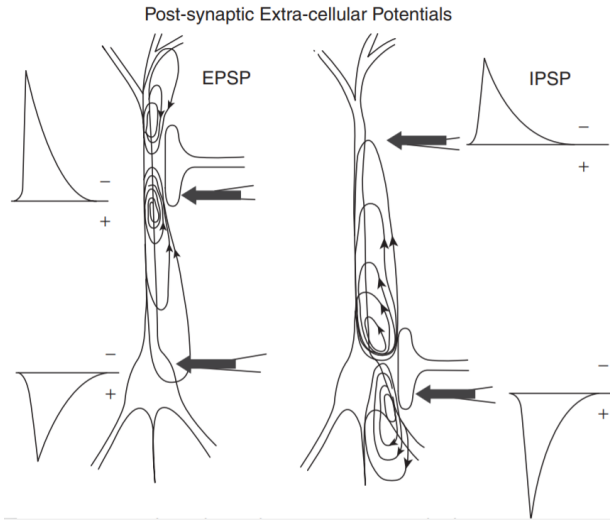

FIGURE 1.7 – Intra- and extracellular current flow in a neuron due to different types of synaptic activation. EPSP : excitatory synapse at the level of the apical dendrite ; the generated current of positive ions flows inwards, causing depolarization of the cell. This results in an active sink at the level of synapse. The extracellularly measured EPSP has a negative polarity at the level of the synapse. At the soma there is a passive source, and the potential has a reversed polarity. IPSP : inhibitory synapse at the level of the soma. A current of negative ions flows inwards causing hyperpolarization of the cell ; this results in an active source at the level of the synapse. The extracellularly measured IPSP has a positive polarity at the level of the soma. At the level of the distal apical dendrite there is a passive sink, and the potential has a reversed polarity [45].

(IPSPs). These two kinds are differentiated based on the type of neurotransmitter and corresponding receptor, and their interaction with specific ionic channels and/or intracellular second messengers.

At the level of a synapse in the case of the EPSP, the transmembrane current is carried by positive ions inwards. In the case of the IPSP, it is carried by negative ions inwards or positive ions outwards. Thus the positive electric current is directed to the extracellular medium in the case of an EPSP, and it is directed from the inside of the neuron to the outside in the case of an IPSP (figure 1.7).

When it comes to EEG recordings, the EEG signal arises mainly from the summation of thousands EPSPs and the IPSPs. The most important point to take into consideration is the geometry of the neuronal sources of electrical activity that gave rise to the scalp EEG signals. The neurons that give the main contribution to the EEG are those that form "open fields" according to the classic description in [39]. Those are the

pyramidal neurons of the cortex, since they are arranged in palisades with the apical dendrites aligned perpendicularly to the cortical surface. This means that longitudinal intracellular currents flow along dendrites or axons, and thus generate electric fields around them.

Pyramidal neurons of the cortex, with their long apical dendrites, generate coherent electric fields when activated with a certain degree of synchrony. We may say that these neurons behave as "current dipoles" that can be detected by sensors placed at a small distance from the skull.

In order to make the next step toward an understanding of how EEG signals recorded outside the skull are generated, we also have to take into consideration the folding of the cortex. The fact that the cortex is folded, forming gyri and sulci, implies that some populations of neurons that are at the top of a gyrus have apical dendrites that are perpendicular to the overlying skull, whereas those that are on the wall of a sulcus are parallel to the skull. The point to note in this respect is that the orientation of the neurons with respect to the skull influences the resulting EEG signal recorded outside the skull. In fact the EEG detects only those electric fields that have a component perpendicular to the skull. These fields are generated by neuronal currents that have a component oriented radially to the skull. In contrast, those currents that are oriented tangentially to the skull do not generate an electric field outside the head. A more elaborated explanation of this point is described in figure 1.8 [45].

1.2.3 Technical Background of EEG

The EEG machine has been under constant improvement since it was introduced in the 1920s by Hans Berger. One channel machines were expanded to machines with 16, 32, 64, 128, and even 256 channels. The development of vacuum tube-based amplifiers has allowed the integrated circuits to become higher in complexity and smaller in size thus leading to devices so small that could be put in patients' pockets instead of being so large that they needed to be pushed around in hospitals. Figure 1.9 shows the block diagram of a modern EEG machine that consists both of digital and analog components [45].

In the next subsections, we will cover the two major component of the EEG machine, the electrodes or the sensors and the amplifiers.

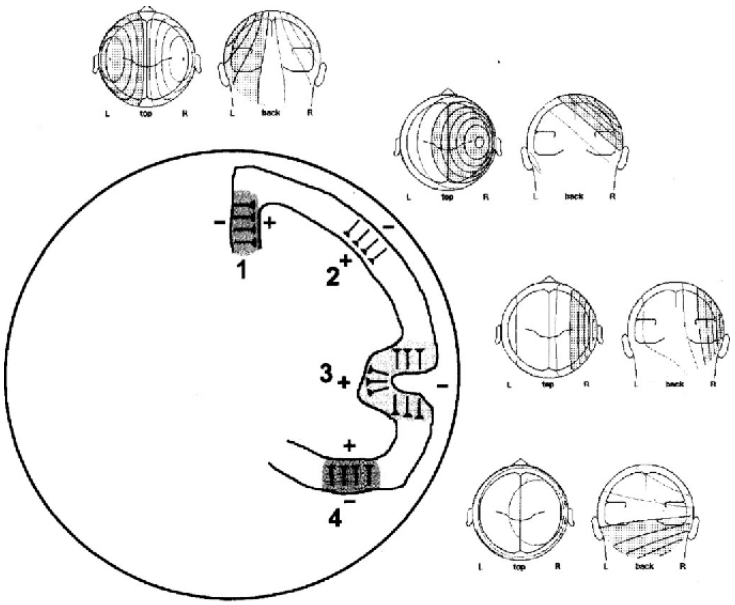

FIGURE 1.8 – Schematic of brain cross-section representing four separate EEG sources. The alignment of the pyramidal neurons is perpendicular to the cortex, thus the EEG electric field is also perpendicular to the cortex. The (+) and (-) show the polarity of the fields generated by the dipoles or the pyramidal neurons of these sources. Top and back views of the scalp EEG of these four separate sources are shown. Sources 2 and 3 generate radial electric fields and the negative voltage maximum is directly above them. in source 3, field from opposing sulcal walls cancel each other and thus only keeping the field that is radial at the bottom to dominate what is detected by the EEG. Sources 1 and 4 produce tangential fields, thus no negative maximum is detected above them, whereas the the negative and positive maxima are detected on either sides in the EEG [45].

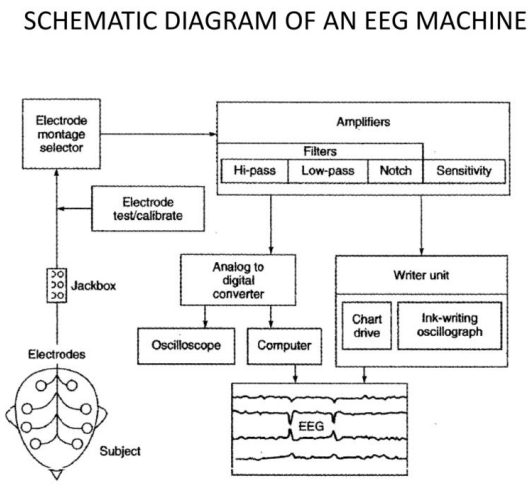

FIGURE 1.9 – Block diagram of a modern EEG machine. In digital EEG machines, the writer unit is replaced by an analog-to-digital converter, computer monitor and a computer that automatically displays and saves the recording of the subject for later diagnosis and allows the use of computerized signal analysis methods.

1.2.4 EEG Electrodes

Electrodes conduct electrical potentials from patient to the EEG machine, usually with help from an conductive electrolyte solution connecting skin to electrode. The electrolyte solution that is used serves to transmit potentials from the brain to the EEG machine and to decrease movement artifacts. Electrodes are made of metal, but not all metals make equally good EEG electrodes. Proper electrodes must be good electrical conductors [45].

When a voltage (such as that from the EEG machine) is applied to an electrode and an electrolyte solution, the double layer between the two is disturbed, and current flows between the electrolyte solution and the electrode. This current is added to the steady-state electrode-electrolyte current. Reversible electrodes are electrodes that do not easily become polarized. One way to produce such electrodes is to deposit a metallic salt containing an ion in common with the conducting solution on the electrode. An example of this is the silver chloride (AgCl) electrode. An electrode like this may be fabricated by immersing silver wire in a solution of electrolyte-containing chloride and placing a positive voltage across the electrode. Chloride ions migrate to the surface of the silver. When a chloride-treated silver electrode comes into contact with NaCl solu-

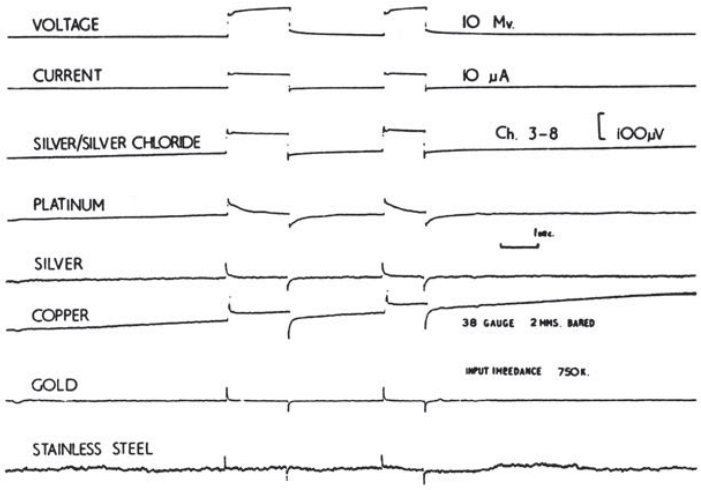

FIGURE 1.10 – The ability of different types of electrodes to reproduce an input square signal of 10mA and 10mV [32].

tion on the skin, currents of Cl^- ions flow freely between the electrode and the solution and prevent the electrode from becoming polarized. Polarization is avoided because the electrode and the solution can communicate with ions that exhibit identical mobilities in solution. Silver chloride electrodes are useful for recording DC and potentials of very low frequency [32] [45].

Figure 1.10 from [32] shows the ability of different types of electrodes to reproduce a square wave test voltage of 10mV. It is noticed that the AgCl electrode gives the best results while others failed to reproduce the low frequency or the DC of the input voltage and current.

1.2.5 Amplifiers

Amplifiers in EEG machines are different from common amplifiers whose sole function is to increase the voltage. In EEG machines amplifiers are much more complex and include filters, voltage dividers, and calibration devices [45].

Typically an amplifier multiplies the input voltage by a constant. In EEG machines, since EEG signals are of very small amplitude, the constant of the amplifier is greater than 1, usually in the range of 2 to 1000. Thus the amplifiers are called step-up

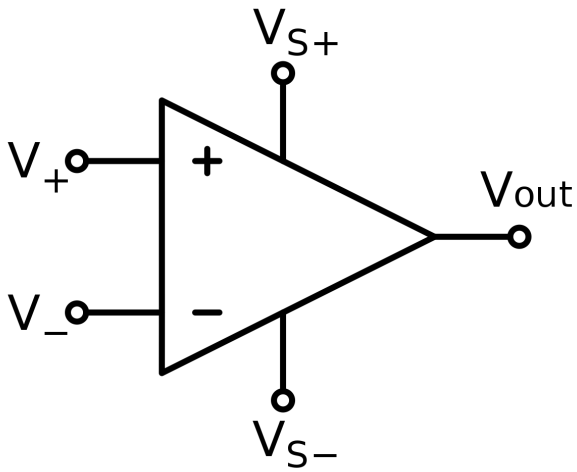

FIGURE 1.11 – Symbol of a differential amplifier. V_{S+} and V_{S-} are power supply of the amplifier. V_{out} is the output voltage which is equal to $A(V_+ - V_-)$, where A is the gain.

amplifiers. The amplification factor is called gain and is expressed as

$$Gain = \frac{V_{out}}{V_{in}}. \tag{1.38}$$

A more common way to express the gain is as a logarithmic ratio where it would be expressed in decibels (dB) :

$$Gain_{dB} = 20 \log \frac{V_{out}}{V_{in}}. \tag{1.39}$$

Signals captured by an electrode are transmitted into a differential amplifier (figure 1.11) that subtracts the signal of one electrode from that of another electrode and amplifies it. Signals common to both inputs are eliminated. Such signals can be called in phase or common mode [45]. This means that they vary together with respect to time. This helps in removing common noise. Line noise of 50Hz is in phase between all electrodes, but differential amplifiers are not ideal and are not able to totally eliminate such noise. The ability of the differential amplifier to reject in phase signals and amplify out of phase signals is measured by the common-mode rejection ratio (CMRR). To calculate the CMRR of an amplifier there are two steps :

1. Feed the same voltage to the two inputs of the differential amplifier. The output in this case is measured and denoted as V_{CM}.
2. Feed the same voltage to only one of the inputs and connect the other to the

ground of the system. The output voltage in that case is measured and denoted as V_d.

In this case

$$CMRR = \frac{V_d}{V_{CM}}. \tag{1.40}$$

An EEG amplifier is good if it has at least a CMRR of 1000. It is important for the reference electrode to be relatively close to the recording electrode. This maximizes the chance of eliminating major noise signals in common. When the reference electrode is distant (for example on the leg), the spaced electrodes act like an antenna and may pick up signals that may exceed the amplifier's common-mode range.

After the signals are subtracted and amplified, they are filtered to remove unwanted frequencies. High-pass filters remove frequencies less than a desired cut-off frequency ; low pass filters remove frequencies greater than a desired cut-off frequency. A common special kind of filter, the notch filter, removes one frequency. This filter is used to remove the line-frequency (50Hz) and reduces as much as possible the noise caused by it.

Mainly after that, the signal is either transmitted to the pen to be printed on a paper or transmitted to the screen and saved digitally in the database for further processing and later diagnosis.

1.3 Epilepsy

Epileptic seizures and epileptic disorders are common in all ages in both sexes. Blume *et al* [18] defined **Epileptic disorders** as chronic neurological conditions characterized by recurrent epileptic seizures. Epileptic seizures are *"transient occurrences of signs and/or symptoms due to abnormal excessive or synchronous neuronal activity in the brain"* [50].

In this thesis we will cover some epileptic disorders of childhood that are called epileptic syndromes because they are defined on precise clinical and EEG criteria. These specific epileptic syndromes are : childhood absence epilepsies (CAE), Landau-Kleffner syndrome including epileptic encephalopathies with Continuous spikes and waves during sleep (CSWS), and benign childhood epilepsy with centrotemporal spikes (BECTS).

1.3.1 Childhood Absence Epilepsy (CAE)

Absence seizures are brief (usually some seconds) generalised epileptic seizures. They are mainly characterized by consciousness impairment and this is where the term "absence" comes from. Impairment of consciousness could range from being complete to partial or even requires special cognitive tests to be detected.

Although typical absences are mainly spontaneous, they could be induced in almost 90% of the patients through hyperventilation. Other factors that may facilitate the occurrence of absences are some photic stimulations, patterns, video games, and thinking [94].

Clinical manifestations of absence seizures are different from patient to another. Consciousness impairment is sometimes not the only clinical manifestation and thus this leads to categorizing absences into two categories [94] :

— simple absences with impairment of consciousness
— complex absences where impairment of consciousness is accompanied with ictal motor manifestations

When comparing incidence rates, complex absences are much more frequent in children knowing that the same patient can have both simple and complex absences.

Simple absences were defined as seizures with *"transient loss of consciousness without conspicuous convulsions. A patient stops for a moment whatever he or she is*

doing, very often turns pale, may drop whatever is in hand... There may be a slight stoop forward, or a slight quivering of the eyelids... The attack usually lasts only a few seconds. The return of the consciousness may be sudden and the patient after the momentary lapse, may be in just the same state as before the attack, may even continue a sentence or action which was commenced before it came on, and suspended during the occurrence" [56]. In less severe cases, absences may not completely stop the patient's activities, but could slow his or her reaction time and speech. In their mildest forms, absences may be unnoticeable to observers (phantom absences) [94].

Figure 1.12 shows the EEG recordings of a child with Childhood Absence Epilepsy during a seizure.

Complex absences are sub-categorized into many subcategories based on the manifestations that accompany the impairment of consciousness. Some of these subcategories are [94] :

Absences with clonic or myoclonic components : These absences are accompanied with clonic or/and myoclonic motor manifestations. They could be rhythmic or arrhythmic and singular or repetitive. The most common motor manifestations are jerking of the eyelids, eyebrows, and eyeballs and jerking of the head.

Absences with atonic components : In some cases, when the absence is severe, the seizure is accompanied with diminution of the muscle tone. In these cases, manifestations such as dropping of the arms or drooping of the head are observed in patients during the seizures. Rarely, the diminution is strong enough to cause falls.

Absences with tonic components : Tonic muscular contractions could sometimes accompany the absence seizures. Such manifestation mainly affect the facial and neck muscles. In some cases, eyes and the head may be pulled backwards or to one side.

It is important to note that absences do not influence the patients' normal life outside the period of the seizure itself. In other words, patients have normal cognitive and physical abilities as the non-epileptic population as long as the seizure is not taking place [24].

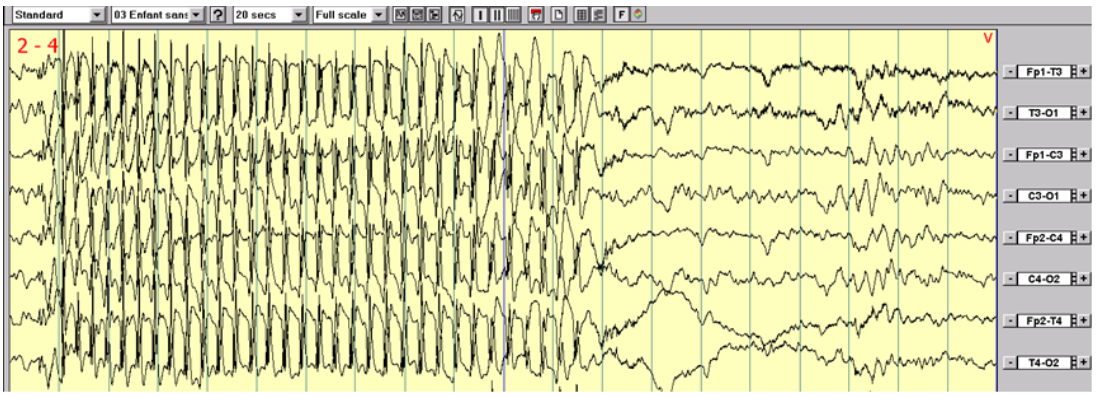

FIGURE 1.12 – The EEG recordings of a child with Childhood Absence Epilepsy during a seizure. The seizures are generalized. Credits to Patrick Van Bogaert.

1.3.2 Epileptic Encephalopathies with Continuous Spikes and Waves during Slow-Wave Sleep Including Landau-Kleffner Syndrome

"Epileptic syndromes with continuous spikes and waves during slow sleep (CSWS) are defined as a cognitive or behavioral impairment acquired during childhood, associated with a strong activation of the interictal epileptiform discharges during NREM sleep – whatever focal or generalized – and not related to another factor than the presence of CSWS."[113]

The onset of the seizures in CSWS is between 2 years and 12 years, peaking at around 5 years [110]. Epilepsy with CSWS is not frequent (0.5% of all children with seizures) [91].

There are typically 3 stages of evolution of epilepsy with CSWS [94].

1. The first stage before the occurrence of the CSWS pattern : The first seizure usually happens at night and in general they are not frequent. The EEG shows multi-focal spikes.

2. The second stage - stage with CSWS : This stage starts some months after the first seizure. A patient can have one or more than one type of seizures. Over 90% of the patients have numerous seizures, sometimes several per day. Infrequent seizure are not common in that case (only 10%).

   The most disturbing clinical feature is the decline of the neuropsychological state. This progresses gradually. The spike localization plays an important role in

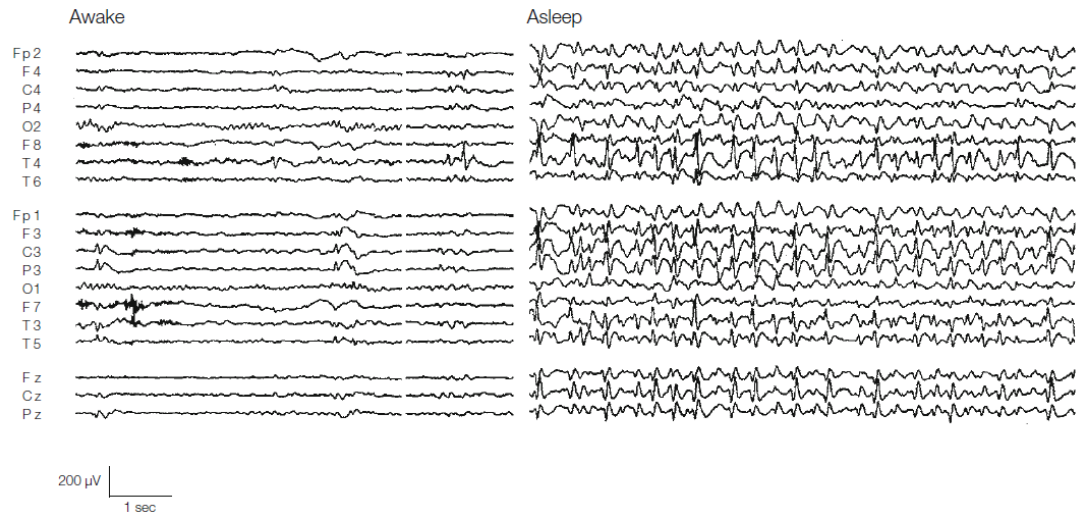

FIGURE 1.13 – The EEG recording of an 8 years old boy with epilepsy with CSWS [94]. The recordings show the significant increase in spike frequency during sleep.

determining the neuropsychological deficits. Frontal and prefrontal CSWS affect the cognitive and executive functioning before damaging the language function. This might be seen as aggressiveness, inattention, and agitation. Temporal lobe CSWS produces mainly linguistic disturbances.

It is worth adding that some studies were also able to identify metabolic disturbances in areas that are remote to the epileptic foci [40][77]. This explains why some neuropsychological disturbances are sometimes not related to the localization of the foci.

3. The third stage of clinico-EEG remission : This stage happens between months to 7 years after the onset. Seizures remit, EEG improves, and neuropsychological state also improves but rarely does the children retain average normality.

Figure 1.13 shows the EEG of an 8 years old boy diagnosed with epilepsy with CSWS. The EEG was recorded during both awake state and asleep state. The figure shows the significant increase in the frequency of spikes during sleep state.

Landau-Kleffner Syndrome

The International League Against Epilepsy (ILAE) identified Landau-Kleffner Syndrome (LKS) in 1989 as "acquired epileptic aphasia" [28]. It was not considered the same epileptic syndrome as "Epilepsy with CSWS" although both are considered to be

"epilepsies and syndromes undetermined as whether they are focal or generalised". A new ILAE definition [46] considers them as a single entity called "epileptic encephalopathy with CSWS including LKS". The justification in [46] was the lack of evidence for mechanistic differences between LKS and CSWS to consider them as separate syndromes. Furthermore, a study in 2006 [114] found significant differences between LKS and epilepsy with CSWS. This led the authors of [114] to conclude that the two disorders could be classified as separate branches of the same disorder.

LKS is not a very frequent epileptic disorder (usually one or two cases per year in highly specialized centres. Its onset is usually between the ages of 2-8 years, and has a 2 :1 male to female ratio [94].

Some clinical manifestation of LKS are :

— **Linguistic abnormalities :** Children with LKS become unable of linking acoustic signals to a semantic value. The diagnosis is often delayed and mistaken to deafness or selective mutism. But in fact most of these children have an audiogram that is normal [94].
  Besides that, children also show language deficits. This can reach a point where LKS can affect linguistic functions with impairment of expressive speech and phonological errors. Finally the child may become entirely mute [94].

— **Cognitive and behavioural abnormalities :** More than 75% of LKS patients show cognitive and behavioural abnormalities. Some common abnormalities are hyperactivity and attention deficit.

— **Seizures :** 75% of LKS patients have seizures and the onset is between 4 and 6 years. Usually seizures are not frequent. Only 20% of LKS patients continue to have seizures after the age of 10 years. Seizure symptoms and types are not well described but they are mainly nocturnal [94].

1.3.3 Benign Childhood Epilepsy with Centrotemporal Spikes (BCECTS)

Benign childhood epilepsy with centrotemporal spike (BCECTS), also called rolandic epilepsy, is a common epileptic syndrome of childhood [79] [80].

The onset of these seizures is from 1 to 14 years, with 75% starting between 7 and 10. It is 1.5 times more frequent in males. Its incidence rate is 10-20 per 100000 children aged between 0-15 years.

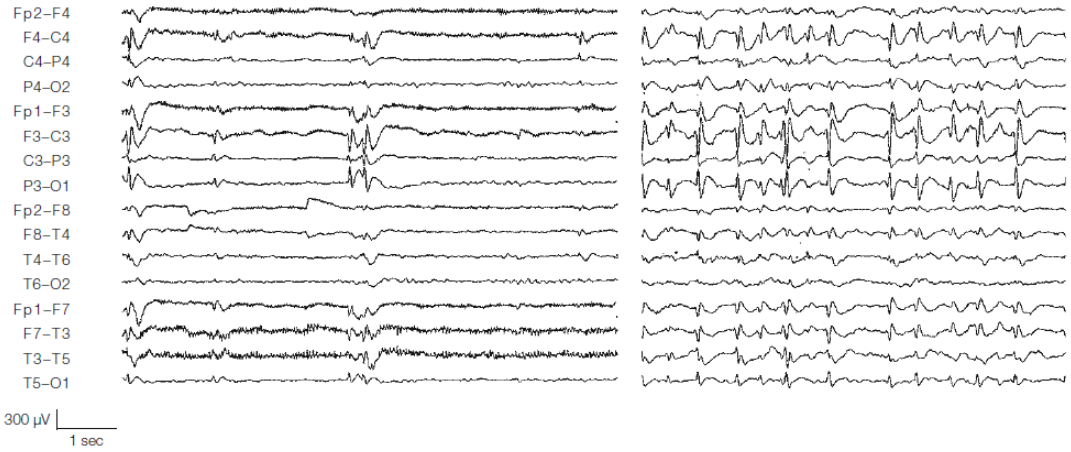

FIGURE 1.14 – The EEG recording of a boy diagnosed with LKS [94].

The main features of BCECTS are [94] :

— **Hemifacial sensorimotor seizures :** This happens in almost 30% of the patients. They are often entirely localised in the lower lip or spread to the ipsilateral hand. It is a sudden, continuous or bursts of contractions that usually last for few seconds. Hemifacial sensory symptoms also involve numbness in the corner of the mouth. They are usually associated with innability to speak and hypersalivation.

— **Oropharyngolaryngeal ictal manifestations :** This happens in 53% of the patients. They are unilateral sensorimotor symptoms inside the mouth. Numbness and paraesthesias are usually diffused on one side or even on one tooth. Motor oropharyngolaryngeal manifestation produces strange sounds like death rattle, gargling and grunting sounds.

— **Arrest of speech :** It happens to 40% of the patients. The child is unable to utter any meaningful word and tries using gestures as a means of communication.

— **Hypersalivation :** It happens is 30% of the patients. It is often associated with oropahryngolaryngeal or hemifacial seizures.

The EEG is very typical, showing CTS that are activated during sleep (figure 1.15). Most children with BCECTS have normal cognitive abilities. However, careful neuropsychological investigations have shown that a lot of patients show subtle impairments affecting various domains (language, attention, memory) in patients with classical BECTS [116] [43] [9]. Moreover, some patients diagnosed as BCECTS evolve to true EE with CSWS. So the concept that BCECTS and EE with CSWS belong to the

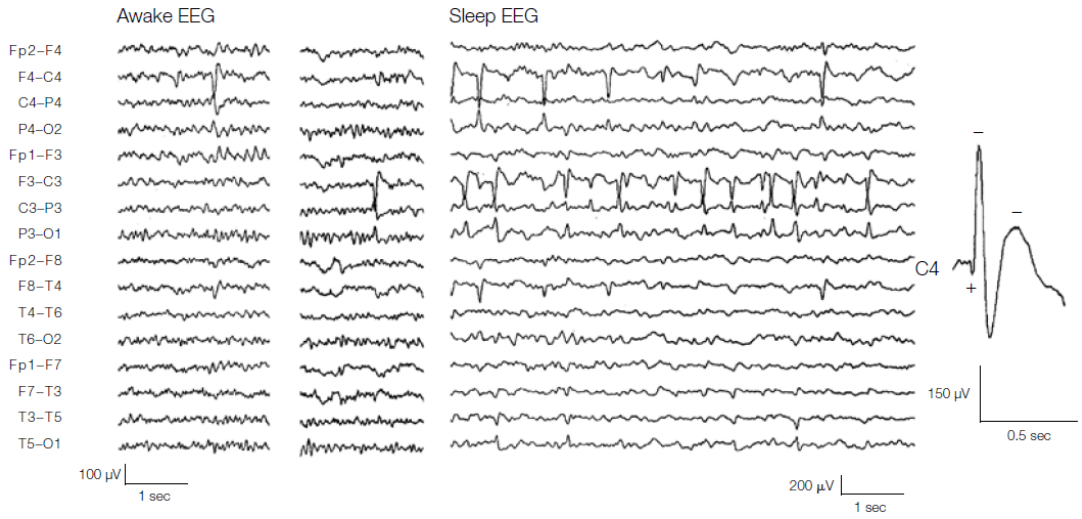

FIGURE 1.15 – The EEG recording of an 11-years old girl with a recorded rolandic seizure who has been in remission since the age of 8 years. The EEG was recorded in both states, awake and asleep. The recording shows that the spikes are mainly central and occur independently on both hemispheres and are more frequent during sleep [94].

same spectrum of epileptic syndromes is now widely accepted [112]. The etiology of these epileptic syndromes is unknown. Structural MRI do not show any lesion. It is hypothesized that genetic factors are involved. Still, some patients show a mutation of a gene that is called GRIN2A.

1.4 Functional Connectivity

Brain connectivity can be categorized into two categories, structural (anatomical) connectivity and functional connectivity. Structural connectivity refers to connections between different brain regions that are established through actual anatomical structures. On the other hand, functional connectivity refers to connections between different brain regions from the statistical relationships of their physiological activity [14].

When it come to studying functional connectivity in neurological disorders, the focus is on how the disorder modifies the brain's networks. Epilepsy is one of the most common neurological disorders that affects the cortical networks and studying it helps better understand its neurobiology and approaches to treatment [15] [69].

In this section, we summarize the findings of the application of functional connectivity on the two most common childhood epilepsies ; BCECTS and CAE. Then we summarize some different methods used to asses functional connectivity from EEG/MEG signals.

1.4.1 Functional Connectivity in BCECTS

Functional connectivity studies of BCECTS mainly focused on network changes in default mode network (DMN), language networks, and executive function.

Default Mode Network (DMN)

The DMN is a "resting state" network because the strength of its functional connectivity increases when subjects are at rest. Usually the DMN weakens during tasks, but it sometimes is involved during some social behaviour tasks which meant that it has a role in facilitating such tasks.

Several studies focused on the DMN changes in BCECTS [75] [93] [77]. The most common finding is the decrease in connectivity strength within some or all the components of the DMN. A study using functional magnetic resonance imaging (fMRI) observed weaker activity at rest in children with BCECTS [93]. Authors of [93] also noticed weaker deactivation of the DMN during the language task. This led them to the conclusion that weaker activations at rest doesn't necessarily mean lower activity in the corresponding brain region, instead it means that the connection or integration between the DMN and other cortical regions is lost. Another study based on fMRI studied

the DMN in 3 groups of resting state : children with BCECTS and Interictal Epileptiform Discharges (IED), children with BCECTS and no IED, and healthy children [75]. Similar to [93], the authors found a decrease in the activity of the DMN. This decrease was only noticed in the group of the children with BCECTS and IED. This lead to the conclusion that IED play the role of weakening the DMN activity.

Other studies focused on the strength of the connectivity between the DMN and the other regions of the brain. The authors of [85] observed a decreased in connectivity between the DMN and the language-related cortical regions. Another study, handled children with CECTS as two groups : with attention-deficit/hyperactivity disorder (ADHD) and without ADHD [126]. This study found that there is increased connectivity between the DMN and the regions in the cortex that are associated to visual tasks in both groups when compared to healthy children.

Language Networks

Language functions are interesting to study in BCECTS patients. Many studies reported language deficits in children with BCECTS [111]. Studying the language deficits in children with BCECTS from the network point of view allows us to better understand the neurological disorders of BCECTS and its atypical forms (Landau-Kleffner syndrome).

Children with BCECTS are found to encounter problems in word generation. Thus, children with BCECTS show altered connectivity patterns involving the inferior frontal gyrus (IFG). Studies [129] [109] [48] showed that the local connectivity within the IFG is altered, with lower connectivity to the temporal lobe and angular gyrus [25], and the supramarginal and superior frontal gyri [89]. A lower connectivity between the left and right IFG was also observed [125].

Another study considered the influence of IED on language networks [127]. This study showed that those discharges lead to the alteration of the connectivity by lower the strength of the network. The result is in consistence with a previous study hypothesizing remote inhibition, that showed that IED lead to the inhibition of remote but functionally connected cortical regions [40].

Executive Functioning and the Frontal Lobe

Despite the fact that children with BCECTS have normal IQ scores, test showed that they have deficits in attention, processing speed, memory, and inhibitory control [7] [38]. All these tasks correspond to what is called executive functioning. The dorsolateral prefrontal cortex, orbitofrontal cortex, and the anterior cingulate cortex are all linked to executive functioning. The executive and the salience networks (SAN) are two resting state networks (RSN) that are associated with "task poistive" states [14].

Several studies pointed out the involvement of the frontal lobe in children with BCECTS. An overall increase in the EEG based connectivity within the frontal and the frontotemporal regions was linked to the presence of IED [2] [29]. In other studies, both increases and decreases in connectivity strength were noted within the frontal regions [85] [83] [29] [115]. This variability was linked to the choice of analytical methods and the regions of interest (ROIs). Finally, other studies reported the decrease in the strength of the within-network connectivity of the dorsal attention network (DAN) [75] [126].

1.4.2 Functional Connectivity in Childhood Absence Epilepsy

As in BCECTS, functional connectivity studies mainly focused on network changes in the DMN, language network, and the executive functioning and the frontal lobe.

Default Mode Network

Similar to BCECTS, the DMN is generally the main network to be analyzed in children with CAE. However, for CAE the analysis is divided into two categories : comparing the brain connectivity in children affected by CAE with that of normal children and comparing within the same individual epochs that are IED-free (no seizures) with epochs containing IED.

A study of connectivity based on fMRI involved 12 CAE affected children and 14 healthy controls [84]. The DMN of the two groups was compared. Only IED-free epochs were included in the analysis. A decrease in the connectivity of the DMN was observed. Three other studies found that the DMN is strongly weakened in epochs with IED when compared to IED-free epochs [132] [128] [76]. These four studies show that the IED play a role in weakening the connectivity of the DMN and that this effect continues to

exist even during the absence of the discharges.

Language Networks

Unlike BCECTS, children with CAE are not known to have language deficits [14]. For this reason, there are no connectivity studies that analysed language connectivity [14]. However, a recent study of language performance in 243 children with different epileptic disorders, including BCECTS and CAE, showed that the children with CAE had a worse performance that those with BCECTS [64]. For this, it is necessary, to perform a study comparing the language networks of CAE and BCECTS.

Executive Functioning and the Frontal Lobe

Children with CAE showed several deficits in executive functions. An analysis of cognitive processing in children with generalized epilepsies found that the deficits in intelligence, processing speed, and memory were found in children with CAE [82]. Changes in connectivity patterns in the frontal lobes are noticed in children with CAE. Most of the studies concluded an increase in the connectivity of the frontal lobe using several connectivity perspectives including EEG [100], magnetocardiography (MEG) [123], and fMRI [10] [48]. The increase of the connectivity in the frontal lobe could be justified by the decrease of the anticorrelation between the DMN and other executive networks as the DAN and the SAN, thus increasing the positive correlation and, in consequence, the functional connectivity.

The dynamic effect of the IED on the brain networks could be studied due to the high frequency of the IED in CAE. Two studies noted the weakening of the attention and executive networks during IED [128] [132]. In another study, the connectivity changes at the beginning of the seizure were analysed [58]. The seizures were linked with an increase in the delta frequency spectrum power on the MEG recording. This frequency band was found to increase the short-range frontal lobe connectivity in [123].

1.4.3 EEG/MEG-Based Functional Connectivity Methods

fMRI has shown to be a very reliable method of functional connectivity. Although fMRI has an excellent spatial resolution, the main (and perhaps only) drawback of fMRI is that it has a bad temporal resolution. For this reason, several methods based

on EEG/MEG were developed to find the brain functional connectivity, since EEG/MEG have a very small temporal resultion (m̃s). These methods can be applied on two levels, the electrode (scalp) level and the source (cortex) level. Since, in this thesis, we are only interested by networks in the cortical level, we will describe several EEG-methods used to project the scalp signals on the cortex and then describe some common methods to find the functional connectivity.

EEG-Based Inverse Solution Algorithms

Based on the equivalent current dipole model, EEG signals recorded from M scalp channels are considered as a linear combination of P source signals.

$$X(t) = GS(t) + N(t), \tag{1.41}$$

where $X(t)$ is the EEG signals, $G[M, P]$ is the lead field matrix, $S(t)$ is the source signals, and $N(t)$ is the noise. Since G is unknown, the EEG inverse problem consists of estimating the unknown sources from $X(t)$. For this reason, several algorithms have been proposed each using different assumptions about spatial and temporal properties. We will present here three commonly used algorithms.

— **Minimum Norm Estimate [60] :** This algorithm is based on a solution with minimum power using the L2 norm to regularize the problem.

$$S_{MNE} = G^T(GG^T + \lambda C)^{-1}G, \tag{1.42}$$

where λ is the regularization parameter and C is the noise covariance matrix.

— **Standardized Low Resolution Brain Electromagnetic Tomography (sLORETA) [95] :** sLORETA standardizes the source distribution estimated from MNE bby the variance of each estimated source.

$$S_{sLORETA} = W_{sLORETA}S_{MNE} \tag{1.43}$$

where $W^2_{sLORETA}$ =diag$(S_{MNE}G)$ =diag$(S_{MNE}(GG^T + C)S^T_{MNE})$.

— **Dynamical Statistical Parametric Mapping (dSPM) [37] :** The dSPM is based on MNE. The normalization matrix in dSPM contains the minimum norm estimates of the noise at each source, derived from the noise covariance matrix,

defined as

$$S_{dSPM} = W_{dSPM} S_{MNE}, \tag{1.44}$$

where $W^2_{dSPM} = \text{diag}(S_{MNE} C S^T_{MNE})$.

EEG-based Connectivity Measures

Lately, EEG/MEG-based functional connectivity methods have been used in order to study brain networks during different states [16] [22] [33] [61] [121] [120]. Five of the commonly known EEG-based connectivity measures are presented here :

— **Cross-Correlation Coefficient (r^2) [21] :** The cross-correlation coefficient measures the linear correlation between to signal or variables x and y. This correlationis calculated as a function of a time delay Θ :

$$r^2_{xy} = \max_{\Theta} \frac{cov^2(x(t), y(t+\Theta))}{(\sigma_{x(t)} \sigma_{y(t+\Theta)})^2}, \tag{1.45}$$

where σ and cov are the standard deviation and the covariance respectively.

— **Mutual Information (MI) [36] :** The mutual information between two signals x and y is

$$I(xy) = H(x) + H(y) - H(xy), \tag{1.46}$$

where I_{xy} is the mutual information between x and y, $H(x)$ and $H(y)$ are the entropy values of x and y respectively, and $H(xy)$ in the bivariate entropy of the two signals x and y.

— **Phase Locking Value (PLV) [72] :** The phase locking value of two signals x and y is

$$PLV_{xy} = |mean(e^{i|\Phi_x(t) - \Phi_y(t)|})|, \tag{1.47}$$

where $\Phi_x(t)$ and $\Phi_y(t)$ are the unwrapped instantaneous phases of signals x and y that may be extracted using the Hilbert transform.

CHAPITRE 2

DEVELOPED ENTROPY MEASURES

2.1 Introduction

In this chapter, three new entropy measures that we developed are introduced. The first, multivariate Improved Weighted Multiscale Permutation Entropy (mvIWMPE), is based on the previously explained multivariate Permutation Entropy (mvMPE) [42], improved multi-scale permutation (IMPE) [8], and weighted permutation entropy (WPE) [47]. It combines the benefits of each method resulting in a method that outperforms the others based on several tests. The second method is sample entropy of multi-channel signals. We introduced this method to resolve the problem that was being encountered when the original multivariate sample entropy had to deal with a relatively large number of channels or variates. The third method we introduce is the time-varying time-frequency complexity measure. It is based on Rényi entropy and singular value decomposition.

2.2 Multivariate Improved Weighted Multiscale Permutation Entropy (mvIWMPE)

Improved Permutation Entropy proved to have more robust results, in terms of variance, than other PE algorithms due to the averaging of τ entropy values of each time scale, but it lacks the concept of considering amplitudes of the signals [8]. Moreover, Weighted Permutation Entropy considers the amplitudes of the signals through the addition of the values of variance instead of incrementing the permutation count, but on the other hand it lacks the low variance in results of the Improved Permutation Entropy [42][47].

We therefore introduced Multivariate Improved Weighted Multiscale Permutation Entropy (mvIWMPE) [67] that combines the advantages of both mvMWPE and IMPE, thus covering the drawbacks that were mentioned for each algorithm.

Hence, the steps for calculating mvIWMPE are as described below.
Considering the multivariate time series $\{x_{m,i}\}_{i=1,\dots,N}$ with N time points and M channels where m represents the channel number $(1 \leq m \leq M)$:

1. For each time scale τ, τ different coarse-grained time series are extracted for

each channel

$$y_{m,j}^{k,\tau} = \frac{1}{\tau} \sum_{i=(j-1)\tau+k}^{j\tau+k-1} x_{m,i}, \tag{2.1}$$

where $1 \leq j \leq \lfloor \frac{N}{\tau} \rfloor$ and $1 \leq k \leq \tau$.

So,

$$\mathbf{Y}^{k,\tau} = \begin{bmatrix} y_{1,1}^{k,\tau} & y_{1,2}^{k,\tau} & y_{1,3}^{k,\tau} & \cdots & y_{1,\lfloor \frac{N}{\tau} \rfloor}^{k,\tau} \\ y_{2,1}^{k,\tau} & y_{2,2}^{k,\tau} & y_{2,3}^{k,\tau} & \cdots & y_{2,\lfloor \frac{N}{\tau} \rfloor}^{k,\tau} \\ \cdots & \cdots & \cdots & \cdots & \cdots \\ y_{M,1}^{k,\tau} & y_{M,2}^{k,\tau} & y_{M,3}^{k,\tau} & \cdots & y_{M,\lfloor \frac{N}{\tau} \rfloor}^{k,\tau} \end{bmatrix}.$$

2. For each k, mvMWPE of $\mathbf{Y}^{k,\tau}$ is calculated as mentioned earlier to obtain $mvWMPE_{k,\tau}^{d,l}$
3. Then mvIWMPE at a certain time scale τ will be calculated as the average of all $mvWMPE_{d,l}^{k,\tau}$ across k

$$mvIWMPE_{(\tau)}^{d,l} = \frac{1}{\tau} \sum_{k=1}^{\tau} mvWMPE_{k,\tau}^{d,l}. \tag{2.2}$$

2.2.1 Validation on Synthetic Data

The perfomance of mvIWMPE is evaluated with synthetic data using white and pink noise, chaotic signals generated from Lorenz system, and deterministic signals from the MIX process. The results are compared with those of mvMPE, mvMWPE, and mvIMPE.

White and Pink Noise

The first test is the application of all the previously mentioned algorithms on multivariate noise signals. Two types of noise signals are used. The first one is the white Gaussian noise (WGN). The second one is the pink noise, which is generated from WGN by dividing the Fourier transform of the WGN by $\sqrt{f}$, thus the power spectrum of the resulting noise would be proportional to $\frac{1}{f}$.

All the generated noise signals have 18 channels and 10000 time points, and are made according to four different mixtures :

1. 18 white noise signals

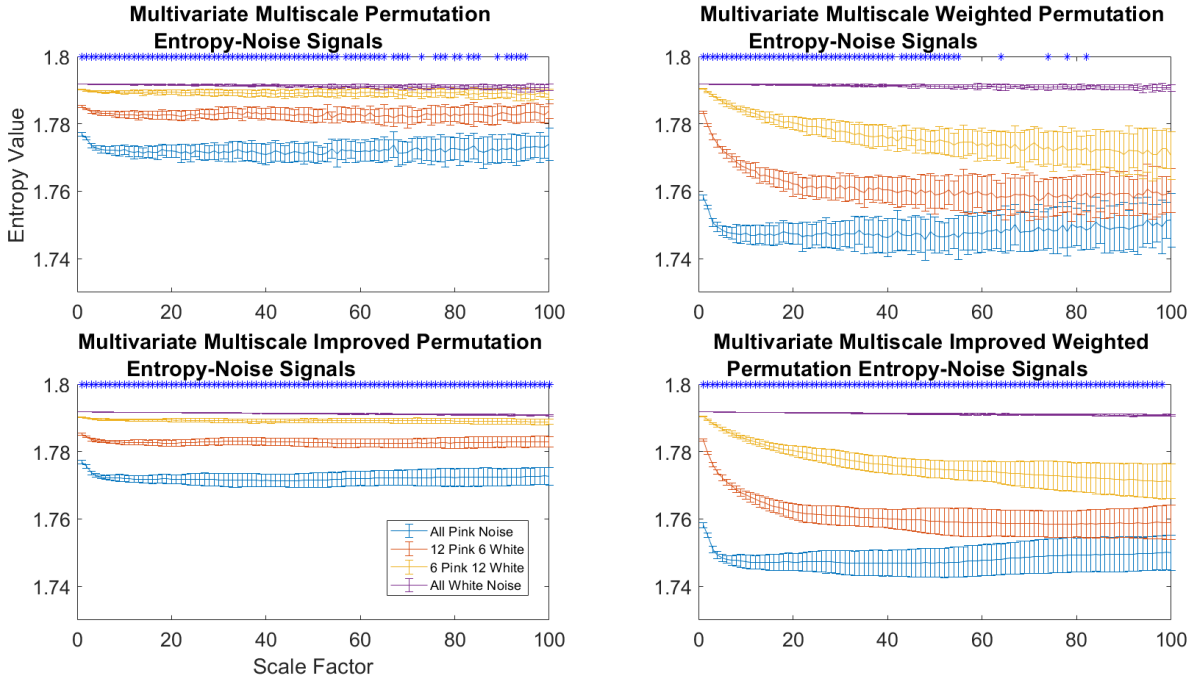

FIGURE 2.1 – Results of the four entropy algorithms on the four different mixtures of white and pink noise signals ($d = 3$ and $l = 1$). For each algorithm, scales where significant differences (based on Friedman test with Bonferroni correction $p < 0.01$) appeared between the results of the four noise mixtures are marked with '*'.

2. 12 white noise signals and 6 pink noise signals
3. 6 white noise signals and 12 pink noise signals
4. 18 pink noise signals

Each group has 30 different realizations. Each of the four algorithms of permutation entropy (mvMPE, mvIMPE, mvMWPE, mvIWMPE) is applied on each of them. The time scales ranges between 1 and 100. To test our method, we use $l = 1$ following Bandt's and Pompe's work [11]. In order to respect the condition of $(d+1)! \leq \lfloor \frac{N}{\tau_{max}} \rfloor$, where $N = 10000$ and $\tau_{max} = 100$, the highest embedding dimension value is $d = 3$. The means and standard deviations of the resulting entropy values are calculated for each group and are presented in Fig. 2.1.

To evaluate the methods, Friedman tests are applied on pairs of results of different signal mixtures for each method. Those that show p-values less than 0.01 with Bonferroni correction are considered to be significantly different. Fig. 2.1 marks by '*', for each method, the scales where the differences are significant between the entropy values of all pairs of the 4 mixtures of signals. mvIMPE shows that all 100 scales have significant differences. mvIWMPE shows similar results with 98 scales having significant differences (only scales 99 and 100 showed no significant differences). Those two methods, in comparison with mvMPE and mvMWPE that show lower number of scales with significant differences, show better performances. Those results show that mvIWMPE outperforms mvMPE and mvMWPE and has similar performance to mvIMPE when applied on noise signals.

Influence of Number of Channels on mvIWMPE

In this test, the effect of increasing the number of channels or variates of the signals is studied. Nine groups of multivariate WGN with 1000 samples are studied. The number of channels ranges between 2 and 10 channels. Each group has 30 realizations. mvIWMPE is applied on those groups with $d = 3$ and $l = 1$. Fig. 2.2 shows that, as the number of channels increases, the values of entropy change become less decreasing and more constant for WGN across scales. This is due to the fact that the increase of number of channels creates more sample vectors to be sorted and distributed across motifs, thus behaving in a manner similar to finding the multiscale entropy of a univariate signal of the concatenated signals of the channels.

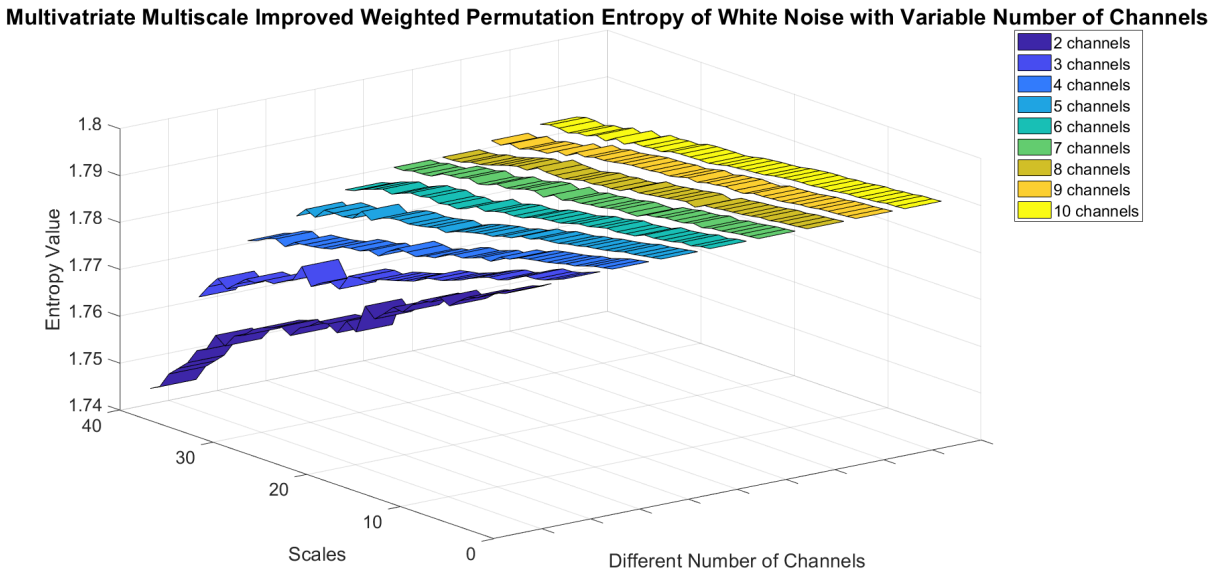

FIGURE 2.2 – Results of mvIWMPE on WGN multivariate signals with different number of channels ranging from 2 to 10 ($d = 3$ and $l = 1$).

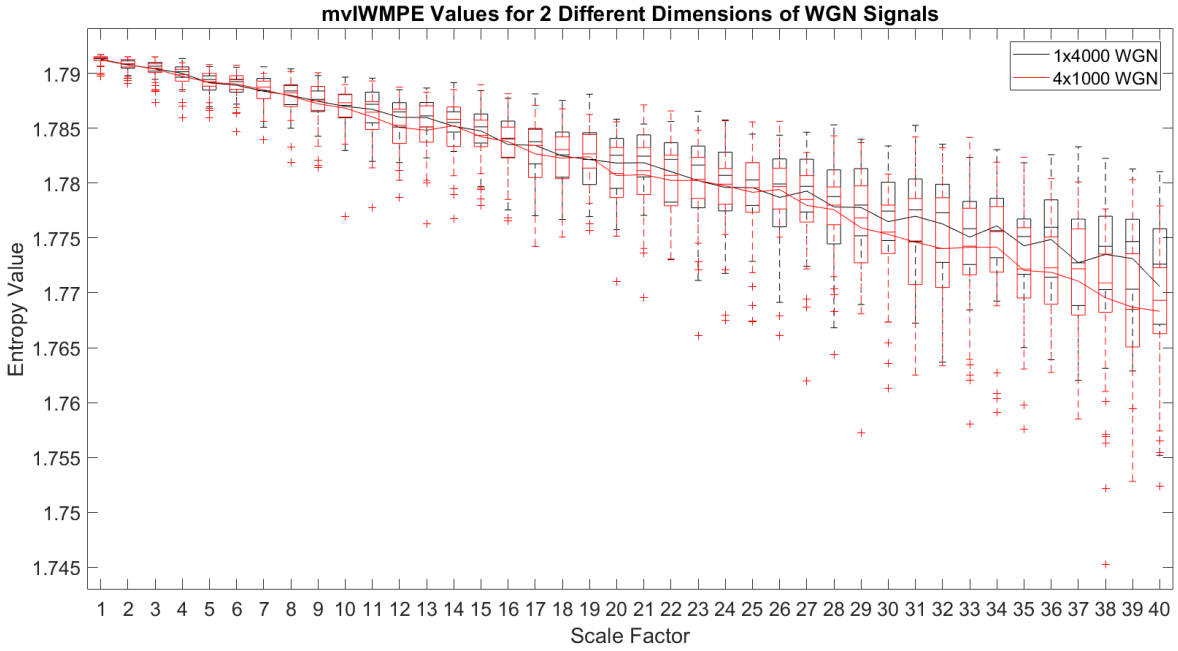

FIGURE 2.3 – Results of mvIWMPE on 1×4000 and 4×1000 WGN signals ($d = 3$ and $l = 1$).

This is supported by the results of Fig. 2.3. mvIWMPE with $d = 3$ and $l = 1$ is applied on 2 groups of WGN, one having a dimension of 1×4000 and the other 4×1000. This way

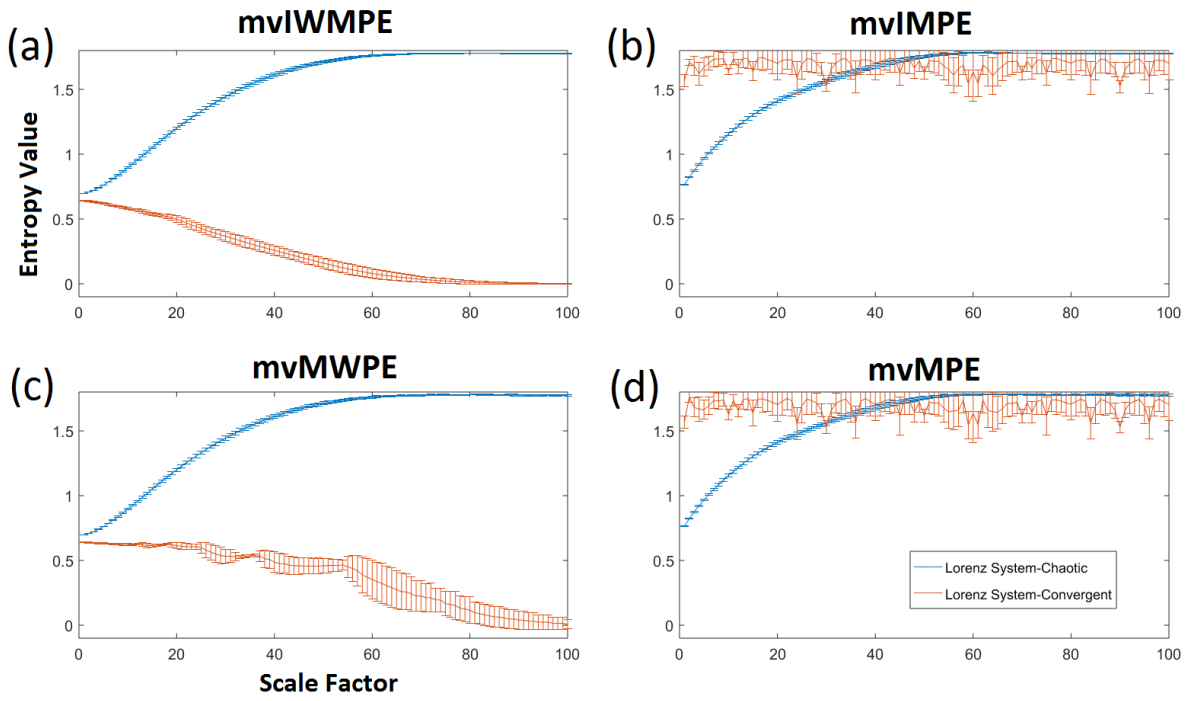

FIGURE 2.4 – Results of (a) mvIWMPE, (b) mvIMPE, (c) mvMWPE, and (d) mvMPE ($d = 3$ and $l = 1$) on the chaotic and convergent signals generated by the Lorenz system.

both groups had the same number of samples (4000). Each group has 30 realizations. The results show that the two groups have similar values of entropy across scales thus signifying that the two groups are being considered as almost the same signal as if the 4 channels are being concatenated to form a univariate signal.

Lorenz System

The Lorenz system [81] is a system of three differential equations that could result in either chaotic or convergent signals based on the parameters. Its equations are

$$\begin{cases} \dfrac{dx}{dt} = \sigma(y - x) \\ \dfrac{dy}{dt} = x(\rho - z) - y \\ \dfrac{dz}{dt} = xy - \beta z \end{cases} . \tag{2.3}$$

In our study we fixed the values of $\sigma = 10$ and $\beta = \dfrac{8}{3}$ and used different values

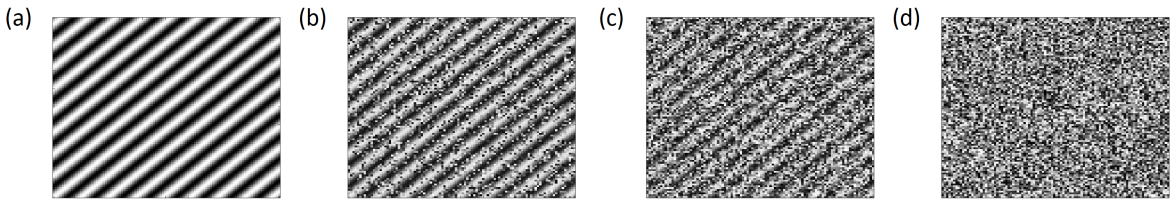

FIGURE 2.5 – The generated MIX process : bidimensional (100×100) signals with different values of p (a) $p = 0$; (b) $p = 0.3$; (c) $p = 0.6$; (d) $p = 1$

of ρ to get different tri-variate chaotic and converging signals. Twenty different values for $0 \leq \rho \leq 1$ result in twenty different converging tri-variate signals. Twenty different values for $23 \leq \rho \leq 33$ result in twenty different chaotic tri-variate signals [102]. The initial point is (0,5,10). All the signals are made up of 10000 time points.

The four permutation entropy algorithms are applied on these signals. The same parameters are used ($d = 3$ and $l = 1$). The results in Fig. 2.4 show that both mvMPE and mvIMPE are not able to differentiate between convergent and chaotic signals. However, the two weighted algorithms show high ability to differentiate between the two types of signals. But when comparing mvMWPE with mvIWMPE, it is noticed that mvIWMPE has lower standard deviation value that reaches 0 for time scales greater than 60, not to mention the smoother curve of the mvIWMPE on converging signals. These results, in addition to the previous ones of noise signals (section 2.2.1), show that mvIWMPE outperforms other methods in differentiating between convergent and chaotic signals with smoother curves across scales. mvIWMPE has also similar good performance to mvIMPE in terms of differentiating between different noise signals.

MIX Process

The last synthetic test that is applied to evaluate the algorithms is MIX process signals. This is based on the test introduced by Pincus *et al* [96]. In order to test the multivariate algorithm, this test is slightly modified to become two dimensional.

The MIX process is used to generate different levels of stochastic signals that range from being purely deterministic to purely stochastic. To generate such signals, set p as a probability with value between 0 and 1. Define $X_{m,n} = \alpha^{-1/2} \sin(\frac{2\pi}{12}(m+n))$,

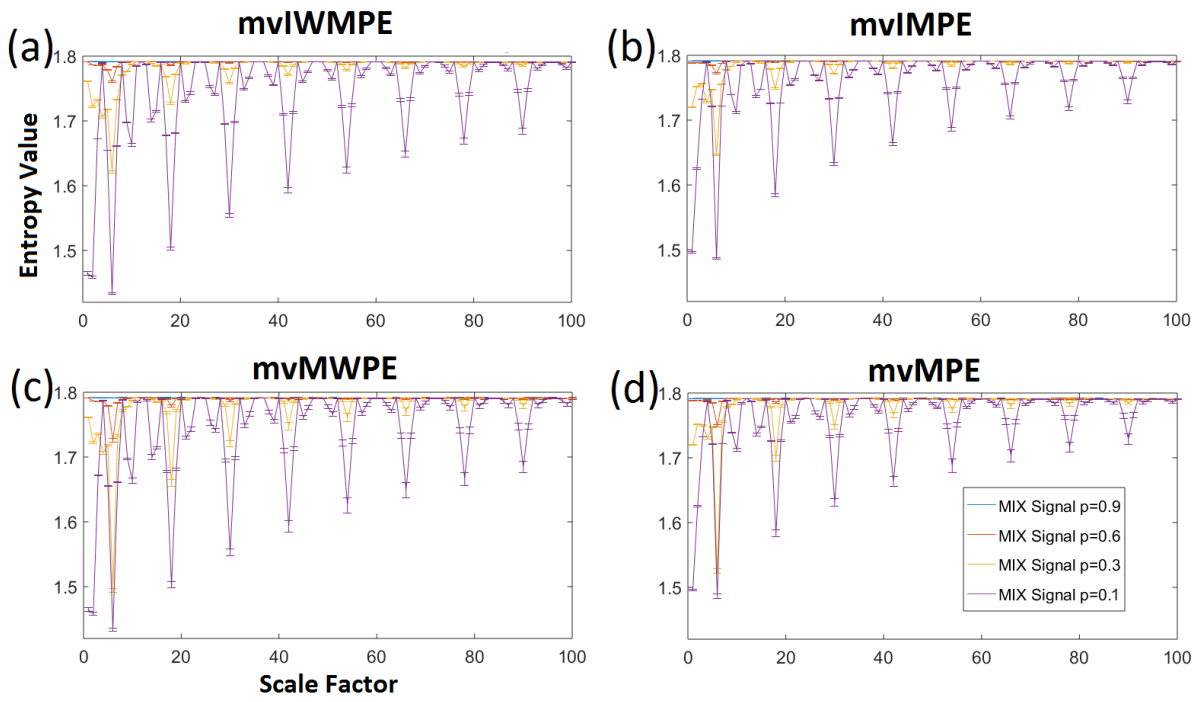

FIGURE 2.6 – Results of (a) mvIWMPE, (b) mvIMPE, (c) mvMWP, and (d) mvMPE ($d = 3$ and $l = 1$) on the different MIX process signals generated by 4 different values of p.

for $1 \leq m \leq M$ and $1 \leq n \leq N$ with α being the amplitude and defined as

$$\alpha = \frac{\sum_{i=1}^{12} \sum_{j=1}^{12} \sin^2(\frac{2\pi}{12}(i+j))}{144}. \tag{2.4}$$

Define $\mathbf{Y}$ as an $M \times N$ matrix of independent identically distributed real random variables having a uniform distribution in the interval $[-\sqrt{3}, \sqrt{3}]$. Define $\mathbf{Z}$ as another $M \times N$ matrix of independent identically distributed real random variables where $Z_{m,n} = 1$ with probability p defined earlier and $Z_{m,n} = 0$ with probability $1 - p$.

Then

$$MIX_{m,n}(p) = (1 - Z_{m,n})X_{m,n} + Z_{m,n}Y_{m,n}. \tag{2.5}$$

So $\mathbf{MIX}(p)$ would be an $M \times N$ matrix that has pMN of its elements corresponding to a random bi-dimensional signal and $(1-p)MN$ elements corresponding to a periodic bi-dimensional signal. Examples of the MIX signals are shown in Fig. 2.5.

To test our algorithm, four values of p are used, $p = 0.1$, $p = 0.3$, $p = 0.6$, and $p = 0.9$. For each value, 30 different 18×10000 signals are generated. Each of the four algorithms of permutation entropy is applied on these signals. The embedding dimension and the lag are unified for all the algorithms as $d = 3$ and $l = 1$. The time scales ranged between 1 and 100. The means and standard deviations of the resulting entropy values are calculated for each group and represented as in Fig. 2.6. The results show that, again, mvIWMPE has the highest differentiation among signals especially for the first ten scales where mvMWPE and mvMPE give very similar results for $p = 0.1$ and $p = 0.3$. It also shows the highest robustness in terms of variance of entropy results for a given type of signal, which can be confirmed by the smaller error bars.

2.2.2 Evaluation on Real EEG Signals

Our new algorithm is also tested on real EEG signals. Two different datasets are processed as mentioned below.

Dataset 1 : Heathy Children

Twenty minutes EEG recording from 6 healthy children at rest (four females and two males, age : 8.8± 2.11 years) were acquired in the Department of Neuropediatrics, Christian-Albrechts-University, Kiel, Germany. These recordings were approved

by the Medical Ethics Committee of the Christian-Albrechts-University, Kiel, Germany, agreement code “D 460/15”.

Subjects were lied down comfortably and rest brain activity was recorded both during eyes open where the subject looked at a fixed picture and eyes closed. The EEG activity was recorded by 128 electrodes (Electrical Geodesics, Inc.) with the Cz electrode as a reference. The sampling rate of all the acquisitions was 1000 Hz. Eyes movements were recorded by two frontal electrodes of the EEG net (E1 and E32) in order to detect drowsiness, and epochs with slow horizontal eyes oscillations were removed from the analysis.

Dataset 2 : Epileptic Patients

The EEG data of 3 epileptic patients recorded in Université Libre de Bruxelles, Hôpital Erasme (agreement of local ethical committee P2015/242) were analyzed. Patient 1 (BE001 from Table 2.2) was diagnosed with epilepsy with CSWS. The epileptic focus was clinically localized on T5 (10-20 system). Patient 2 (BE003 from Table 2.2) was diagnosed with atypical benign childhood epilepsy with centrotemporal spikes (BECTS) with the focus being on C3 (10-20 system). Patient 3 (BE004 from Table 2.2) was diagnosed with BECTS with the focus being on C3 (10-20 system).

All patients had their resting-state EEG recorded while they were lying down for around 20 minutes and alternating between eyes open and eyes closed every minute. The acquisition was done using high density EEG (HD-EEG) with 256 electrodes (Electrical Geodesics, Inc.). The reference was the Cz electrode and the sampling frequency was 1000 Hz.

Preprocessing

We filtered the acquired signals by a bandpass FIR filter of a transition bandwidth of 0.22 Hz obtained by an order of 15000. The cut-off frequencies of the filter are 0.5 Hz and 45 Hz. We also applied independent component analysis (ICA) [62] on each subject individually to remove artifacts caused by blinking or movement.

For dataset 1, we extracted 30 epochs of 10 seconds for each case (eyes open and eyes closed) from each subject. Some of these epochs in some subjects were overlapping (maximum of five seconds overlap).

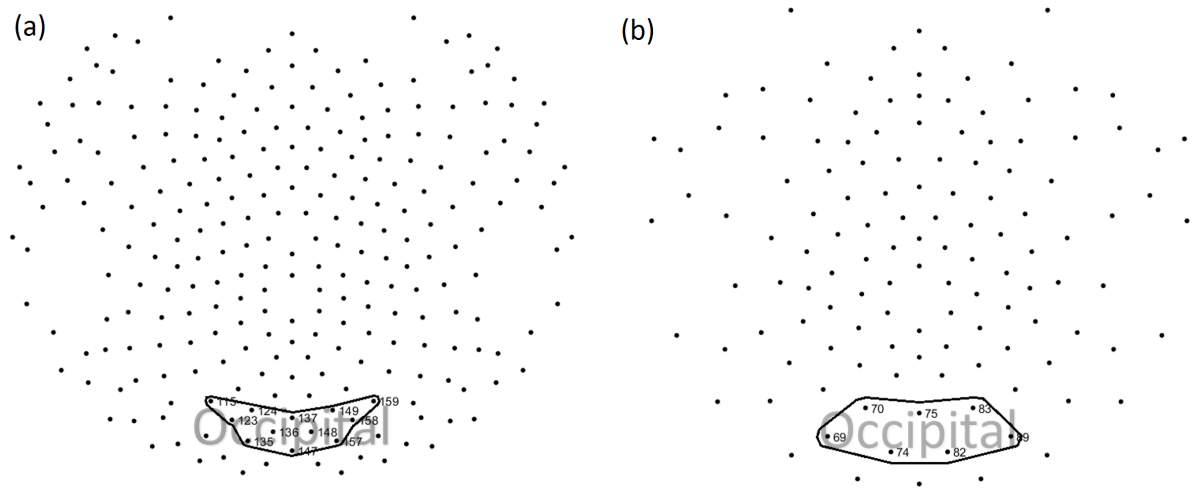

FIGURE 2.7 – The occipital region of interest on the (a) 256-channels EEG net and on the (b) 128-channels EEG net.

For dataset 2, we extracted 40 non-overlapping epochs of 1 second for each case (eyes open and eyes closed) from each subject. The reason for choosing only one second epochs is the appearance of spikes, or interictal epileptiform discharges (IED) and we are interested in epochs without those spikes. For this, the datasets were examined by Prof. Patrick Van Bogaert in order to select epochs with no spikes.

Previous studies showed that the main difference between eyes open and eyes closed in terms of EEG is the presence of the alpha rhythm in the occipital region during the eyes closed case [45]. For this reason, the analysis was performed for that region only. We defined the set of electrodes for each EEG net that covered the occipital region with the help of a neurophysiologist. Figure 2.7 shows the occipital region for each net used.

All of the preprocessing was done using the EEGLAB [41] toolbox for Matlab R2016b.

Results of EEG Signals Evaluation

The goal of this evaluation was to see whether mvIWMPE maintains higher ability of differentiation between two states when applied to real EEG signals, which in our case are eyes open and eyes closed. The four multivariate algorithms of permutation entropy were then applied on the epoched signals of each subject in each dataset, with

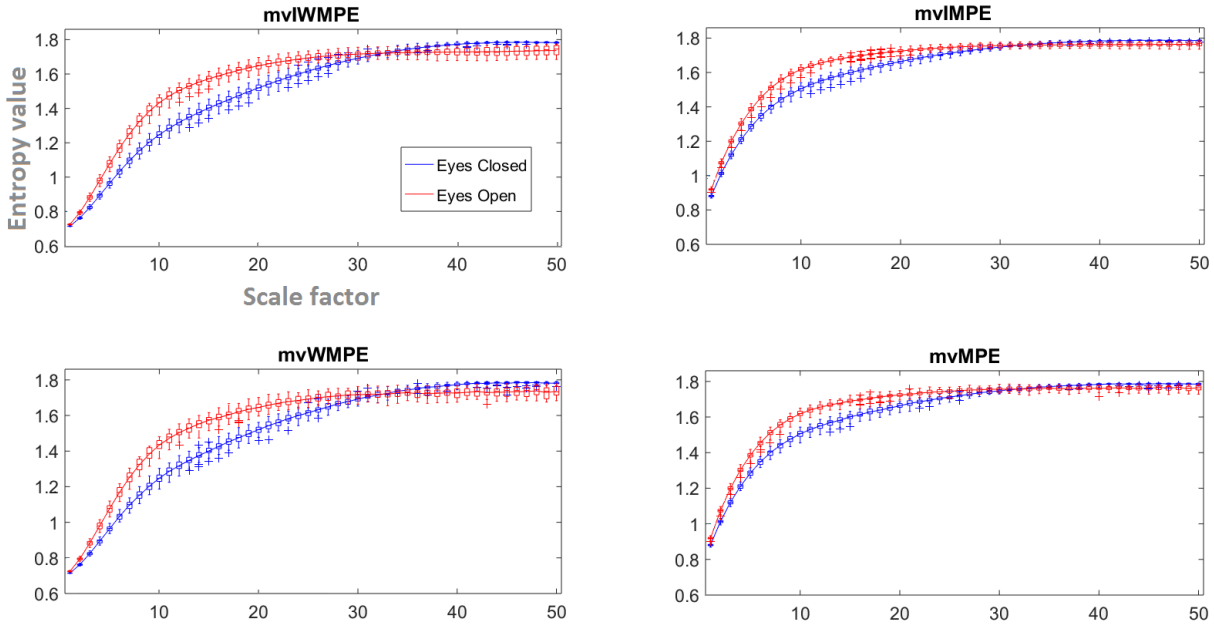

FIGURE 2.8 – Resulting curves of the application the 4 permutation entropy methods (mvMPE, mvIMPE, mvMWPE, and mvIWMPE) on one of the subjects of Dataset 1. The methods were applied on 30 epochs of eyes open (red curve) and 30 epochs of eyes closed (blue curve).

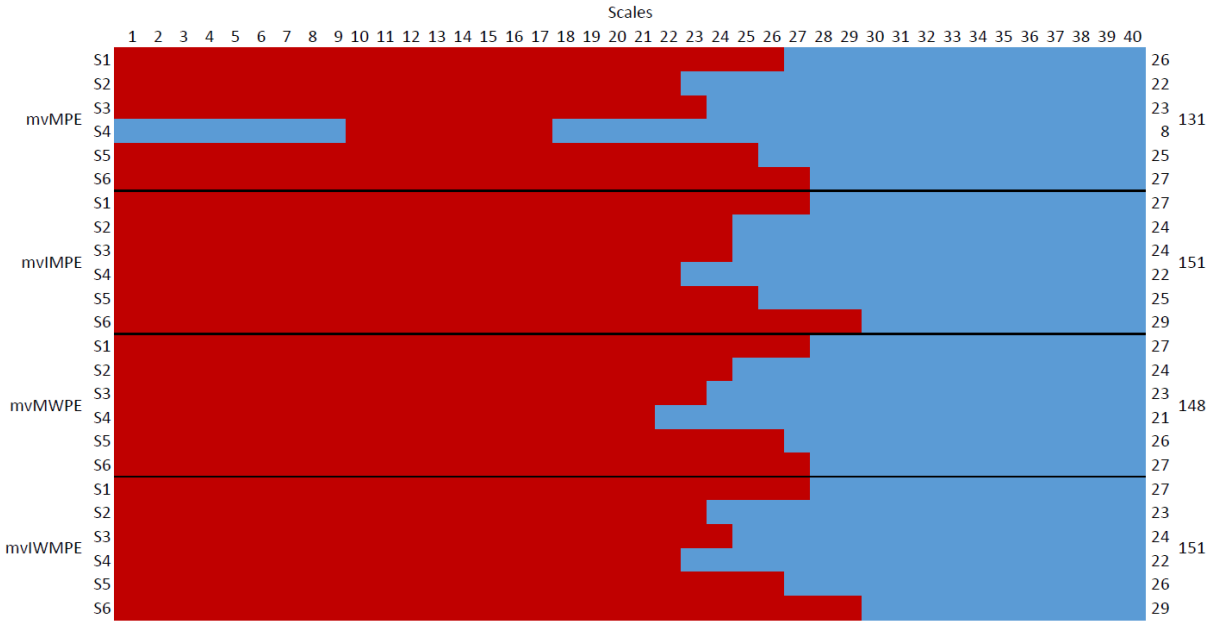

FIGURE 2.9 – Results of Friedman tests with Bonferroni correction on the results of the 4 permutation entropy methods (mvMPE, mvIMPE, mvMWPE, and mvIWMPE) on Dataset 1. Scales that had corrected p-values less than 0.01 were considered to have eyes open entropy value to be significantly higher than that of eyes closed and labeled in red while others are labeled in blue. The total number of scales with significant differences for each subject and for each method is given at the end of each row.

$d = 3$ and $l = 1$ in a time scale ranging from 1 to 40.

In general, all the curves had a common form which is similar to that of the chaotic signals of the Lorenz system (a decaying increase of entropy value with respect to time scale) (example in figure 2.8). However it is worth mentioning that each subject behaved differently in a certain normal range and resulted in different curves that differentiated eyes open from eyes closed entropy values. Thus, averaging the results across subjects would diminish this differentiation for such relatively small number of subjects. For this reason, each subject was studied separately.

The results for all subjects showed that entropy values were lower in the case of eyes closed, for scales less than 30. This was expected since, as mentioned in section 2.2.2, the eyes closed state is characterized by the alpha waves that makes the recorded EEG signals more periodic and thus less complex. The reason behind having 30 as the maximum scale where the entropy of eyes closed signal was less than the entropy of eyes open signals is that the coarse-graining window becomes larger than

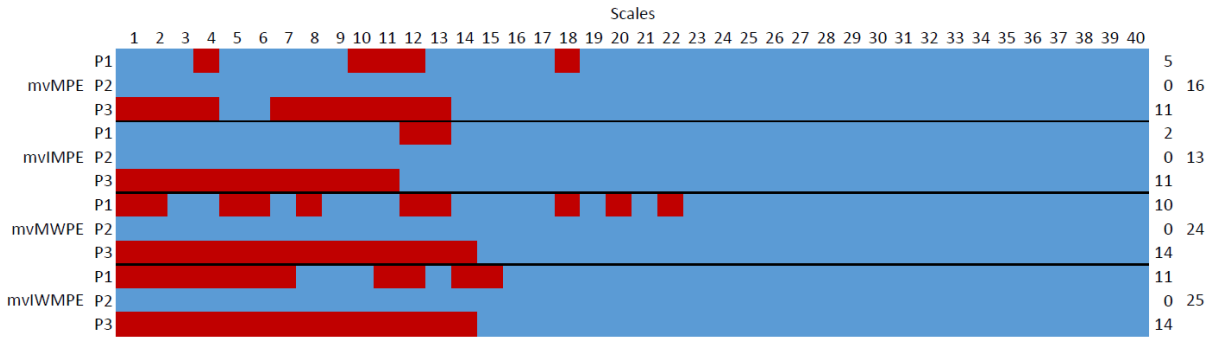

FIGURE 2.10 – Results of Friedman tests with Bonferroni correction on the results of the 4 permutation entropy methods (mvMPE, mvIMPE, mvMWPE, and mvIWMPE) on Dataset 2. Scales that had corrected p-values less than 0.01 were considered to have eyes open entropy value to be significantly higher than that of eyes closed and labeled in red while others are labeled in blue. The total number of scales with significant differences for each patient and for each method is given at the end of each row.

the alpha oscillation at this scale.

For all subjects in both datasets, Friedman tests were applied on the results of the eyes open and eyes closed condition to evaluate whether we have significant differences between the two results. Scales with Bonferroni corrected p-values less than 0.01 were considered to be significantly different. Only significant differences of scales less than 30 were considered. Figures 2.9 and 2.10 summarize the results of the Friedman tests for both datasets. Scales labeled in red had the entropy values of eyes open significantly higher than those of eyes closed. The total number of scales in red is given for each subject or patient and for each method in each dataset. For dataset 1, both mvIMPE and mvIWMPE had the highest number of scales in red (151) showing that both have good ability in differentiating between signals of eyes open and eyes closed states. For dataset 2, mvIWMPE had the highest number of scales in red (25) showing the best ability in differentiating between the two cases of EEG signals.

It is worth mentioning that dataset 1 had epochs of 10 seconds while dataset 2 had epochs of 1 second. This is the reason why the results of dataset 1 have much higher number of scales in red as for longer signals each method gave more precise results due to the increase in the number of embedding vectors to be grouped into motifs. This also highlights the fact that, for shorter signals, mvIWMPE shows better performance than the other permutation entropy methods as shown in Fig. 2.10.

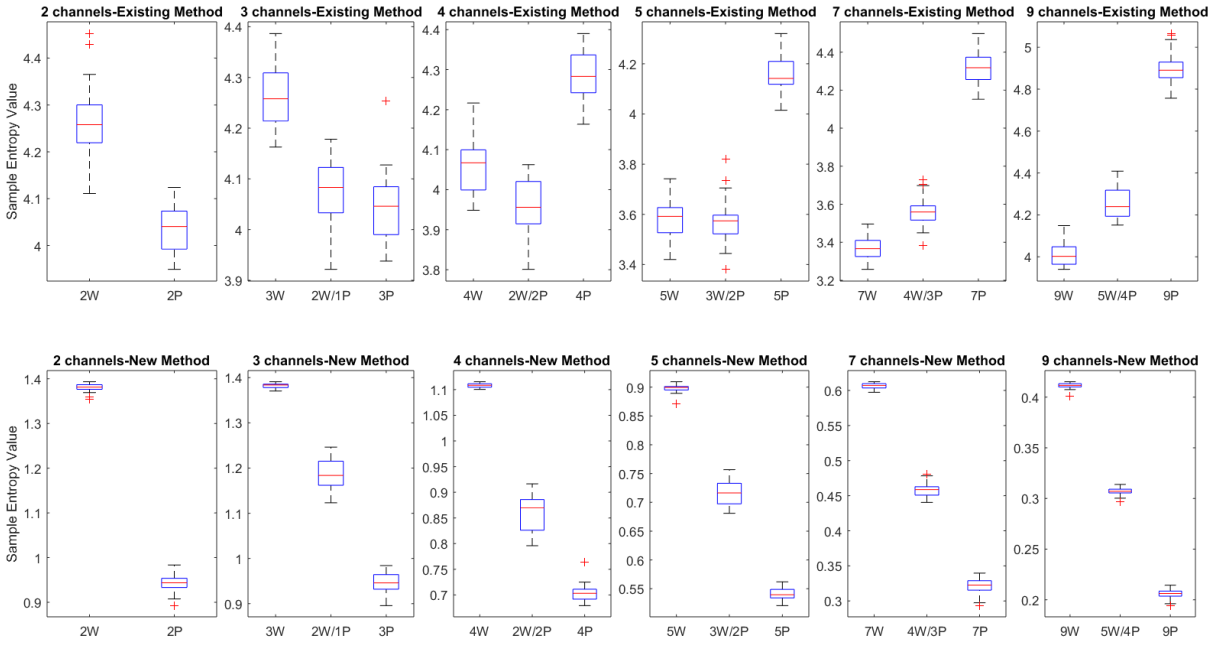

FIGURE 2.11 – Results of multivariate sample entropy for the existing multivariate sample entropy and the new one we proposed applied on white Gaussian (noted as W) and pink noise (noted as P), and a mixture of them (noted as xW/yP where x is the number of white Gaussian noise channels and y is the number of pink noise channels). Each signal had 5000 samples and 30 realizations. For both methods, the threshold was $r = 0.15\times$standard deviation of the normalized signal and $m = 2$ for all the channels.

2.2.3 Conclusion

We proposed a multiscale permutation entropy-based method to compute irregularity of multivariate complex signals. This method, called mvIWMPE, has the advantages of being robust and able to discriminate between different states in a single signal. The efficiency of mvIWMPE and its performances compared to mvMWPE, mvIMPE, and mvMPE was proven in synthetic and human EEG signals.

2.3 Sample Entropy of Multi-channel Signals

It was noticed that the multivariate sample entropy method explained in chapter 1 shows erroneous results when the number of channels increases (see Figs. 2.11 and 2.12). To address this issue, we propose a new way to calculate sample entropy for

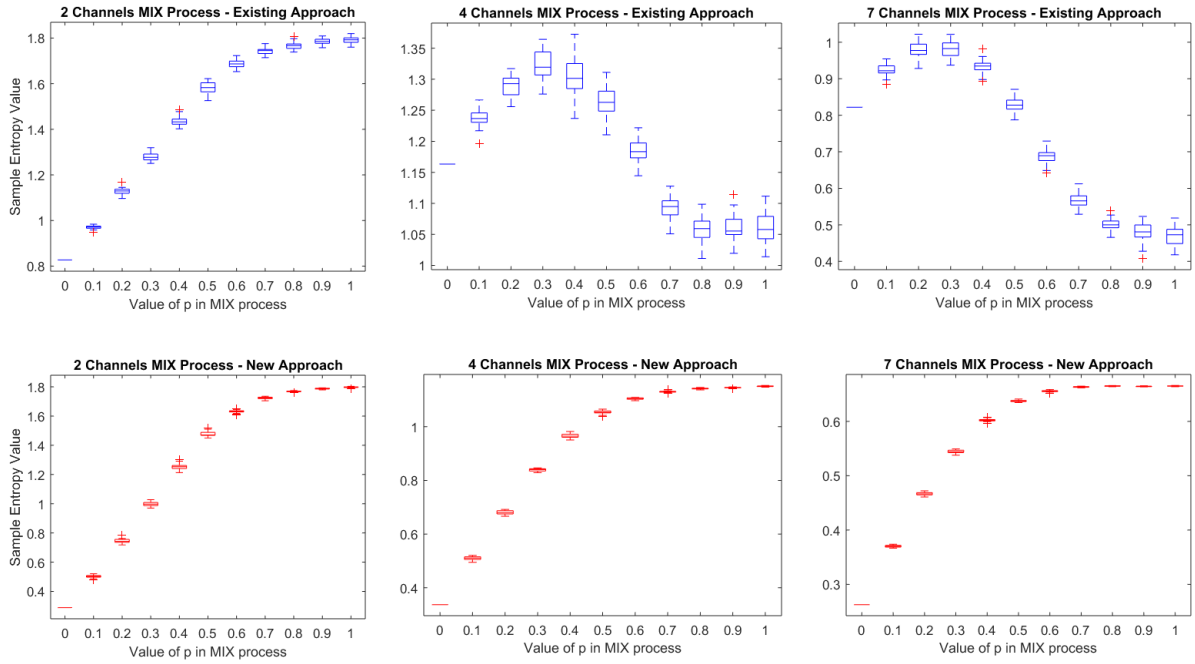

FIGURE 2.12 – Results of the existing multivariate sample entropy and the new one we proposed applied on MIX signals with varying number of channels. The value of p ranges between 0 and 1 with a step 0.1. Each signal has a length of 5000 samples and 30 realizations. For both methods, the threshold is $r = 0.15\times$standard deviation of the normalized signal and $m = 2$ for all the channels.

multivariate time series, as described below.

Let $\{x_1^k, \ldots, x_i^k, \ldots, x_N^k\}$ be a multivariate time series of length N with $1 \leq k \leq K$ being the index of the variate and let $\mathbf{M} = [m_1, m_2, \ldots, m_K]$ be the multivariate embedding dimension vector. To calculate the sample entropy for this multivariate signal :

1. For each variate k, generate the DV subspace : $\mathbf{X}_{m_k}^k(i) = [x_i^k, x_{i+1}^k, \ldots, x_{i+(m_k-1)}^k]$, where $i = 1, 2, \ldots, N-(m_k-1)$ and m_k is the corresponding embedding dimension for the variate k.

2. For each variate k, calculate the distances between all the possible vector pairs. Any type of distance between vectors could be used. Here we use the Chebyshev distance as it is commonly used in previous papers dealing with sample entropy [4][5][99]. Since there are $N-(m_k-1)$ vectors, this means there are $\alpha = \dfrac{(N-(m_k-1))(N-m_k)}{2}$ possible distances without including self-distances.

3. Count the number of instances $A_{m_k}^k(r)$ where the distances are less than a predefined threshold r.

4. Define the frequency of occurrence as $B_{m_k}^k(r) = \dfrac{A_{m_k}^k(r)}{\alpha}$.

5. Extend the dimension from m_k to m_k+1 and repeat steps 1 to 4. The new number of possible distances between pairs is $\beta = \dfrac{(N-m_k)(N-m_k-1)}{2}$. So the frequency of occurrence for the extended case will be : $B_{m_k+1}^k(r) = \dfrac{A_{m_k+1}^k(r)}{\beta}$, where $A_{m_k+1}^k(r)$ is the number of instances where the extended DV pairs had distances less than r.

6. Repeat all the above steps for all the variates of the time series $1 \leq k \leq K$.

7. The sample entropy of the multivariate time series is :

$$mvSampEn_{new} = -\ln \frac{\sum_{k=1}^{K} B_{m_k+1}^k(r)}{\sum_{k=1}^{K} B_{m_k}^k(r)}. \tag{2.6}$$

The channel-wise computation of distances and frequencies of occurrence, followed by a global integration, makes this approach much more robust, as it will be confirmed immediately.

2.3.1 Validation on Synthetic Data

To study the effect of increasing the number of channels on the existing multivariate sample entropy and the one we proposed, we apply both algorithms on synthetic data with varying number of channels and study the behavior of the results.

White and Pink Noise

For this test, 3 types of multivariate noise signals are used :

1. Pure white Gaussian noise (WGN).
2. Pure pink noise (power spectrum proportional to $1/f$).
3. A mixture of WGN and pink noise.

These signals have a length of $N = 5000$ samples and each type has 30 realizations. The existing method and the new one were applied on these signals while the number of channels increased gradually from 2 to 9. For both methods, the threshold was $r = 0.15\times$standard deviation of the normalized signal and $M = [m_k] = 2$ for $1 \leq k \leq K$.

Figure 2.11 shows that, for the existing method, the entropy value of the pure WGN signals is higher than that of the pure pink noise for signals with 2 and 3 channels. This is the normal case, since white noise is more irregular than pink noise [35]. But as the number of channels is higher than 3, the sample entropy value of white noise drops below that of the pink noise and the difference between white and pink noise becomes larger. For the new proposed method the sample entropy value of WGN remains larger than that of pink noise regardless of the number of channels of the noise signals. Also, the value of sample entropy for the mixtures of the two noises is always between those of pure WGN and pink noise. This proves that the new proposed method gives more consistent relative results and is not dependent on the number of channels as the existing method is.

MIX process

In this test we evaluate the results of both methods as the multivariate signals gradually change from periodic to uniform random signals with respect to number of channels.

MIX process signals [96] are signals that range from periodic to completely random as the value of the parameter p ranges from 0 to 1. The two methods were applied on

multivariate MIX processes with $0 \leq p \leq 1$ for various number of channels. The length of the signals was $N = 5000$ samples and we used 30 realizations. For both methods the threshold was $r = 0.15\times$standard deviation of the normalized signal and $m = 2$ for all the channels.

Figure 2.12 shows the results of the two methods on multivariate MIX process signals with 2, 4, and 7 channels. It is expected that sample entropy value is minimum for $p = 0$ as the signals are purely periodical. This value should increase as the value of p increases and the signal becomes more random. This is the case for both methods when the number of channels is 2. But, as the number of channels increases, the results of the existing method shows an increase in sample entropy value for $0 \leq p \leq 0.3$. Then, the value starts decreasing for $0.3 \leq p \leq 1$ and even drops below the value of $p = 0$. By opposition, for the proposed, method the value of sample entropy, as expected, increases as the value of p increases. This, once again, shows that the proposed method is more consistent and is not dependent on the number of channels. It could therefore be applied for a higher number of channels without risking getting erroneous values.

2.3.2 Results on EEG Data

Epilepsy, as described in chapter 1, is a very commonly studied pathology using EEG. It is a neurological disorder characterized by the recurrence of epileptic seizures. Besides, most epileptic patients present, in the interictal state, or the state when no seizures occur, interictal epileptiform discharges (IED).

Cognitive deficits are common in childhood epilepsy and have multifactorial origins : underlying etiology, anti-epileptic drugs, seizures and IED. In some epilepsy syndromes like BECTS and CSWS, the cognitive deficits are believed to be strongly related to the frequency of spikes [119]. Some anti-epilepticdrugs (AED) may lower the frequency of the spikes. For patients with BECTS, a decrease in the number of spikes was reported when the patients were treated with sulthiame [13]. The same effect takes place on patients diagnosed with CSWS when they are treated with levetiracetam [3].

In this application we will focus on the resting state, without IED, of EEG recordings of patients with the aforementioned syndromes. We hypothesize that the treatment will impact the complexity of the EEG signal. We will evaluate the sample entropy of the recorded EEG before and after treatment to see if it would imply an increase in

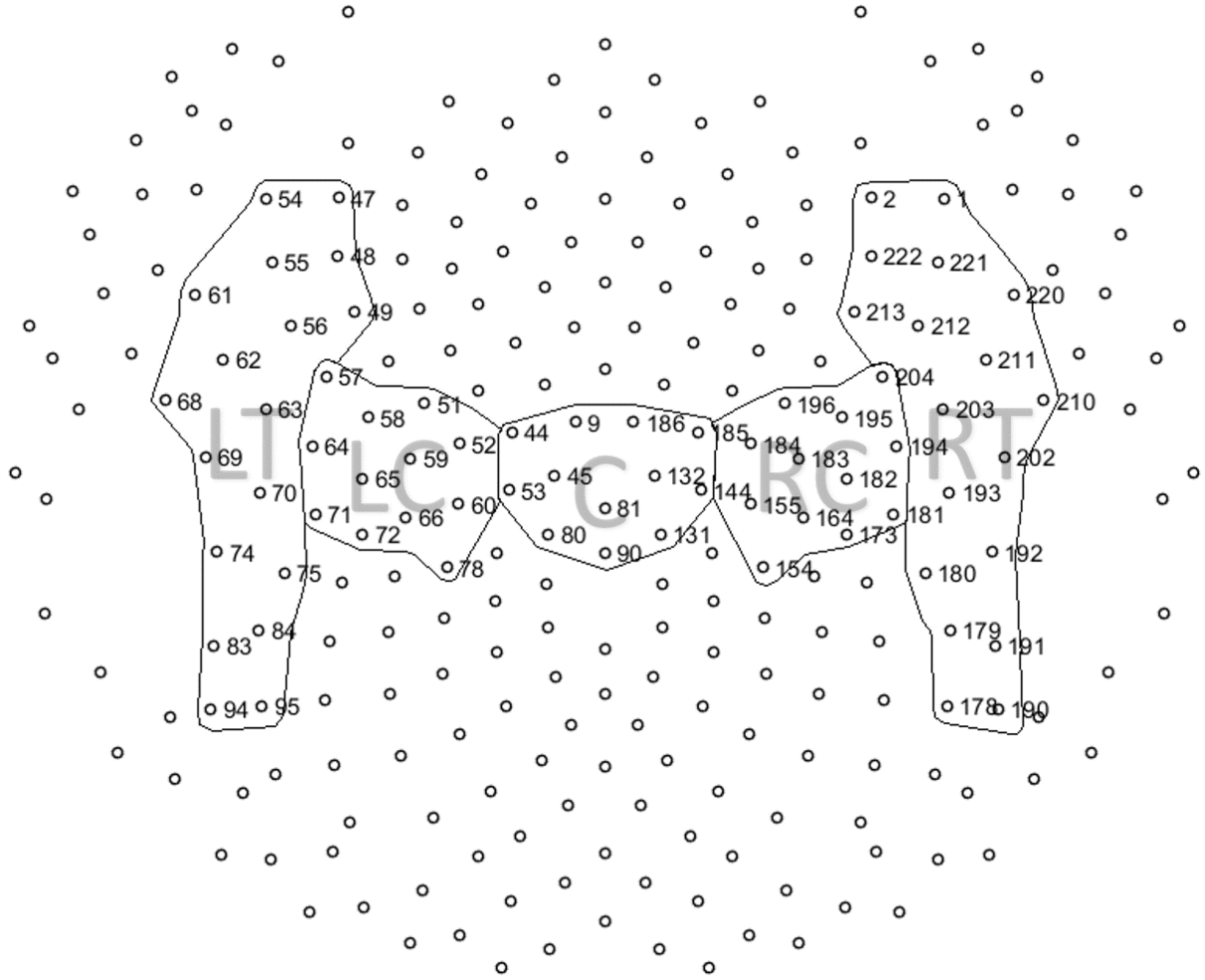

FIGURE 2.13 – The five regions where the entropy was calculated. LT : Left Temporal. LC : Left Central. C : Central. RC : Right Central. RT : Right Temporal.

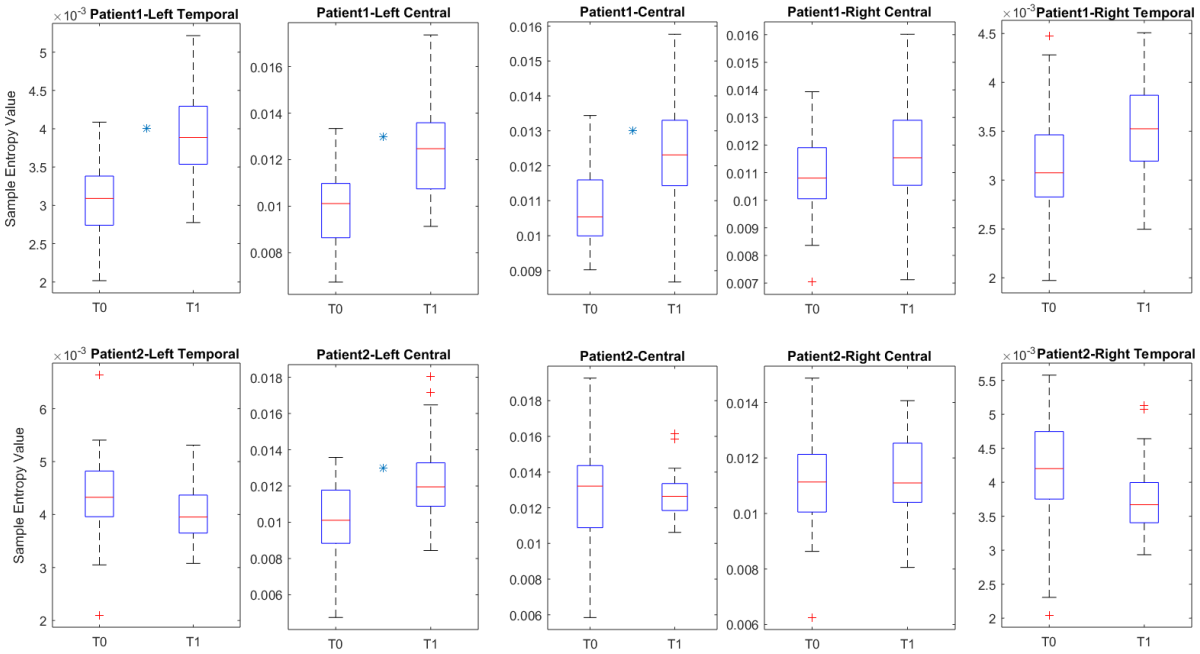

FIGURE 2.14 – Results obtained with the proposed sample entropy method on 40 epochs of the two sessions (T0 being the baseline and T1 being 4 to 6 weeks after T0 while a certain AED was successfully administered in this period) for two subjects. The method was applied on the 5 regions (LT, LC, C, RC, and RT). Epochs are 1 second long (1000 Hz). The threshold was $r = 0.15\times$standard deviation of the normalized signal and $m = 2$ for all the channels. Regions with statistically significant differences between T0 and T1 are marked with '*'. Friedman test was applied with significance threshold p-value$= 0.02$ with Bonferroni correction.

irregularity after treatment : it is known that signals from healthy subjects present higher irregularity than those of pathological subjects [20][130].

Recordings

The EEG data of 2 epileptic patients (BE003 and BE004 detailed in table 2.2) recorded in Université Libre de Bruxelles, Hôpital Erasme (agreement of local ethical committee P2015/242) were analyzed. Patient 1 (8 years old female) was diagnosed with atypical BECTS. The epileptic focus was clinically localized on C3 (10-20 system). Patient 2 (9 years old male) was diagnosed with BECTS with the focus being on C3 (10-20 system).

For each patient, two sessions of recordings were made, T0 being the baseline and T1 being 4 to 6 weeks after T0 while a certain AED was successfully administered in this period. Patient 1 was treated with valproate and lamotrigine, while Patient 2 was treated with levetiracetam.

Both patients had their resting state EEG recorded while they were lying down for around 20 minutes. The acquisition was done using high density EEG (HD-EEG) with 256 electrodes (Electrical Geodesics, Inc.). The reference was the Cz electrode and the sampling frequency was 1000 Hz.

Preprocessing and Application

We processed all the recordings in the same way. A high order band-pass filter between 0.5 Hz and 45 Hz with a transition bandwidth of 0.22 Hz was applied. Then, we applied independent component analysis (ICA) [62] in order to isolate artifact-related components and discard them before reconstructing the artifact-free signals. Finally, the signals were visually examined by a trained neurophysiologist to identify the spikes (as described earlier), and 40 spike-free epochs with eyes open (1 second long) were extracted from each session recording.

Five regions of interest were taken from the 256 electrodes (Central (C), Left Central (LC), Right Central (RC), Left Temporal (LT), and Right Temporal (RT)). Figure 2.13 shows the position of those regions with respect to the whole net. We are interested in those regions because this is where we expect the irregularity change to take place since the foci, as mentioned in Sec. 2.3.2, are central and temporal (since it is the nature of the syndromes). The new proposed sample entropy method was

applied on the epoched multivariate signals of those five regions. The threshold was $r = 0.15\times$standard deviation of the normalized signal and $m = 2$ for all the channels.

Results and Discussion

For both patients, the sample entropy results are presented in Fig. 2.14. To objectively define the significance of the entropy changes, a Friedman test was applied on the results. The regions with p-values < 0.02, with Bonferroni correction for multiple comparisons, are considered to have significant differences between T0 and T1, and are marked with '*'.

For Patient 1, C, LC, and LT regions show a significant increase in sample entropy value. This suggests that the patient is responding with the medication and is approaching the healthy case [20][130]. Besides, the regions that showed the significant increase are in correspondence with the clinical localization of the focus (T5). Patient 2 shows significant increase for only the LC region. This could have the same explanation as for Patient 1. The region of significance is also in correspondence with the clinical localization of the focus (C3). These results confirm the findings done in a previous study [31] as the irregularity of the EEG signals increased after almost one month of treatment.

2.3.3 Conclusion

Sample entropy has been commonly used in several fields, especially medical. In this paper, we reviewed the sample entropy approach and its existing multivariate extension and proposed a new approach for sample entropy of multivariate signals. Existing and proposed methods were applied on synthetic data. Results showed that the proposed method overcomes the drawback of the existing method that fails to handle relatively large numbers of channels. Moreover, our method was applied to real EEG data showing its reliability.

	$y_1(t)$	$y_2(t)$	Ratio
Rényi H_R^α	13.97	14.02	0.996
NoC N^α	1.555	1.617	0.961
SVD H_V	1.177	1.295	0.909
mean($H_R^\alpha(t)$)	10.66	10.74	0.992
std($H_R^\alpha(t)$)	0.4514	0.3855	1.171
TV($H_R^\alpha(t)$)	2.262	4.482	**0.505**
mean($N^\alpha(t)$)	1.558	1.625	0.958
std($N^\alpha(t)$)	0.473	0.438	1.079
TV($N^\alpha(t)$)	2.366	4.475	**0.498**
mean($H_V(t)$)	0.3215	0.5871	**0.548**
std($H_V(t)$)	0.3233	0.286	1.130
TV($H_V(t)$)	3.679	6.697	**0.549**

TABLE 2.1 – Rényi entropy, number of components (NoC) based on Rényi entropy, and SVD entropy of the signal shown in figure 2.15, along with the means, standard deviations (std), and total variations (TV) of its time-dependent versions. Parameters : $\alpha = 2$ and $\Delta t = 101$. The ratio of the value calculated for y_1 to that calculated for y_2 is represented in the last column. The bold values correspond to ratios that are significantly different from 1.

2.4 Time-varying Time-Frequency Complexity Measures

This research was published in IEEE transactions on biomedical engineering, volume 65, issue 8 [31].

In chapter 1 we illustrated the capabilities of the TF entropies to differentiate signals based on the amount of information they carry. While the Rényi entropy focuses on the number of components, the SVD entropy focuses on their (non)stationarity. Yet, for very simple signals of different complexities, both might be unable to see a significant difference between them.

Let us consider the signals $y_1(t)$ and $y_2(t)$ shown in figure 2.15. Although they may look similar, $y_2(t)$ is indeed more complex, since it carries more information (two transients onset against only one). But the fact that both spectrograms have the same integral value makes the Rényi entropy unable to differentiate them. Also, since one TFR can be obtained from the other by simply permutating columns, the singular values are the same, and so does the SVD entropy. This can be confirmed on Table 2.1.

A time-varying approach for these complexity measures is needed not only to detect

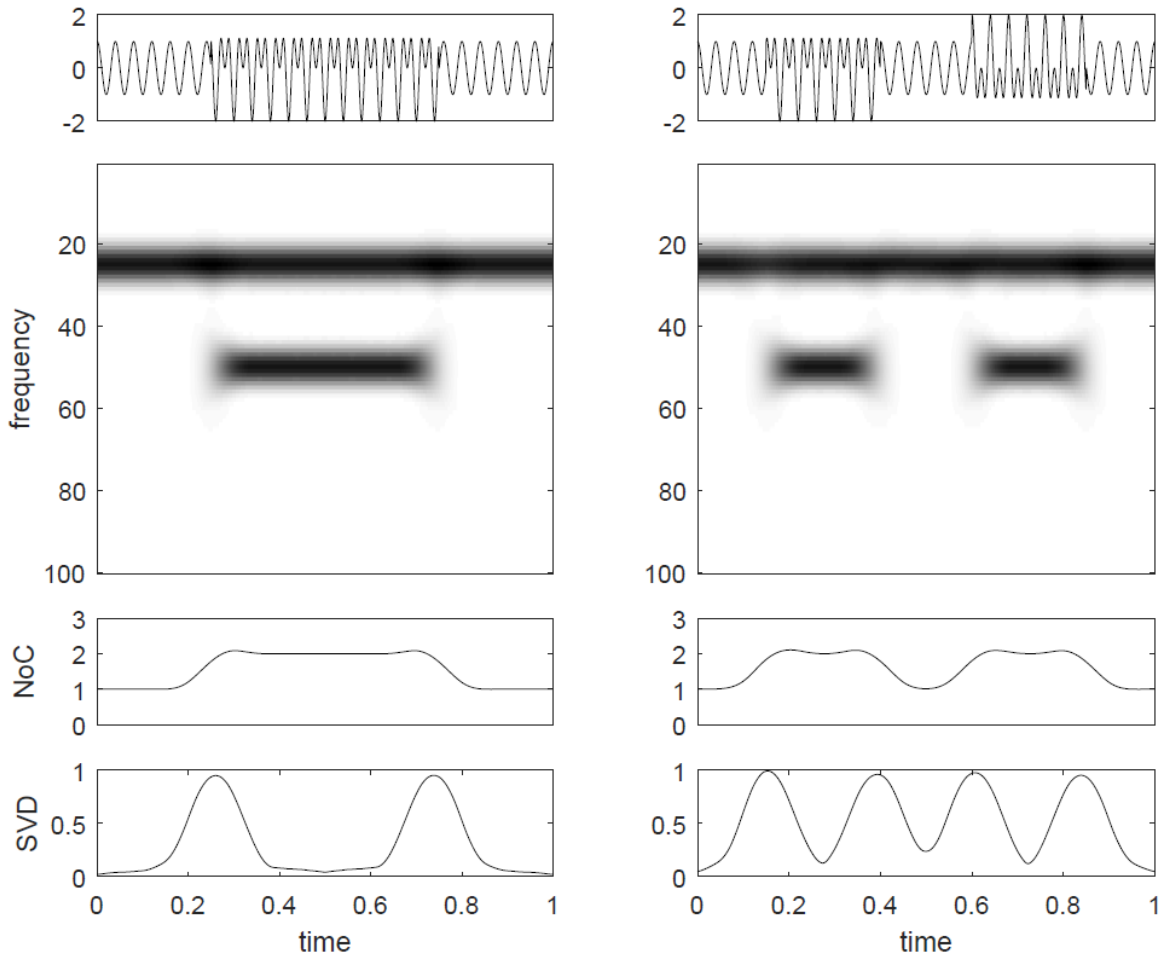

FIGURE 2.15 – Signals of different complexities, their spectrograms, and time-varying entropies. Left : pure tone plus one transient of half duration. Right : pure tone plus two transients of quarter duration each. In both cases, the signals are defined for $0 \leq t \leq T = 1$ and were generated with a sampling frequency of $f_s = 1000$. The spectrograms were obtained with a Hann window of 200 samples, and for $0 \leq f \leq 100$. For each signal, the instantaneous number of components (NoC) and singular value decomposition (SVD) are also represented.

when a change occurred, but also to characterize the signals as a whole in a non-local manner. The marginal statistics of these time-varying quantities are useful to this purpose. The short-time Rényi entropy was introduced in [107]. For a slice of width Δt the local Rényi entropy is defined as

$$H_R^\alpha(R_x;t) = \frac{1}{1-\alpha}\log_2 \int_{t-\Delta t/2}^{t+\Delta t/2} \int \tilde{R}_x{}^\alpha(\tau,f)d\tau df, \tag{2.7}$$

where $\tilde{R}_x(t,f) = R_x(t,f)/\int_{t-\Delta t/2}^{t+\Delta t/2} R_x(a,b)dadb$ is the locally normalized time-frequency representation. It should be noted that, in general, $H_R^\alpha(R_x) \neq \int H_R^\alpha(R_x;t)dt$ due to the nonlinearity of the logarithm and to the local normalization. A time-varying estimation of the number of components is constructed as [107]

$$N_x^\alpha(t) = 2^{H_R^\alpha(R_x;t) - \breve{H}_R^\alpha(t)}, \tag{2.8}$$

where $\breve{H}_R^\alpha(t)$ is the time-varying Rényi entropy of a pure tone.

The mean, standard deviation, and total variation of $H_R^\alpha(R_{x_{1,2}};t)$ are presented in table 2.1. Total variation is

$$TV_x = \int |x'(t)|dt. \tag{2.9}$$

The ratio between the results of the two signals is also presented. Ratios that are significantly different from 1 are highlighted. While the first two quantities show no difference, total variation was able to differentiate between the two signals with higher values for the one that carries more information ($y_2(t)$). The counting property of this entropy can be confirmed in the third row of figure 2.15 where it can be appreciated how $N_x^\alpha(t)$ acts as an instantaneous counter.

The same approach could be taken with SVD entropy. We propose here to define a time-varying version of this complexity measure by taking the singular value decomposition of a slice of width Δt of the time frequency representation :

$$R_x(\tau,f) = \sum_{n=1}^{\inf} \hat{\sigma}_{n,t}\hat{u}_{n,t}(\tau)\hat{v}_{n,t}(f), \tag{2.10}$$

for $t - \Delta t/2 \leq \tau \leq t + \Delta t/2$. Then, the local SVD entropy is

$$H_V(t) = -\sum_n \frac{\hat{\sigma}_{n,t}}{\sum_n \hat{\sigma}_{n,t}} \log_2\left(\frac{\hat{\sigma}_{n,t}}{\sum_n \hat{\sigma}_{n,t}}\right). \tag{2.11}$$

For those windows where the signal is more stationary, the time-varying SVD entropy would attain low values, while where the instantaneous frequency varies faster, the values would be increased. Specifically, for those windows where the signal has constant frequency we expect a null value. As the window advances into the transition zone the value would increase up to $\log_2(2) = 1$ when the center of the window corresponds with the onset time of one of the transients. The value then decreases again to zero as the window advances out of the transition. The fourth row of figure 2.15 depicts the values of $H_V(R_x; t)$, confirming our explanation. The difference between the two signals is now evident. Table 2.1 presents the mean, standard deviation, and total variation of this quantity for the two signals. The differentiation becomes clear. For the Rényi entropy, a common value of $\alpha = 2$ was used in [103]. A window of $\Delta t = 101$ samples was used for all the time-varying quantities.

2.4.1 Real EEG Data from Epileptic Patients

The EEG recordings of patients with BECTS are quite remarkable due to the presence of spikes over the centrotemporal regions (unilateral or bilateral) with a biphasic or triphasic appearance and a relatively high amplitude [70]. Studies suggest that cognitive deficits might be correlated with the frequency of spikes [88] [119]. This should prompt the clinician to lower this spike discharge frequency using antiepileptic drugs (AED). However this issue remains controversial as AED may, by their own, create or aggravate pre-existing cognitive dysfunction. A decreasing of the amount of spikes in patients with BECTS after being medicated with sulthiame was reported [13]. A syndrome quite close to BECTS is epileptic encephalopathies with CSWS, whose patients were reported to diminish the frequency of spikes after medication with levetiracetam [3]. This study also showed that the clinical improvement of some patients was associated to decreased diffusion of the IED over the whole scalp even if the frequency of spikes was not decreased [3]. Moreover, the temporal association between clinical improvement and decrease of spikes is not always strict [112]. Taken together, this highlights that other methods to analyze EEG are needed. In the past years, a lot of studies attempted to correlate cognitive outcome with the resting state activity in various neurological conditions including epilepsy.

We will focus our attention on resting state signals, i.e. epochs without IED. Knowing that signals from healthy subjects present larger complexity [20] [63] [130], we wonder

if this will be confirmed on resting state signals of patients with BECTS and related conditions before and after medication. Does the complexity of the resting state signals increase after proper medication ? If positive, we expect to compute larger values of entropy on these epochs corresponding to recordings after medication. This procedure would allow for a better monitoring of the treatment.

A second question we will address is : Is this difference big enough as to separate the signals into two disjoint clusters ? If positive, the time-frequency complexity features are good enough for classification task.

Database

The EEG data of 3 epileptic patients acquired in Universite Libre de Bruxelles, Hopital Erasme (agreement of local ethical committee number P2015/242) were analyzed. Patients were studied at baseline (T0) and about 4-6 weeks after a change of the AED regimen aimed to reduce IED (T1). Table 2.2 shows a summary of clinical data, diagnoses, AED at T0 and T1, and IED quantification on awake and sleep EEG using a spike-wave index (SWI) during sleep and an EEG grade that assesses the diffusion of IED, as previously proposed [3]. It was concluded from the visual analysis and quantification of the SWI during non-rapid eye movement (NREM) sleep, performed by an experienced neurophysiologist, that patient BE001 did not respond to the change of AED (a benzodiazepine), and that patients BE003 and BE004 showed impressive EEG improvement after introduction of levetiracetam.

For the acquisitions, all the subjects were lied down comfortably and brain activity was recorded both during eyes open and eyes closed. The activity was recorded by 256 electrodes (hdEEG) with the Cz electrode as reference. The sampling frequency was 1000 Hz.

Patient (number, age, gender)	BE001, 10, M	BE003, 8, F	BE004, 9, M	BE006, 10, F	BE007 9, M	BE009 9, F	BE011, 9, M	BE012, 8, F	BE014 7, F
Diagnosis	Epilespsy with CSWS	Atypical BECTS	BECTS	CAE	Epilepsy with CSWS-LKS	CAE	CAE	CAE	BECTS
Localization of IED acording to 10-20 system	T5	C3	C3		T3 F8				C3 C4
Treatment at T0	LTG ETS	VPA LTG	None	None	None	VPA	None	LTG	VPA
Treatment at T1	LTG CLB ETS	VPA LEV	LEV	ETS	Cortisone	VPA LTG	ETS	LTG ETS	None
SWI at T0 and T1	75% T0, 67% T1	75% T0, 50% T1	60% T0, 70% T1	3% T0, 1% T1	42% T0, 1% T1	47% T0, 41% T1	20% T0, 1% T1	7% T0, 1% T1	30% T0, 25% T1
EEG grade at T0	3 (W and S)	3 (W and S)	3 (W and S)		2 S				1 S
EEG grade at T1	3 (W and S)	0 W, 1 S	1 (W and S)		1 S				1 S

TABLE 2.2 – Summary of the database. M : Male, F : Female, LTG : Lamotrigine, ETS : Ethosuximide, CLB : Clobazam, LEV : Levetiracetam, VPA : Valproate, W : Awake, S : NREM Sleep. SWI calculations and EEG grades were performed as detailed in [3].

Preprocessing and selection of epochs

The preprocessing stage consisted of three steps : band-pass filtering, artifact removal and selection of spike-free epochs. For the first task, we applied a high-order filter between 0.5 Hz and 45 Hz, with a transition bandwidth of 0.22 Hz. We used Independent Component Analysis (ICA) [62] to remove artifacts by discarding those sources identified as artifacts before reconstruction. For the selection of epochs, a trained neurophysiologist visually isolated the spikes in order to obtain spike-free epochs of 1 second of duration. These epochs are the signals we analyzed, playing the role of $\{x(i)\}$ of the previous sections. The choice of the length of the epochs was conditioned by the fact that one patient presented only 12 non-consecutive seconds of spikefree signals at T0. We were forced to segment this data into 12 epochs of 1 second, and proceed in the same way for the other two patients (although with more epochs). Shorter epochs would be affected by border effects. Therefore, an epoch of one second is a good trade-off between border effects and the difficulty of having longer spike-free segments.

Features

The features to be used will be : total number of components based on Rényi entropy (to be referred as NoC in the figures), mean of time-varying number of components (MN), standard deviation of time-varying number of components (SN), total SVD entropy (VT), and mean of time-varying SVD entropy (MV). For every one of the epochs e, $e = 1 \dots E$, we compute the five mentioned features, C^p, $p = 1 \dots 5$, for every electrode. Then, we define the features for a whole region $\Re$ as the mean of the corresponding feature for that epoch among the electrodes belonging to that specific region (see figure 2.16 for the regions and electrodes) :

$$C_e^{\Re,p} = \frac{1}{\#\Re} \sum_{i \in \Re} C_{i,e}^p, \tag{2.12}$$

where $\#\Re$ is the cardinality of the set $\Re$.

Results and discussion

We begin analyzing the results for patient BE004. We processed $E = 30$ epochs of 1 second of duration during eyes open for both baseline (T0) and after six weeks on

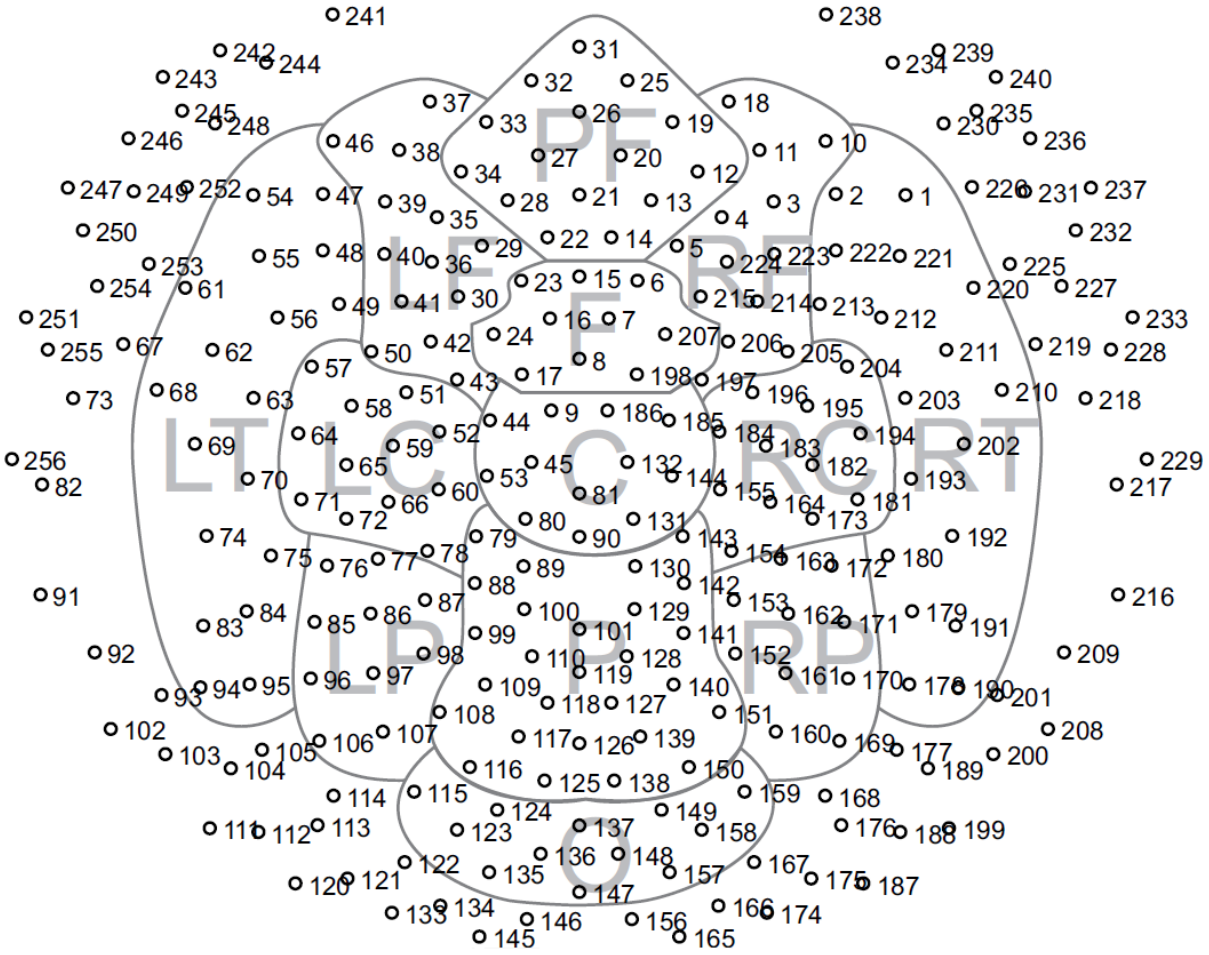

FIGURE 2.16 – Thirteen regions of interest from the hdEEG (256 channels) recordings. PF : Pre-Frontal. F : Frontal. RF : Right Frontal. LF : Left Frontal. C : Central. RC : Right Central. LF : Left Central. RT : Right Temporal. LT : Left Temporal. P : Parietal. RP : Right Parietal. LP : Left Parietal. O : Occipital.

levetiracetam (T1). The values for the five features for the thirteen regions (region-wise computed as in 2.12) can be appreciated on boxplots in figure 2.17. It can be seen how, in general, the features attain higher values for those epochs corresponding to T1. In order to objectively measure this increase, we performed a Friedman test for every feature and for every region, and mark with an asterisk ('*') those with $p < 0.05$. The increasing of the features is observed on most of the regions, especially in the frontal area (regions prefrontal, frontal, and right and left frontal) with 12 out of 20 features experiencing it ; and in the centrotemporal area (regions central, right and left central, and right and left temporal) with 21 out of 25 features with a significant increase. We also test the features for a decreasing complexity on T1 with negative results. The fact that the major increasing is observed on the centrotemporal area is relevant since studies have shown that these regions are the sources of IED in BECTS. These results shed light on our first question : the complexity on the resting state signals may increase after proper medication.

In order to evaluate the capability of these features to perform a classification task, we performed a Principal Component Analysis (PCA) [65] for every feature on every region. Then, the first principal component (a mere linear combination of the five features) was used as the sole feature for binary classification. The ROC curves obtained for different values of the discrimination threshold are presented on figure 2.18, along with the areas under the curves (AUC). The best results again are on the centrotemporal area, with an AUC higher than 0.93 for left central region, i.e. the region of the brain where IED were localized in this patient. Now we may be able to answer our second question : when used combined, these time varying time-frequency entropy measures are able to perform a classification task with good results when analyzing EEG data from epileptic patients.

For patient BE003 we were able to isolate only $E = 12$ epochs without any spike because of the large amount of spikes present on the T0 recording. The results are summarized on Table 2.3. We mark with asterisks ('*') those features that present a significant difference ($p < 0.05$, Friedman test). As with the previous example, the results are good enough as to evidence the difference between the T0 recording and the T1 (six weeks on levetiracetam). We observed an even performance across regions. We also present the AUCs, with the best results on the centrotemporal area, with an AUC up to 1 for the central region. These remarkable results must be considered carefully since they might be conditioned by the small sample.

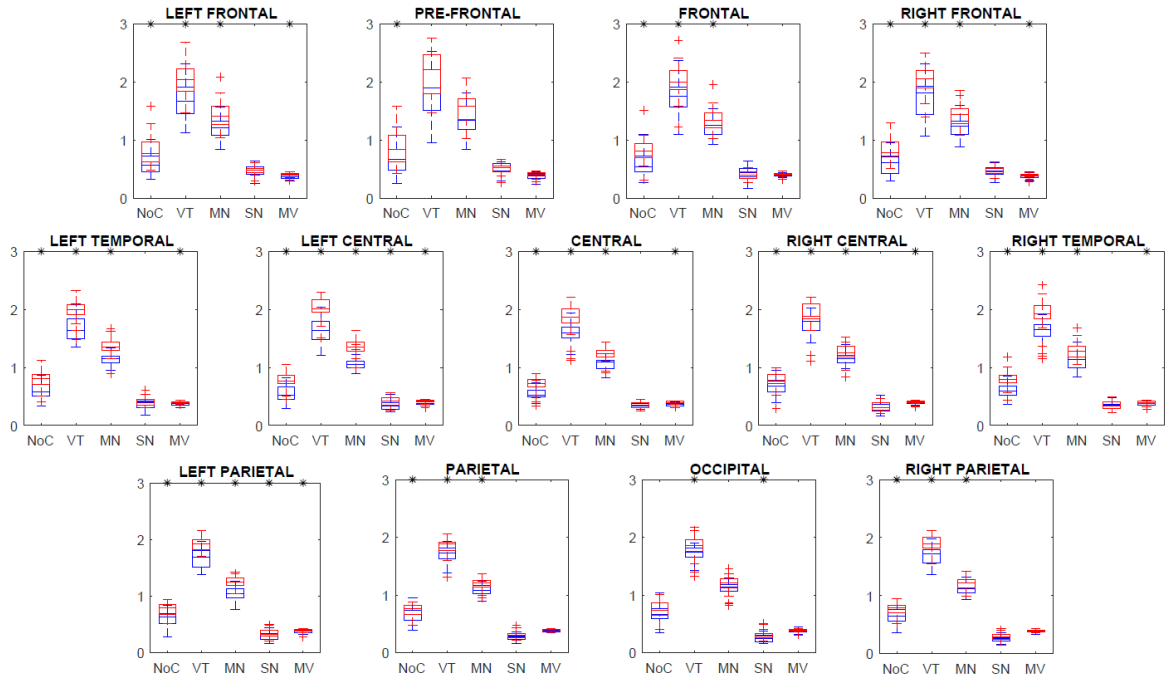

FIGURE 2.17 – Results of the 5 features (NoC, VT, MN, SN, and MV) for the 30 epochs (for each of T0 and T1) of the 13 regions for patient BE004. The baseline records (T0) are shown in blue, while the records after six weeks on leveteracitam (T1) are shown in red. Those features that present significant differences ($p < 0.05$ in a Friedman test) are indicated with a star ('*'). NoC : Number of Components. VT : total SVD entropy. MN : mean of the time-varying number of components. SN : standard deviation of the time-varying number of components. MV : mean of the time-varying SVD entropy. Parameters : Hann window of 200 samples. $\Delta t = 21$ samples. $\alpha = 2$.

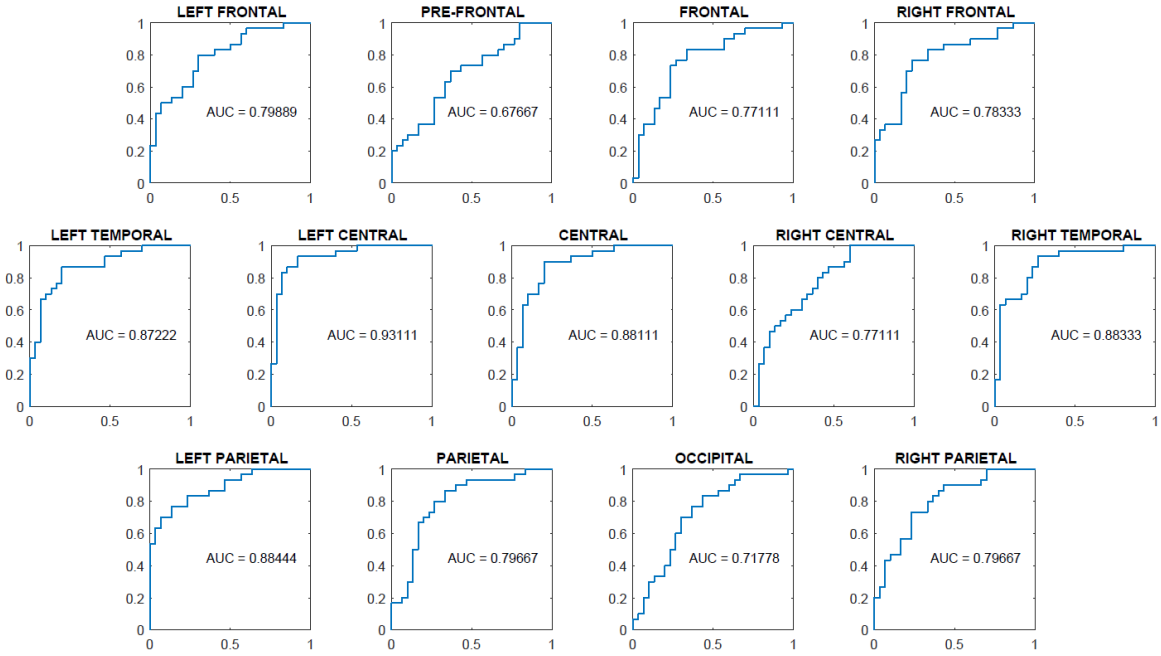

FIGURE 2.18 – The ROC curves for the 13 regions for patient BE004 obtained for different values of the discrimination threshold. The ROC curves were performed on the first principal component obtained via PCA on the five features (NoC, VT, MN, SN, and MV). The horizontal axes correspond to 1-specificity, while the vertical axes correspond to sensitivity. The areas under the curves (AUC) are also shown.

Region	NoC	VT	MN	SN	MV	AUC
Pre-frontal	*	*	*		*	0.972
Frontal		*	*		*	0.917
Right Frontal	*	*	*		*	0.938
Left Frontal	*	*	*		*	0.993
Central	*	*	*		*	1.000
Right Central		*	*		*	0.944
Left Central	*	*	*	*	*	0.979
Right Temporal		*	*		*	0.979
Left Temporal	*	*	*	*	*	0.993
Parietal	*	*	*		*	1.000
Right Parietal	*	*	*		*	0.986
Left Parietal	*	*	*	*	*	0.972
Occipital	*	*	*		*	1.000

TABLE 2.3 – Summary of the results of the comparison of the values of the five feautures (NoC, VT, MN, SN, and MV) of the patient BE003 (T0 vs T1) using Friedman test. Parameters : Hann Window of 200 samples for stft, $\alpha = 2$, $\Delta t = 21$. Significant differences are marked with '*' (significance level : $p < 0.05$). $E = 12$ epochs.

The results for patient BE001 are presented in a summarized manner in Table 2.4. Here we analyzed 30 epochs. The results are, in general, worse than those of the other two patients : less features present significant differences and the AUCs have lower values. This is the patient who did not present an improvement of the EEG. This could suggest that the complexity measures here presented are more sensitive than visual analysis of EEG to appreciate changes related to drugs.

All the records were analyzed using a Hann window of 200 samples for the STFT, a value of $\alpha = 2$ for the Rényi entropy, and $\Delta t = 21$ for the time-varying entropy measures. In all cases, we only considered eyes open epochs because of two reasons : the first one is that in this state there are less IED in some patients, and the second one is because it is the highest complexity state (it is known that the stronger alpha rhythm during eyes closed drives the complexity down).

The global scheme here applied on high density EEG recordings might also be applied on other types of neurophysiological signals, such as regular EEG or magnetoencephalography (MEG). As long as there is a difference in complexity between two states or populations, the procedure proposed here may reveal it. Here, besides the global entropies, we used marginal statistics of their time-varying versions, but other features derived from the same complexity measures might be used as well.

Region	NoC	VT	MN	SN	MV	AUC
Pre-frontal	*	*	*	*	*	0.711
Frontal	*	*	*	*	*	0.716
Right Frontal			*			0.679
Left Frontal		*	*	*		0.862
Central				*		0.604
Right Central				*		0.590
Left Central	*	*	*	*		0.793
Right Temporal		*	*	*	*	0.739
Left Temporal	*	*	*	*	*	0.933
Parietal	*	*	*	*	*	0.779
Right Parietal		*	*	*		0.732
Left Parietal	*	*	*	*	*	0.882
Occipital	*	*	*	*	*	0.858

TABLE 2.4 – Summary of the results of the comparison of the values of the five features (NoC, VT, MN, SN, and MV) of the patient BE001 (T0 vs T1) using Friedman test. Parameters : Hann Window of 200 samples for stft, $\alpha = 2$, $\Delta t = 21$. Significant diferences are marked with '*' (significance level : $p < 0.05$). $E = 30$ epochs.

2.4.2 Conclusion

We applied the global time-frequency entropies along with statistics from their time-varying counterparts to a particular problem : the analysis of the resting state EEG recordings from the epileptic patients before and after proper medication.

The results show an increase in the complexity for most of the regions of the brain. This increase could be used, along with the clinical exam, neurophysiological tests, and the decreasing in the amount of the spikes, to better monitoring the treatment of the patients. The complexity features also show that, when combined, they are able to perform classification between the state before and after proper medication. We made no use of the preestablished EEG frequency bands, which may sometimes slightly differ between authors, but considered the whole frequency content of the signal instead, with no *a priori* band separation.

The complexity measures presented here can be applied to a wider range of problems. For instance, in epilepsy, the time-varying versions are suitable for the prediction of epileptic seizures. A deeper study of the regional changes of the complexities should shed light on the localization of the epileptic foci.

CHAPITRE 3

FUNCTIONAL CONNECTIVITY BASED ON MUTUAL INFORMATION USING MVIWMPE

3.1 Introduction

In this thesis our aim is to use entropy measures in order to assess functional connectivity. The authors of [117] showed that regional neural complexity and network functional connectivity may be two related aspects of brain's information processing : the more complex regional neural activity, the higher functional connectivity this region has with other brain regions. They also showed that multi-scale entropy, at high and low frequencies may represent local and distributed information processing across brain regions. These results (although validated only in mice [117]) are promising in terms of the application of multi-scale entropy in functional connectivity studies. Another study showed, using optical voltage imaging, that the synchrony of functional connectivity and multi-scale entropy are positively correlated at small scales and negatively correlated at large scales [78]. This study showed that functional connectivity and multi-scale entropy are effective biomarkers for brain states, and provide a promising viewpoint to unify these two principal domains in human brain data analysis. Based on this and for the sake of applying multi-scale entropy measures in assessing functional connectivity in human subjects, we introduce a new method to calculate functional connectivity based on scalp EEG recordings. The method is based on mutual information that uses mvIWMPE as the entropy measure. We at first validate the ability of this method to find resting state networks that were found using functional MRI (fMRI). We then evaluate inter-subject variability and intra-subject variability of this method coupled with several node and global network measures. Finally, we apply this method on EEG data we recorded from epileptic children with three types of epilepsy : childhood absence epilepsy, CSWS, and BECTS.

3.2 Method

This functional connectivity approach [66] is based on mutual information with the following equation

$$I(\mathbf{x}, \mathbf{y}) = H(\mathbf{x}) + H(\mathbf{y}) - H(\mathbf{x}, \mathbf{y}). \tag{3.1}$$

$I(\mathbf{x}, \mathbf{y})$ is the mutual information between two signals, $\mathbf{x}$ and $\mathbf{y}$. $H(\mathbf{x})$ and $H(\mathbf{y})$ are the entropies of $\mathbf{x}$ and $\mathbf{y}$ respectively and $H(\mathbf{x}, \mathbf{y})$ is the bivariate entropy of signals $\mathbf{x}$ and $\mathbf{y}$.

The novelty of this study is that we used mvIWMPE that we introduced in [67] to calculate the mutual information. mvIWMPE was explained in details in chapter 2. So in other words, the muatual information equation would be

$$I_s(\mathbf{x},\mathbf{y}) = mvIWMPE_s(\mathbf{x}) + mvIWMPE_s(\mathbf{y}) - mvIWMPE_s(\mathbf{x},\mathbf{y}), \tag{3.2}$$

where $1 \leq s \leq \tau$, s is the time scale, and τ is the maximum time scale to calculate mvIWMPE. Finally,

$$I(\mathbf{x},\mathbf{y}) = \sum_{s=1}^{\max \tau} I_s(\mathbf{x},\mathbf{y}), \tag{3.3}$$

which can be considered as an aggregation of the mutual information at different scales.

3.3 Evaluation on EEG data

3.3.1 Dataset

Sixteen-minute high-density EEG recordings from 4 healthy children at rest (2 females and 2 males, age : 9.875 ± 1.956 years) were acquired in Department of Pediatric Neurology, Centre Hospitalier Universitaire, Angers, France. These recordings were approved by ethical committee agreement (N° ID CPP : 2016-A01783-487).

Subjects were asked to lie down comfortably and the resting-state brain activity was recorded during eyes open, where the subjects looked at a fixed target on a wall facing them, and eyes closed, without sleeping. The EEG activity was recorded by 256 electrodes (Electrical Geodesic Inc.) with the Cz electrode as a reference. The sampling rate of the acquisitions was 1 kHz.

Individual MRI for each subject was also recorded in Department of Pediatric Neurology, Centre Hospitalier Universitaire, Angers, France.

3.3.2 Preprocessing

By visually inspecting all the EEG recordings, 74 channels were removed from the recordings of all the patients for being contaminated with a significant amount of muscle activity and to conserve symmetry between the left and right hemispheres. The signals

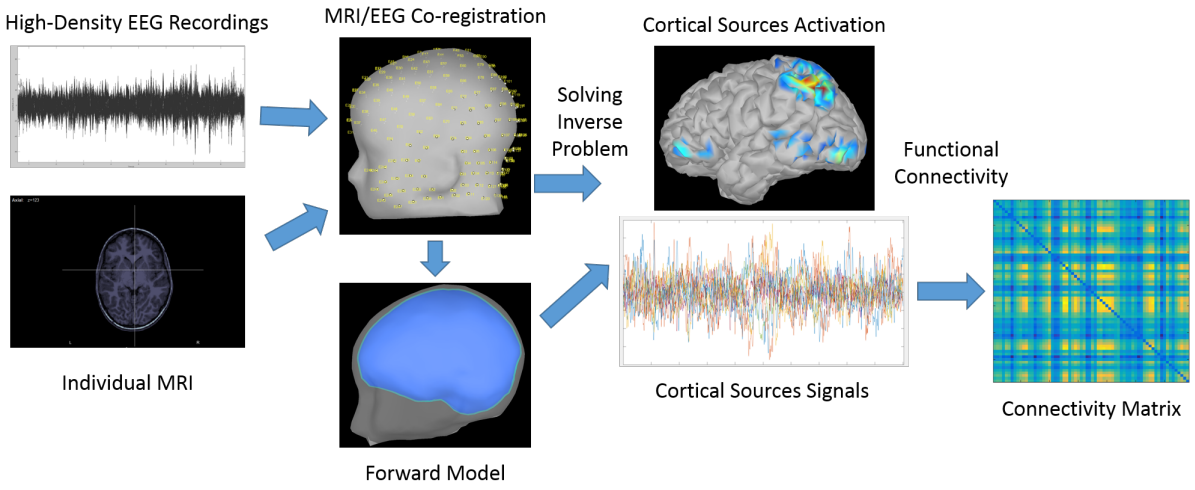

FIGURE 3.1 – Pipeline to estimate functional connectivity from EEG signals. The process involves MRI/EEG Co-registration, finding the forward model, estimating cortical source signals by solving an inverse problem, and finally calculation of the connectivity matrix of the source signals.

were filtered by a bandpass FIR filter of a transition bandwidth of 0.22 Hz. The cut-off frequencies were 0.5 Hz and 45 Hz. From each subject, 10 eyes-closed artifact-free epochs of 10 seconds each were extracted. These steps were performed using Brainstorm [108] and EEGLAB [41].

To construct a realistic head model for each subject, the individual MRI was segmented using the Freesurfer software [49]. After the coregistration of the EEG data with the segmented MRI data, the lead field matrix for the cortical mesh of 15000 vertices was computed using OpenMEEG [57] according to the Boundary Element Method (BEM) [59].

Using the constructed lead field matrices and the 182 signals from the electrode level for each of the epochs, 15000 source signals were estimated on the cortical level. This was done by solving the inverse problem according to the Minimum Norm Estimate (MNE) [60] method. Those 15000 source signals were reduced to 68 regional signals according to the Desikan-Killiany [44] atlas. Figure 3.1 shows the pipeline that was followed to prepare the data for acquiring the connectivity matrices.

3.3.3 Functional Connectivity

The epochs from all the subjects were grouped into one group to get relatively general results rather than subject-related results. For each of the 40 epochs on the source level, we applied the mvIWMPE-based mutual information between all the signals of the 68 regions. $\max \tau$ was set to 10 and we used the default value of the embedding dimension d as in [67], $d = 3$. This resulted in a 68×68 symmetrical connectivity matrix for each epoch. Each matrix was thresholded keeping the highest 10% of values and zeroing the rest.

Each calculated connectivity matrix can be represented as a graph with 68 nodes and edges between nodes, with the entries of the matrix being the weights of these edges. In this sense, we can quantify each node with several network measures [101]. In our study, we used :

— Betweenness Centrality [53] : The betweenness centrality of node i is calculated as

$$BC_i = \frac{1}{(n-1)(n-2)} \sum_{h,j \in \mathcal{N}, h \neq j, h \neq i, j \neq i} \frac{\rho_{hj}(i)}{\rho_{hj}}, \tag{3.4}$$

where $\mathcal{N}$ is the set of nodes, n is the number of nodes, ρ_{hj} is the number of shortest paths between node h and node j, and $\rho_{hj}(i)$ is number of shortest paths between node h and node j passing through node i. The higher the value of BC for a node the more important that node is in the graph.

— Strength : The strength of a node i is the sum of the weights of all of its edges

$$S_i = \sum_{j \in \mathcal{N}} w_{i,j}, \tag{3.5}$$

where $\mathcal{N}$ is the set of nodes, and $w_{i,j}$ is the weight of the edge between node i and node j.

— Node Clustering Coefficient [92] : The clustering coefficient of a node i is calculated as

$$C_i = \frac{2t_i^w}{S_i(S_i-1)} = \frac{\sum_{j,h \in \mathcal{N}} (w_{ij} w_{ih} w_{jh})^{\frac{1}{3}}}{S_i(S_i-1)}, \tag{3.6}$$

where $\mathcal{N}$ is the set of nodes, t_i^w is the geometric mean of triangles around node i, and S_i is the strength of node i.

— Vulnerability [55] : The vulnerability of a node i is calculated as

$$V_i = \frac{E - E_i}{E}, \tag{3.7}$$

where E is the global efficiency of the network and E_i is the global efficiency of the network after removing node i. Global efficiency [73] of network is calculated as :

$$E = \frac{1}{n} \sum_{i \in \mathcal{N}} \frac{\sum_{j \in \mathcal{N}, j \neq i} (d_{ij}^w)^{-1}}{n-1}, \tag{3.8}$$

where d_{ij}^w is shortest weighted path length between node i and node j.

Those 4 network measures were calculated for each node of the 40 estimated networks. A Wilcoxon signed-rank test with Bonferroni correction (68×4 multiple comparisons) was applied on each measure of each node. The value of the measure of a node was considered significant if the test showed that the values of the measure were significantly higher than the median of that measure across all nodes. The level of significance was $p_{adjusted} < 0.05$.

3.3.4 Results and Discussion

Functional magnetic resonance imaging (fMRI) is one of the techniques used to find functional connectivity in the cortex during several states. During resting-state, fMRI was able to identify several main networks that were called resting-state networks (RSNs) [87]. In our study we used 5 main RSNs that are the Auditory Network (AUD), Dorsal Attentional Network (DAN), Default Mode Network (DMN), Salience Network (SAN), and Visual Network (VIS). Based on their localization, and based on previous studies [68], we were able to correspond 44 regions from the Desikan-Killiany atlas to to the 5 RSNs, while 24 regions did not correspond to any of the aforementioned RSNs. Figure 3.2 represents the 68 regions (nodes) grouped according to their corresponding RSN if they correspond to one and grouped as 'Other' if they do not correspond to any. For each node, Fig. 3.2 shows whether each of the 4 network measures is significant or not. For betweenness centrality, only one node was significant and it corresponded to SAN. For clustering coefficient, 24 nodes were considered significant. 20 of those nodes corresponded to RSNs (9/12 DAN, 6/14 DMN, 4/8 SAN, and 1/8 VIS). For the vulnerability and strength, we got similar results. 29 were considered significant with 24 of them corresponded to RSNs (2/2 AUD, 9/12 DAN, 6/14 DMN, 5/8 SAN, and 2/8

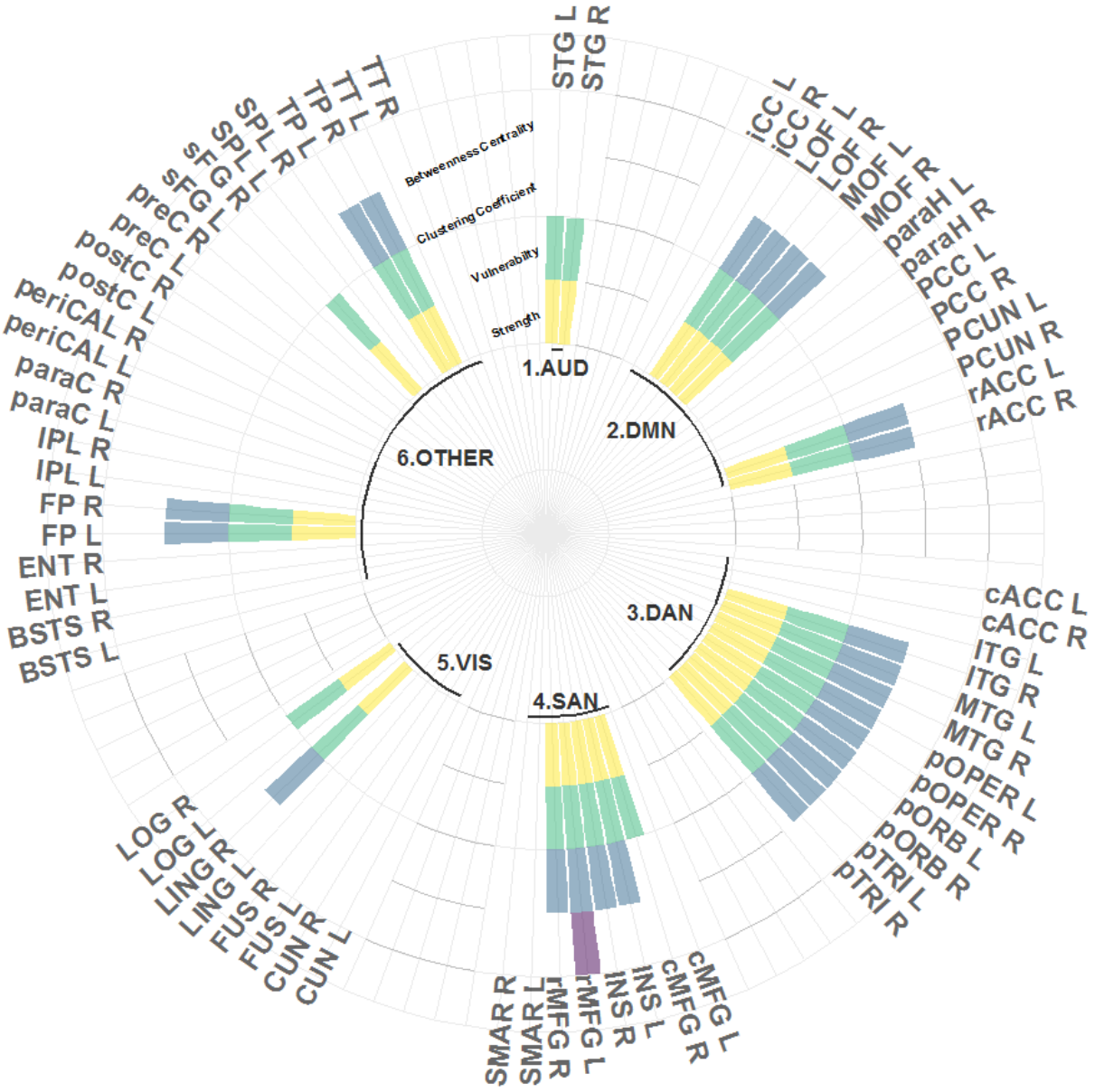

FIGURE 3.2 – Results of Wilcoxon Signed-Rank Test with Bonferroni Correction when comparing the 4 measures (Betweenness Centrality, Clustering Coefficient, Vulnerability, and Strength) values of a node with respect to the median of all the values of that measure. Significance level is $p_{adjusted} < 0.05$. Nodes were grouped according to their localization with respect to previously defined Resting-State Network (RSN) based on fMRI. AUD : Auditory Network, DAN : Dorsal Attentional Network, DMN : Default Mode Network, SAN : Salience Network, VIS : Visual Network.

VIS).

During resting-state, we expect the most important nodes to be corresponding to the RSNs. Our results show that, in terms of clustering coefficient, 83.3% of the significant nodes correspond to RSNs with only 16.7% corresponding to others, and in terms of strength and vulnerability, 82.8% of the significant nodes correspond to RSNs with only 17.2% corresponding to others. Besides, our proposed method was able to conserve symmetry of the nodes, where for most of the significant nodes the corresponding regions on both hemispheres were significant. These results show that our method is able to detect functional networks in the cortex efficiently and without the need to band-pass filter the EEG source signals into narrow frequency bands as several other methods require for networks estimation.

3.4 Validation of the Method

To further validate this method, we applied several additional tests. Our aim was to study inter-subject and intra-subject variability on the method. For this, we had two datasets. The first dataset was recorded from a group of healthy children. The second dataset was recorded from a group of epileptic children. The tests were based on the values of the following network measures :

- Node Measures result in a value per node :
  - Closeness Centrality [54] : The closeness centrality of a node i is defined as

$$(L_i)^{-1} = \frac{n-1}{\sum_{j \in N, j \neq i} d_{ij}}, \tag{3.9}$$

    where n is the number of nodes, N is the set of all nodes, and d_{ij} is the shortest distance between nodes i and j.
  - Node Clustering Coefficient [92] : Detailed in section 3.3.3.
  - Strength : Detailed in section 3.3.3.
- Global Measures result in a value per network :
  - Characteristic Path Length [118] : The characteristic path length is described as

$$L = \frac{1}{n} \sum_{i \in N} \frac{\sum_{j \in N, j \neq i} d_{ij}}{n-1}, \tag{3.10}$$

    where n is the number of nodes, N is the set of all nodes, and d_{ij} is the

shortest distance between nodes i and j.

— Clustering Coefficient [118] : Clustering coefficient is the average of all node clustering coefficients.

$$C = \frac{1}{n} \sum_{i \in N} C_i, \tag{3.11}$$

where C_i is the node clustering coefficient of node i described in section 3.3.3

— Global Efficiency [73] : The global efficiency of a network is defined in section 3.3.3.

3.4.1 Influence of Inter-subject Variability

To study inter-subject variability on the method we used the dataset of the healthy children. This is the same dataset used in section 3.3.1.

By visually inspecting all the EEG recordings, 74 channels were removed from the recordings of all the patients for being contaminated with a significant amount of muscle activity and to conserve symmetry between the left and right hemispheres. The signals were filtered by a bandpass FIR filter of a transition bandwidth of 0.22 Hz. The cut-off frequencies were 0.5 Hz and 45 Hz. ICA [62] was applied on the recordings to remove all muscle artifacts and eye blinks. Bad channel detection was used based on the PREP pipeline [17] to detect the bad channels and interpolate them. From each subject, 10 eyes-open artifact-free epochs of 10 seconds each were extracted. These steps were performed using Brainstorm [108] and EEGLAB [41].

To construct a realistic head model for each subject, the individual MRI was segmented using the Freesurfer software [49]. After the coregistration of the EEG data with the segmented MRI data, the lead field matrix for the cortical mesh of 15000 vertices was computed using OpenMEEG [57] according to the Boundary Element Method (BEM) [59].

Using the constructed lead field matrices and the 182 signals from the electrode level for each of the epochs, 15000 source signals were estimated on the cortical level. This was done by solving the inverse problem according to the Minimum Norm Estimate (MNE) [60] method. Those 15000 source signals were reduced to 68 regional signals according to the Desikan-Killiany [44] atlas. The introduced connectivity approach was applied on the 68 resulting signals of each epoch.

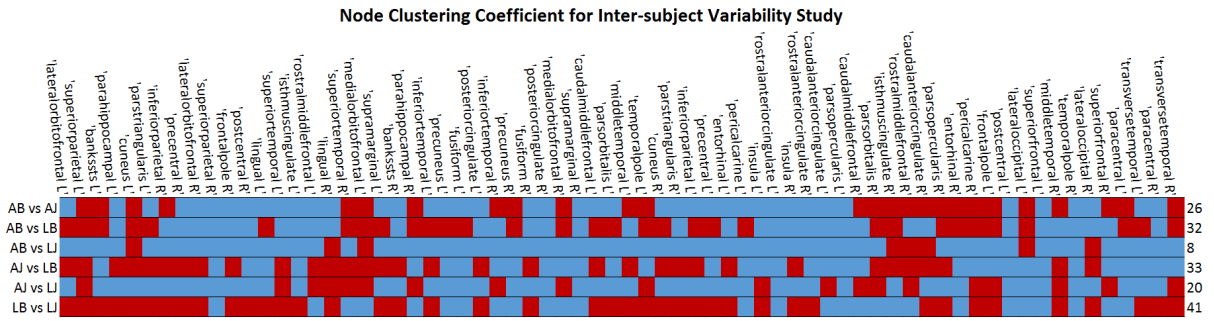

FIGURE 3.3 – Results of the 6 inter-subject comparisons of the values of the node clustering coefficient using Wilcoxon sign-rank test. The significance level is $p = 0.05$. Bonferroni correction of a factor of 68 is applied on the p-values. Regions below the significance level are considered significantly different and are marked in red. Non-significantly different regions are marked in blue. The number of regions that are significantly different per comparison is displayed on the right end of the figure.

This resulted in 10 connectivity matrices per subject. For the sake of ease of demonstration of the test results, we will call the subjects AJ, LJ, AB, and LB. The three node measures was calculated for each node of the 10 networks for every subject. Similarly, the 3 global measures were calculated for each network.

For each node measure, after obtaining the 40 values per node (10 per subject), 6 comparisons were performed using Wilcoxon sign-rank test with Bonferroni correction (by a factor of 68) comparing 10 values against 10 values per node (figures 3.3 3.4 and 3.5) :

— AB vs LB
— AB vs AJ
— AB vs LJ
— LB vs AJ
— LB vs LJ
— AJ vs LJ

The nodes with tests that had corrected p-values less than the significance level of 0.05 where considered significantly different.

For each global measure, after obtaining 40 values (10 per subject), the same six comparisons were performed using Wilcoxon sign-rank test comparing 10 values of one subject against 10 values of another subject, this time with no need for the Bonferroni correction. The tests that had p-values less than the significance level of 0.05 were considered significantly different (table 3.1).

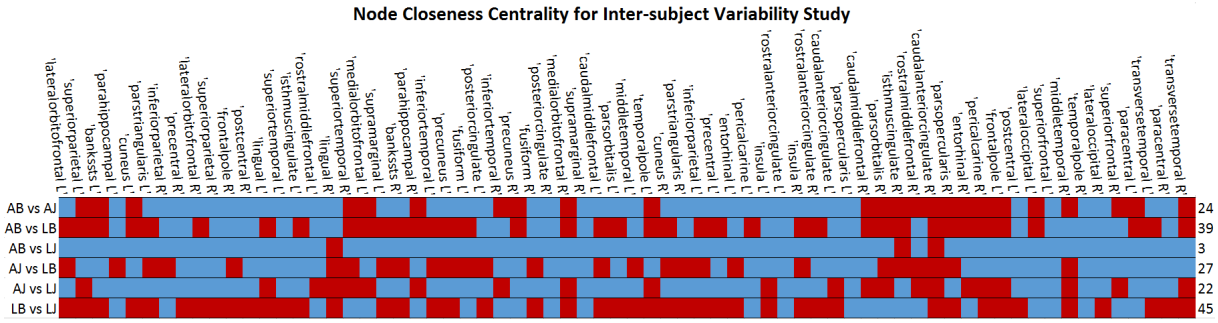

FIGURE 3.4 – Results of the 6 inter-subject comparisons of the values of the node closeness centrality using Wilcoxon sign-rank test. The significance level is $p = 0.05$. Bonferroni correction of a factor of 68 is applied on the p-values. Regions below the significance level are considered significantly different and are marked in red. Non-significantly different regions are marked in blue. The number of regions that are significantly different per comparison is displayed on the right end of the figure.

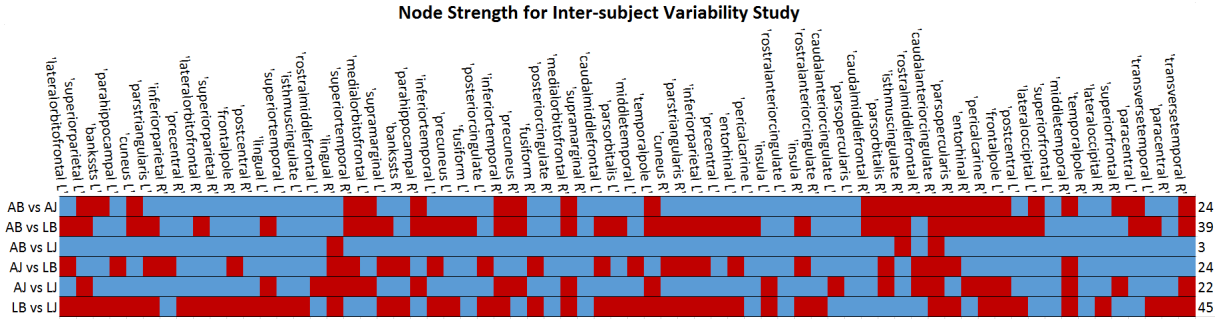

FIGURE 3.5 – Results of the 6 inter-subject comparisons of the values of the node strength using Wilcoxon sign-rank test. The significance level is $p = 0.05$. Bonferroni correction of a factor of 68 is applied on the p-values. Regions below the significance level are considered significantly different and are marked in red. Non-significantly different regions are marked in blue. The number of regions that are significantly different per comparison is displayed on the right end of the figure.

Results Discussion

As described in the earlier section, 2 types of measures were compared. To begin with the node measure, figures 3.3, 3.4, and 3.5 show the regions where the comparisons of pair of values of each node showed significant differences. Significantly different values here means that the values are not consistent from subject to another and that the method gives different values from subject to subject. Otherwise, the regions where the comparisons of the pair of values of each node showed no significant differences means that the methods here gave similar values and that the Wilcoxon sign-rank test was not able to differentiate between the values of the same node of the two compared subjects. For the node clustering coefficient, figure 3.3 shows the results of the tests. Red squares mark the regions where the tests showed that the values compared are significantly different and blue squares mark the regions where the tests showed that the values compared are not significantly different. As seen in the figure, 38.2% of the regions have significantly different values for the comparison between AB and LB, 47.1% for the comparison between AB and AJ, 11.8% for the comparison between AB and LJ, 48.5% for the comparison between LB and AJ, 29.4% for the comparison between LB and LJ, and 60.3% for the comparison between AJ and LJ. All the comparisons except AB and LJ had a lot of nodes or regions that have significantly different values. Similarly, figure 3.4 shows the results of the tests of closeness centrality of the nodes. Figure 3.5 shows the results of the tests of strength of the nodes. The same pattern can be observed where all the comparisons except AB and LJ showed a lot of significantly different regions. This shows that we can not perform inter-subject analysis using this method and applying the node network measures on its results.

Similar procedure was done for the three global measures, characteristic path length, global clustering coefficient, and global efficiency. The six comparisons are represented in table 3.1. As shown, all the comparisons except AB and LJ had p-values that are less than 0.05. This means that all the values of the all the pairs except AB and LJ are significantly different. As mentioned for the node measures, this means that we also can not perform inter-subject analysis using the method and applying global measures on its results due to the inconsistent results from subject to subject.

	Characteristic Path Length	Clustering Coefficient	Efficiency
AB vs LB	0.0003*	0.0003*	0.0003*
AB vs AJ	0.0002*	0.0002*	0.0003*
AB vs LJ	0.7912	0.7912	0.7912
LB vs AJ	0.0078*	0.0078*	0.0089*
LB vs LJ	0.0013*	0.0013*	0.0013*
AJ vs LJ	0.0004*	0.0004*	0.0004*

TABLE 3.1 – The p-values of the comparisons of the values of the global measures done using the Wilcoxon sign-rank test. Each subject had 10 values per measure. Comparisons with tests that have p-values less than 0.05 are considered significantly different and are marked with a '*'.

3.4.2 Influence of Intra-subject Variability

To study the influence of intra-subject variability on the method, we used the same dataset as in sections 3.3.1 and 3.4.1. The study was made by comparing networks extracted from the beginning of the sixteen minutes EEG recording with networks extracted from the end of the recording. The same preprocessing steps that were mentioned in section 3.4.1 were used here but instead of extracting 10 random spike-free epochs, 10 spike-free epochs were extracted from the beginning (first 5 minutes) of the recording of each subject in the eyes-open condition and other 10 spike-free epochs were extracted from the end (last 5 minutes) of the recording of each subject. All the epochs are 10 seconds-long.

This resulted in 20 connectivity matrices, 10 corresponding to the beginning of each recording and 10 corresponding to the end of the recording. The same node and global network measures that were presented in section 3.4 were calculated for each network. Our aim here was to compare for each subject the values of the measures obtained at the beginning of the recording session with the values obtained at the end of the recording. Therefore, for each value of the measures, only one comparison was made per subject, comparing the 10 values obtained at the beginning of the recording with the 10 values obtained at the end.

For each subject and for each node measure, after obtaining the 20 values, the comparison was made using the Wilcoxon sign-rank test with Bonferroni correction (by a factor of 68) comparing, per node, 10 values of the beginning of the recording against 10 values of the end (figures 3.6, 3.7, and 3.8).

For each subject and for each global measure, after obtaining 20 values (10 per

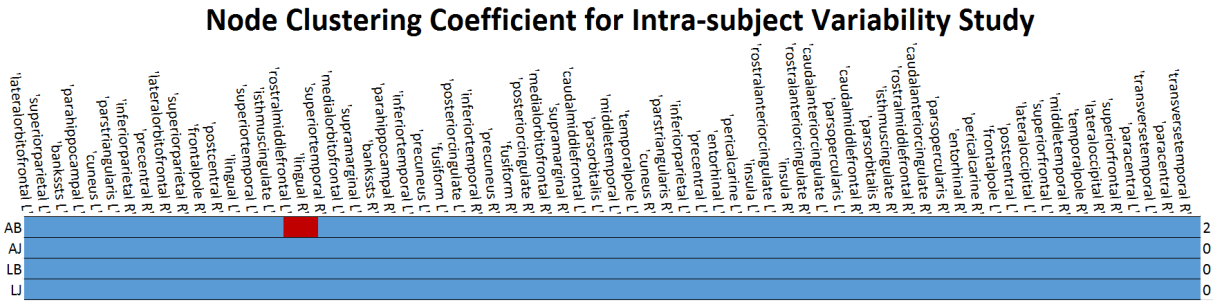

FIGURE 3.6 – Results of the 4 intra-subject comparisons of the values of the node clustering coefficient using Wilcoxon sign-rank test. The significance level is $p = 0.05$. Bonferroni correction of a factor of 68 is applied on the p-values. Regions below the significance level are considered significantly different and are marked in red. Non-significantly different regions are marked in blue. The number of regions that are significantly different per comparison is displayed on the right end of the figure.

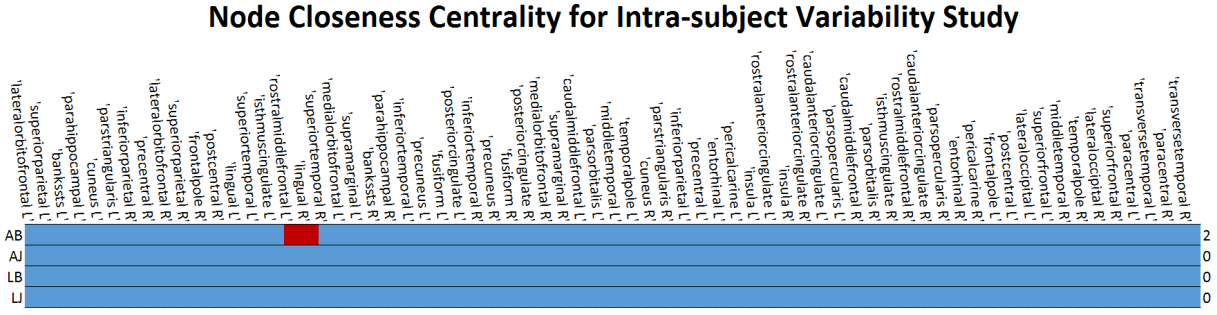

FIGURE 3.7 – Results of the 4 intra-subject comparisons of the values of the node closeness centrality using Wilcoxon sign-rank test. The significance level is $p = 0.05$. Bonferroni correction of a factor of 68 is applied on the p-values. Regions below the significance level are considered significantly different and are marked in red. Non-significantly different regions are marked in blue. The number of regions that are significantly different per comparison is displayed on the right end of the figure.

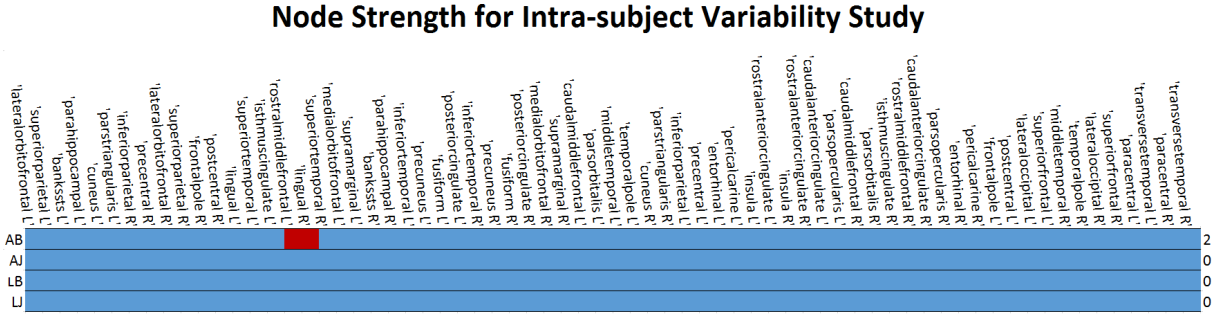

FIGURE 3.8 – Results of the 4 intra-subject comparisons of the values of the node strength using Wilcoxon sign-rank test. The significance level is $p = 0.05$. Bonferroni correction of a factor of 68 is applied on the p-values. Regions below the significance level are considered significantly different and are marked in red. Non-significantly different regions are marked in blue. The number of regions that are significantly different per comparison is displayed on the right end of the figure.

	Characteristic Path Length	Clustering Coefficient	Efficiency
AB	0.18	0.21	0.24
AJ	0.38	0.38	0.38
LB	0.27	0.27	0.27
LJ	0.9	0.9	0.9

TABLE 3.2 – The p-values of the comparisons of the values of the global measures done using the Wilcoxon sign-rank test. Each subject had 20 values per measure. 10 values corresponding to the beginning of the recording were compared against 10 values corresponding to the end of the recording. Comparisons with tests that have p-values less than 0.05 are considered significantly different.

subject), the comparison was made using the Wilcoxon sign-rank test comparing 10 values of the beginning of the recording against 10 values of the end, this time with no need for the Bonferroni correction. The tests that had p-values less than the significance level of 0.05 were considered significantly different (table 3.2).

Results Discussion

When taking a look at the node measure, figures 3.6, 3.7, and 3.8 show the regions where the comparisons of pair of values of each node showed significant differences. Significantly different values here means that the values are not consistent from epoch to epoch within the same subject and that the method gives different values every time. Otherwise, the regions where the comparisons of the pair of values of each node showed no significant differences means that the methods here gave similar values and that the Wilcoxon sign-rank test was not able to differentiate between the values of the same node of the two compared subjects. For the node clustering coefficient, figure 3.6 shows the results of the tests. Red squares mark the regions where the tests showed that the values compared are significantly different. Blue squares mark the regions where the tests showed that the values compared are not significantly different. As seen in the figure, 3% of the regions have significantly different values for the comparison among AB, and none for the comparisons among AJ, LB, and AJ. All the comparisons had very few to no nodes or regions that are significantly different values. Similarly, figure 3.7 shows the results of the tests of closeness centrality of the nodes and figure 3.8 shows the results of the tests of strength of the nodes. The same pattern can be observed where all the comparisons showed very few to no significantly different regions. This shows that intra-subject variability does not influence the results and the consistency of the method. Thus, the calculation of node measures based on our method can be used to study the state of a subject at different times.

Similar procedure was done for the three global measures, characteristic path length, global clustering coefficient, and global efficiency. The four comparisons are represented in table 3.2. As shown, all the comparisons had p-values that are greater than 0.05. This means that all the values of the all the epochs within a single subject are similar and the Wilcoxon sign-rank test is not able to differentiate between them. As mentioned for the node measures, this means that we can apply the method to perform intra-subject analysis and apply global measures on its results due to the consistent results within one subject.

3.4.3 Application on Epileptic Patients

After the validation on the control subjects to prove that the results of the method are not influenced by intra-subject variability, the method and the network measures were applied on EEG signals from epileptic children. A dataset of 6 epileptic children was used here.

Sixteen-minute high-density EEG recordings from 6 epileptic children at rest (BE006, BE007, BE009, BE011, BE012, and BE014) were acquired in Department of Pediatric Neurology, Centre Hospitalier Universitaire, Angers, France. These recordings were approved by ethical committee agreement (N° ID CPP : 2016-A01783-487). Four of the children were diagnosed with childhood absence epilepsy and are labelled as A1, A2, A3, and A4. One was diagnosed with CSWS-LKS and is labelled as B1 and one was diagnosed with BECTS and is labelled as B2.

For the acquisitions, subjects were asked to lie down comfortably and the resting-state brain activity was recorded during eyes open, where the subjects looked at a fixed target on a wall facing them, and eyes closed, without sleeping. The EEG activity was recorded by 256 electrodes (Electrical Geodesic Inc.) with the Cz electrode as a reference. The sampling rate of the acquisitions was 1 kHz.

The EEG of each subject was recorded twice. The first time is when the patient first enters the hospital (before any treatment) and is labelled as T0. The second time is 4 to 6 weeks after T0 where certain anti-epileptic drugs (AEDs) were given to the child during this time. The second session is labelled T1.

Individual MRI for each subject was also recorded in Department of Pediatric Neurology, Centre Hospitalier Universitaire, Angers, France.

By visually inspecting all the EEG recordings, 74 channels were removed from the recordings of all the patients for being contaminated with a significant amount of muscle activity and to conserve symmetry between the left and right hemispheres. The signals were filtered by a bandpass FIR filter of a transition bandwidth of 0.22 Hz. The cut-off frequencies were 0.5 Hz and 45 Hz. ICA [62] was applied on the recordings to remove all muscle artifacts and eye blinks. Bad channel detection was used based on the PREP pipeline [17] to detect the bad channels and interpolate them. From each of T0 and T1 of each subject, 10 eyes-open artifact-free epochs of 10 seconds each were extracted. These steps were performed using Brainstorm [108] and EEGLAB [41].

To construct a realistic head model for each subject, the individual MRI was segmented using the Freesurfer software [49]. After the coregistration of the EEG data

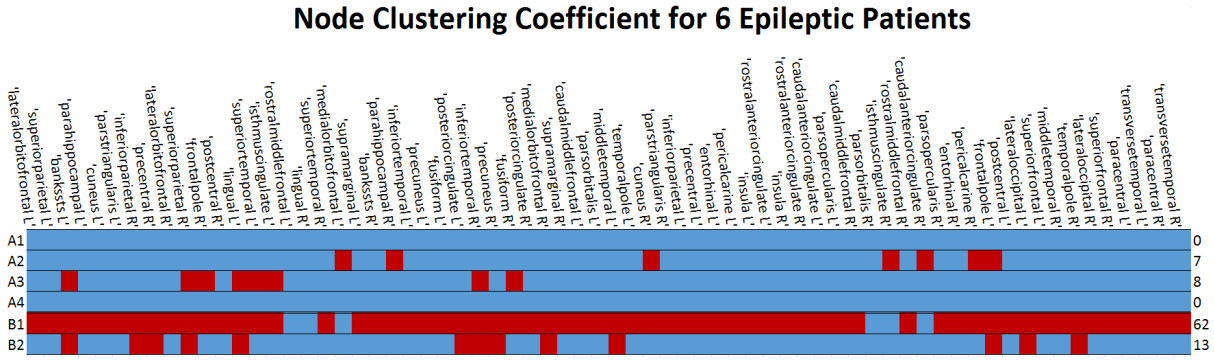

FIGURE 3.9 – Results of the comparisons of the values of the node clustering coefficient using Wilcoxon sign-rank test of the 6 epileptic patients between T_0 and T_1. The significance level is $p = 0.05$. The significance level is $p = 0.05$. Bonferroni correction of a factor of 68 is applied on the p-values. Regions below the significance level are considered significantly different and are marked in red. Non-significantly different regions are marked in blue. The number of regions that are significantly different per comparison is displayed on the right end of the figure.

with the segmented MRI data, the lead field matrix for the cortical mesh of 15000 vertices was computed using OpenMEEG [57] according to the Boundary Element Method (BEM) [59].

Using the constructed lead field matrices and the 182 signals from the electrode level for each of the epochs, 15000 source signals were estimated on the cortical level. This was done by solving the inverse problem according to the Minimum Norm Estimate (MNE) [60] method. Those 15000 source signals were reduced to 68 regional signals according to the Desikan-Killiany [44] atlas. The introduced connectivity approach was applied on the 68 resulting signals of each epoch.

For each subject this resulted in 20 connectivity matrices, 10 from the T0 session and 10 from the T1 session. The same node and global network measures that were presented in section 3.4 were calculated for each network. Our aim here is to study the differences between the T0 session and the T1 session. Therefore, for each measure, the values of one subject at T0 are compared with the values of the same subject at T1 using the Wilcoxon sign-rank test. For the node measures Bonferroni correction with a factor of 68 was applied on the significance level.

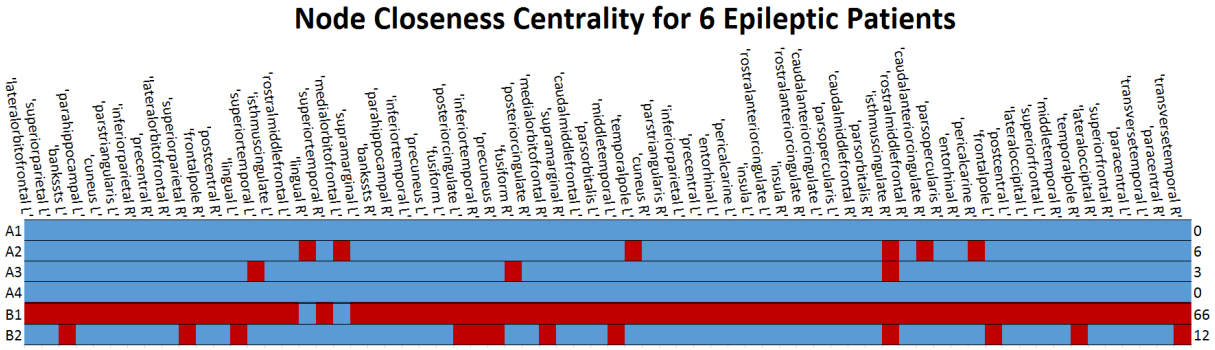

FIGURE 3.10 – Results of the comparisons of the values of the node closeness centrality using Wilcoxon sign-rank test of the 6 epileptic patients between T_0 and T_1. The significance level is $p = 0.05$. Bonferroni correction of a factor of 68 is applied on the p-values. Regions below the significance level are considered significantly different and are marked in red. Non-significantly different regions are marked in blue. The number of regions that are significantly different per comparison is displayed on the right end of the figure.

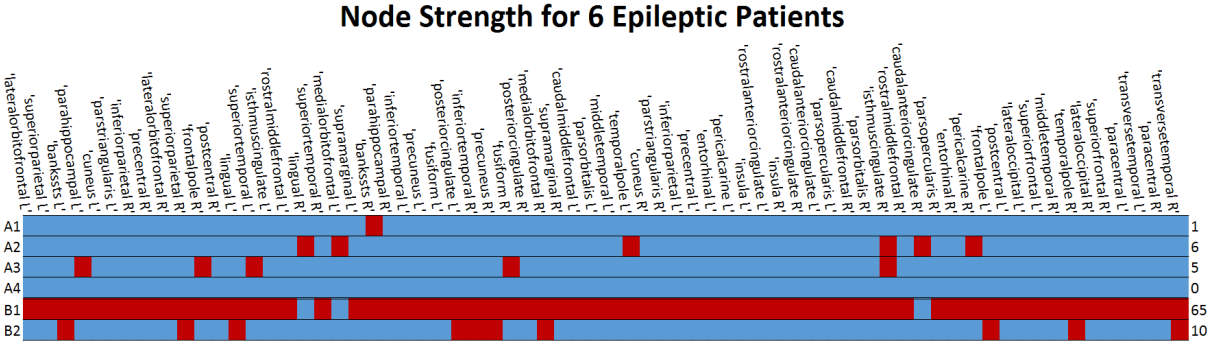

FIGURE 3.11 – Results of the comparisons of the values of the node strength using Wilcoxon sign-rank test of the 6 epileptic patients between T_0 and T_1. The significance level is $p = 0.05$. The significance level is $p = 0.05$. Bonferroni correction of a factor of 68 is applied on the p-values. Regions below the significance level are considered significantly different and are marked in red. Non-significantly different regions are marked in blue. The number of regions that are significantly different per comparison is displayed on the right end of the figure.

	Characteristic Path Length	Clustering Coefficient	Efficiency
A1	0.054	0.054	0.054
A2	0.678	0.678	0.734
A3	0.071	0.071	0.071
A4	0.791	0.791	0.791
B1	0.00018*	0.00018*	0.00018*
B2	0.571	0.623	0.623

TABLE 3.3 – The p-values of the comparisons of the values of the global measures done using the Wilcoxon sign-rank test. Each epileptic patient had 20 values per measure. 10 values corresponding to T0 session (before any treatment) were compared against 10 values corresponding to T1 session (4 to 6 weeks after T0 and start of treatment). Comparisons with tests that have p-values less than 0.05 are considered significantly different and are marked with '*'.

Results and Discussion

The results of the 6 comparisons between T0 and T1 are represented in figures 3.9 to 3.11 and table 3.3.

For the patients A1 to A4, the results of node measures represented in figures 3.9 to 3.11 showed 15/272 (5.5%) nodes with significant differences for node clustering coefficient, 9/272 (3.3%) nodes with significant differences for node closeness centrality, and 12/272 (4.4%) nodes with significant differences for node strength. The results of the global measures represented in table 3.3 showed no significant differences between T0 and T1 of the 4 patients.

For patient B1 (with CSWS-LKS), the results of the node measures represented in figures 3.9 to 3.11 showed 62/68 (91.2%) nodes with significant differences for node clustering coefficient, 66/68 (97.1%) nodes with significant differences for node closeness centrality, and 65/68 (95.6%) nodes with significant differences for node strength. The results of the global measures represented in table 3.3 showed that all the global measures calculated at T1 were significantly different from those calculated at T0.

For patient B2 (with BECTS), the results of the node measures represented in figures 3.9 to 3.11 showed 13/68 (19.1%) nodes with significant differences for node clustering coefficient, 12/68 (17.6%) nodes with significant differences for node closeness centrality, and 10/68 (14.7%) nodes with significant differences for node strength. The results of the global measures represented in table 3.3 showed that all the global measures calculated at T1 were not significantly different from those calculated at T0.

Table 2.2 shows that the patients A1, A2, A3, A4, and B2 showed no changes

FIGURE 3.12 – Holter EEG recordings during sleep of patient B1 at T0. The recordings show very frequent IEDs on two foci T3 and F8.

clinically. This can be seen in terms of the grades and the SWI. These observations come in parallel with the statistical results of the network measures of those patients, as a relatively small number of nodes are significantly different between T0 and T1. The same can be said for the global measures as none of the global measures of these patients showed significant differences between T0 and T1.

On the other hand table 2.2 shows that the patient B1 showed much improvement between T0 and T1. This can also be noticed from the Holter EEG recordings of that patient (figures 3.12 and 3.13). If we take a look at the node measures for B1 we can see that almost all the nodes of that subject showed significant differences between T0 and T1. The results are repeated for all three network measures. This is in parallel with the clinical results as B1 was completely aphasic at T0 and after one month recovered language at T1. The same thing can be said for the global measures. All the global measures were significantly different from T0 to T1 and this also confirms the previous findings.

3.5 Conclusion

From this preliminary study of our introduced functional connectivity approach, we noticed that the results given based on this method were the same as the clinical results of each patient. The coherence of the results was noticed on patients that clinically did not change from T0 to T1 and also on the patient that clinically showed a strong change

FIGURE 3.13 – Holter EEG recordings during sleep of patient B1 at T1. The recordings show reduced frequency of IEDs compared with T0. Even remaining IEDs have diminished amplitudes.

(improvement) from T0 to T1.

Future studies to assess the method would be by presenting concrete results showing the methods ability of extracting networks based on short-time epochs (around 1 second). This ability was already noticed from the method but later work should give solid results on this hypothesis. Besides, comparing the introduced method with other functional connectivity methods that are found in the literature could be an important step to better evaluate the method's potential in calculating functional connectivity and extracting networks.

CONCLUSION

In this thesis, we developed a new entropy approach based on permutation entropy, the multivariate improved weighted multi-scale permutation entropy (mvIWMPE). When applied on synthetic multivariate signals and compared with other multivariate methods based on permutation entropy, we found out that our method has better ability of differentiating signals than multivariate multi-scale permutation entropy (mvMPE) and multivariate multi-scale weighted permutation entropy (mvMWPE). The advantage of our method over multivariate improved multi-scale permutation entropy (mvIMPE) is that it introduced the weighting factor that includes in the calculations the amplitudes of the signal samples. We finally applied this method on real EEG signals from healthy children to successfully differentiate between two states, eyes open and eyes closed.

We developed another multivariate entropy approach that is based on sample entropy. This developed approach was compared with the existing approach by processing synthetic signals with varying number of variates with the existing method and with our method. It was noticed that both methods gave similar results when applied on small number of variates (2 or 3) but our method gave better results when the number of channels was greater than that. Our method was also applied on EEG signals of epileptic patients at two time points of their treatment. The results came in correspondence with the clinical diagnosis that was performed in the hospital on whether the patients were improving or not.

A third complexity measure was developed based on a time-varying time-frequency approach. This measure was also applied on synthetic signals and then on real EEG signals from the same epileptic patients that were used in the multivariate sample entropy study. By extracting several features from the results and comparing them at different time points of the treatment, the results also came in correspondence with what was found from the clinical diagnosis in the hospital.

Finally, we introduced a new functional connectivity approach based on mvIWMPE and mutual information (MI). We first tested this method's ability in extracting networks whose significant nodes correspond to the known resting state networks (RSNs) extracted using the functional magnetic resonance imaging (fMRI). For this reason we

applied the method on cortical signals calculated from EEG signals of healthy children. After extracting the networks, we extracted node and global network measures from the networks and tested their values in order to identify the significant nodes. The methods succeeded in having most of the fMRI RSN-corresponding nodes significant. We then intended to study the influence of inter-subject variability on the method. So, we applied the method on the same healthy children, but this time for the sake of comparing the values of the extracted network measures across subjects. This method failed to give consistent results across subject, which meant that we can not use to compare different subjects. After that, we intended to test the influence of intra-subject variability on the method. So we performed a similar comparison using network measures, but this time comparing values within the same subject. The method showed that it gives consistent results within the same subject. This meant that we can use this method to study subjects at different times. So, we used this method to study the states of epileptic patients at different times of their treatment. The results were based on the type of epilepsy that each patient was diagnosed with.

This work opens the door to many other questions and applications of the method. So in the future, our first step would be to compare the results of the method we introduced with other methods that are already known in the literature (for example phase locking value [72] and power envelope oscillation [121]). Further work should include a much larger dataset including all the subjects (here, the data from all the subjects are not processed yet) we recorded in our work and perhaps even record additional subjects.

It is also important to note here that most of the epileptic patients recorded had a third session (T2) which is six months after T0. So this opens the door to evaluate the states of the patients even after longer times. Future work would include these sessions and record and evaluate new T2 sessions for the remaining subjects.

As mentioned in the previous section, we also aim to test the limits of our method to calculate connectivity by shortening the time segments as much as possible to reach almost 1 sec at 1000 Hz sampling rate. This will help in evaluating the connectivity in patients that have a lot of spikes in their recordings.

Another point we are curious to explore is the analysis of connectivity during the eyes closed states. Would the networks change a lot? Would the higher frequency of spikes during eyes closed state influence the connectivity in the spike-free epochs during the same state?

The introduction of other new entropy methods allows us to think of using these methods (as with mvIWMPE) in connectivity approaches to evaluate the patients. The time-frequency approach [31] succeeded in detecting the changes around the epileptic focus in the patients. Would that be valuable if adapted to a connectivity approach ?

We also are curious to study the time course of the changes in complexity during and after the spikes. What happens directly after the spikes and how long does the influence persist ? We also intend to study, during the spike, the regions that are remote to the focus of the spike and do not show IEDs in EEG recordings. Are those regions also influenced ? Do they record changes in complexity too ?

All these points are of our interest and we are willing to address in the future. Of course finding some answers to those points will open a path for deeper investigations and further questions.

BIBLIOGRAPHIE

[1] Kari Modalsli AABERG et al., « Incidence and prevalence of childhood epilepsy : a nationwide cohort study », in : *Pediatrics* 139.*5* (2017), e20163908.

[2] Azeez ADEBIMPE, Emilie BOUREL-PONCHEL et Fabrice WALLOIS, « Identifying neural drivers of benign childhood epilepsy with centrotemporal spikes », in : *NeuroImage : Clinical* 17 (2018), p. 739-750.

[3] Alec AEBY et al., « Levetiracetam efficacy in epileptic syndromes with continuous spikes and waves during slow sleep : experience in 12 cases », in : *Epilepsia* 46.*12* (2005), p. 1937-1942.

[4] Mosabber Uddin AHMED et Danilo P MANDIC, « Multivariate multiscale entropy : A tool for complexity analysis of multichannel data », in : *Physical Review E* 84.*6* (2011), p. 061918.

[5] Mosabber Uddin AHMED et Danilo P MANDIC, « Multivariate multiscale entropy analysis », in : *IEEE Signal Processing Letters* 19.*2* (2012), p. 91-94.

[6] Orly ALTER, Patrick O BROWN et David BOTSTEIN, « Singular value decomposition for genome-wide expression data processing and modeling », in : *Proceedings of the National Academy of Sciences* 97.*18* (2000), p. 10101-10106.

[7] Yılmaz AY et al., « Neuropsychologic impairment in children with rolandic epilepsy », in : *Pediatric neurology* 41.*5* (2009), p. 359-363.

[8] Hamed AZAMI et Javier ESCUDERO, « Improved multiscale permutation entropy for biomedical signal analysis : Interpretation and application to electroencephalogram recordings », in : *Biomedical Signal Processing and Control* 23 (2016), p. 28-41.

[9] Maria Giuseppina BAGLIETTO et al., « Neuropsychological disorders related to interictal epileptic discharges during sleep in benign epilepsy of childhood with centrotemporal or Rolandic spikes », in : *Developmental medicine and child neurology* 43.*6* (2001), p. 407-412.

[10] X BAI et al., « Resting functional connectivity between the hemispheres in childhood absence epilepsy », in : *Neurology* 76.*23* (2011), p. 1960-1967.

[11] Christoph BANDT et Bernd POMPE, « Permutation entropy : a natural complexity measure for time series », in : *Physical review letters* 88.*17* (2002), p. 174102.

[12] Richard G BARANIUK et al., « Measuring time-frequency information content using the Rényi entropies », in : *IEEE Transactions on Information theory* 47.*4* (2001), p. 1391-1409.

[13] Thomas BAST et al., « The influence of sulthiame on EEG in children with benign childhood epilepsy with centrotemporal spikes (BECTS) », in : *Epilepsia* 44.*2* (2003), p. 215-220.

[14] Joshua J BEAR, Kevin E CHAPMAN et Jason R TREGELLAS, « The epileptic network and cognition : What functional connectivity is teaching us about the childhood epilepsies », in : *Epilepsia* (2019).

[15] Boris C BERNHARDT, Leonardo BONILHA et Donald W GROSS, « Network analysis for a network disorder : the emerging role of graph theory in the study of epilepsy », in : *Epilepsy & Behavior* 50 (2015), p. 162-170.

[16] Gaelle BETTUS et al., « Interictal functional connectivity of human epileptic networks assessed by intracerebral EEG and BOLD signal fluctuations », in : *PloS one* 6.*5* (2011), e20071.

[17] Nima BIGDELY-SHAMLO et al., « The PREP pipeline : standardized preprocessing for large-scale EEG analysis », in : *Frontiers in neuroinformatics* 9 (2015), p. 16.

[18] Warren T BLUME et al., « Glossary of descriptive terminology for ictal semiology : report of the ILAE task force on classification and terminology », in : *Epilepsia* 42.*9* (2001), p. 1212-1218.

[19] Boualem BOASHASH, Ghasem AZEMI et John M O'TOOLE, « Time-frequency processing of nonstationary signals : Advanced TFD design to aid diagnosis with highlights from medical applications », in : *IEEE Signal Processing Magazine* 30.*6* (2013), p. 108-119.

[20] William BOSL et al., « EEG complexity as a biomarker for autism spectrum disorder risk », in : *BMC medicine* 9.*1* (2011), p. 18.

[21] Mary AB BRAZIER et JS BARLOW, « Some applications of correlation analysis to clinical problems in electroencephalography », in : *Electroencephalography and clinical Neurophysiology* 8.*2* (1956), p. 325-331.

[22] Matthew J BROOKES, Mark William WOOLRICH et Gareth R BARNES, « Measuring functional connectivity in MEG : a multivariate approach insensitive to linear source leakage », in : *Neuroimage* 63.*2* (2012), p. 910-920.

[23] M BUREAU, « Continuous spikes and waves during slow sleep », in : *CSWS) : definition of the syndrome," in Continuous Spikes and Waves During Slow Sleep, A. Beaumanoir, M. Bureau, L. Deonna, L. Mira, and CA Tassinari, Eds* (1995), p. 17-26.

[24] Rochelle CAPLAN et al., « Childhood absence epilepsy : behavioral, cognitive, and linguistic comorbidities », in : *Epilepsia* 49.*11* (2008), p. 1838-1846.

[25] Sihan CHEN et al., « The focal alteration and causal connectivity in children with new-onset benign epilepsy with centrotemporal spikes », in : *Scientific reports* 8.*1* (2018), p. 5689.

[26] Weiting CHEN et al., « Characterization of surface EMG signal based on fuzzy entropy », in : *IEEE Transactions on neural systems and rehabilitation engineering* 15.*2* (2007), p. 266-272.

[27] Weiting CHEN et al., « Measuring complexity using fuzzyen, apen, and sampen », in : *Medical Engineering & Physics* 31.*1* (2009), p. 61-68.

[28] Commission on CLASSIFICATION et Terminology of the INTERNATIONAL LEAGUE AGAINST EPILEPSY, « Proposal for revised classification of epilepsies and epileptic syndromes », in : *Epilepsia* 30.*4* (1989), p. 389-399.

[29] Béla CLEMENS et al., « Increased resting-state EEG functional connectivity in benign childhood epilepsy with centro-temporal spikes », in : *Seizure* 35 (2016), p. 50-55.

[30] Leon COHEN, *Time-frequency analysis*, t. 778, Prentice hall, 1995.

[31] Marcelo A COLOMINAS et al., « Time-Varying Time–Frequency Complexity Measures for Epileptic EEG Data Analysis », in : *IEEE transactions on biomedical engineering* 65.*8* (2017), p. 1681-1688.

[32] R COOPER, *Osselton. JW, & Shaw. J'. C.(1980). EEG technology*.

[33] Nicolas COQUELET et al., « The electrophysiological connectome is maintained in healthy elders : a power envelope correlation MEG study », in : *Scientific reports* 7.*1* (2017), p. 13984.

[34] Madalena COSTA, Ary L GOLDBERGER et C-K PENG, « Multiscale entropy analysis of biological signals », in : *Physical review E* 71.*2* (2005), p. 021906.

[35] Madalena COSTA, Ary L GOLDBERGER et C-K PENG, « Multiscale entropy analysis of complex physiologic time series », in : *Physical review letters* 89.*6* (2002), p. 068102.

[36] Thomas M COVER et Joy A THOMAS, « Elements of Information Theory John Wiley & Sons », in : *New York* 68 (1991), p. 69-73.

[37] Anders M DALE et al., « Dynamic statistical parametric mapping : combining fMRI and MEG for high-resolution imaging of cortical activity », in : *Neuron* 26.*1* (2000), p. 55-67.

[38] Julia DANIELSSON et Franz PETERMANN, « Cognitive deficits in children with benign rolandic epilepsy of childhood or rolandic discharges : a study of children between 4 and 7 years of age with and without seizures compared with healthy controls », in : *Epilepsy & Behavior* 16.*4* (2009), p. 646-651.

[39] Rafael Lorente DE NO, *A study of nerve physiology*, t. 131, Rockefeller Institute for Medical Research, 1947.

[40] Xavier DE TIÈGE et al., « Metabolic evidence for remote inhibition in epilepsies with continuous spike-waves during sleep », in : *Neuroimage* 40.*2* (2008), p. 802-810.

[41] Arnaud DELORME et Scott MAKEIG, « EEGLAB : an open source toolbox for analysis of single-trial EEG dynamics including independent component analysis », in : *Journal of neuroscience methods* 134.*1* (2004), p. 9-21.

[42] Bin DENG et al., « Multivariate multi-scale weighted permutation entropy analysis of EEG complexity for Alzheimer's disease », in : *Cognitive neurodynamics* 11.*3* (2017), p. 217-231.

[43] Thierry DEONNA, « Rolandic epilepsy : neuropsychology of the active epilepsy phase. », in : *Epileptic disorders : international epilepsy journal with videotape* 2 (2000), S59-61.

[44] Rahul S DESIKAN et al., « An automated labeling system for subdividing the human cerebral cortex on MRI scans into gyral based regions of interest », in : *Neuroimage* 31.*3* (2006), p. 968-980.

[45] John S EBERSOLE et Timothy A PEDLEY, *Current practice of clinical electroencephalography*, Lippincott Williams & Wilkins, 2003.

[46] Jerome ENGEL JR, « Report of the ILAE classification core group », in : *Epilepsia* 47.*9* (2006), p. 1558-1568.

[47] Bilal FADLALLAH et al., « Weighted-permutation entropy : A complexity measure for time series incorporating amplitude information », in : *Physical Review E* 87.*2* (2013), p. 022911.

[48] Jiajia FANG et al., « Altered language network in benign childhood epilepsy patients with spikes from non-dominant side : A resting-state fMRI study », in : *Epilepsy research* 136 (2017), p. 109-114.

[49] Bruce FISCHL, « FreeSurfer », in : *Neuroimage* 62.*2* (2012), p. 774-781.

[50] Robert S FISHER et al., « Epileptic seizures and epilepsy : definitions proposed by the International League Against Epilepsy (ILAE) and the International Bureau for Epilepsy (IBE) », in : *Epilepsia* 46.*4* (2005), p. 470-472.

[51] Patrick FLANDRIN, *Time-frequency/time-scale analysis*, t. 10, Academic press, 1998.

[52] Andrew M FRASER et Harry L SWINNEY, « Independent coordinates for strange attractors from mutual information », in : *Physical review A* 33.*2* (1986), p. 1134.

[53] Linton C FREEMAN, « A set of measures of centrality based on betweenness », in : *Sociometry* (1977), p. 35-41.

[54] Linton C FREEMAN, « Centrality in social networks conceptual clarification », in : *Social networks* 1.*3* (1978), p. 215-239.

[55] Vladimir GOL'DSHTEIN, GA KOGANOV et Gregory I SURDUTOVICH, « Vulnerability and hierarchy of complex networks », in : *arXiv preprint cond-mat/0409298* (2004).

[56] William Richard GOWERS, *Epilepsy and other chronic convulsive diseases : their causes, symptoms, and treatment*, Old Hickory Bookshop, 1901.

[57] Alexandre GRAMFORT et al., « OpenMEEG : opensource software for quasistatic bioelectromagnetics », in : *Biomedical engineering online* 9.*1* (2010), p. 45.

[58] Disha GUPTA, Pauly OSSENBLOK et Gilles van LUIJTELAAR, « Space–time network connectivity and cortical activations preceding spike wave discharges in human absence epilepsy : a MEG study », in : *Medical & biological engineering & computing* 49.*5* (2011), p. 555-565.

[59] William S HALL, « Boundary element method », in : *The Boundary Element Method*, Springer, 1994, p. 61-83.

[60] Matti S HÄMÄLÄINEN et Risto J ILMONIEMI, « Interpreting magnetic fields of the brain : minimum norm estimates », in : *Medical & biological engineering & computing* 32.*1* (1994), p. 35-42.

[61] Mahmoud HASSAN et al., « EEG source connectivity analysis : from dense array recordings to brain networks », in : *PloS one* 9.*8* (2014), e105041.

[62] Aapo HYVÄRINEN, Juha KARHUNEN et Erkki OJA, *Independent component analysis*, t. 46, John Wiley & Sons, 2004.

[63] Leon D IASEMIDIS, « Epileptic seizure prediction and control », in : *IEEE Transactions on Biomedical Engineering* 50.*5* (2003), p. 549-558.

[64] DC JACKSON et al., « Language function in childhood idiopathic epilepsy syndromes », in : *Brain and language* 193 (2019), p. 4-9.

[65] Ian T JOLLIFFE, « Principal component analysis : a beginner's guide—II. Pitfalls, myths and extensions », in : *Weather* 48.*8* (1993), p. 246-253.

[66] Mohamad El Sayed Hussein JOMAA et al., « A new mutual information measure to estimate functional connectivity : preliminary study », in : *41st Annual International Conference of the IEEE Engineering in Medicine and Biology Society*, 2019.

[67] Mohamad El Sayed Hussein JOMAA et al., « Multivariate improved weighted multiscale permutation entropy and its application on EEG data », in : *Biomedical Signal Processing and Control* 52 (2019), p. 420-428.

[68] Aya KABBARA et al., « The dynamic functional core network of the human brain at rest », in : *Scientific reports* 7.*1* (2017), p. 2936.

[69] Mark A KRAMER et Sydney S CASH, « Epilepsy as a disorder of cortical network organization », in : *The Neuroscientist* 18.*4* (2012), p. 360-372.

[70] Uri KRAMER, « Atypical presentations of benign childhood epilepsy with centrotemporal spikes : a review », in : *Journal of child neurology* 23.*7* (2008), p. 785-790.

[71] J KURTHS et al., « Measures of complexity in signal analysis », in : *AIP Conference Proceedings*, t. 375, 1, AIP, 1996, p. 33-54.

[72] Jean-Philippe LACHAUX et al., « Measuring phase synchrony in brain signals », in : *Human brain mapping* 8.*4* (1999), p. 194-208.

[73] Vito LATORA et Massimo MARCHIORI, « Efficient behavior of small-world networks », in : *Physical review letters* 87.*19* (2001), p. 198701.

[74] Jonatan LERGA, Nicoletta SAULIG et Vladimir MOZETIČ, « Algorithm based on the short-term Rényi entropy and IF estimation for noisy EEG signals analysis », in : *Computers in biology and medicine* 80 (2017), p. 1-13.

[75] Rong LI et al., « Epileptic discharge related functional connectivity within and between networks in benign epilepsy with centrotemporal spikes », in : *International journal of neural systems* 27.*07* (2017), p. 1750018.

[76] Wei LIAO et al., « Dynamical intrinsic functional architecture of the brain during absence seizures », in : *Brain Structure and Function* 219.*6* (2014), p. 2001-2015.

[77] Noémie LIGOT et al., « Default mode network hypometabolism in epileptic encephalopathies with CSWS », in : *Epilepsy research* 108.*5* (2014), p. 861-871.

[78] Mianxin LIU et al., « Assessing spatiotemporal variability of brain spontaneous activity by multiscale entropy and functional connectivity », in : *NeuroImage* 198 (2019), p. 198-220.

[79] P LOISEAU et M BEAUSSART, « The seizures of benign childhood epilepsy with rolandic paroxysmal discharges », in : *Epilepsia* 14.*4* (1973), p. 381-389.

[80] PIERRE LOISEAU et BERNARD DUCHÉ, « Benign childhood epilepsy with centrotemporal spikes », in : *Cleve Clin J Med* 56.*suppl 1* (1989), p. 17-22.

[81] Edward N LORENZ, « Deterministic nonperiodic flow », in : *Journal of the atmospheric sciences* 20.*2* (1963), p. 130-141.

[82] A LOUGHMAN, SC BOWDEN et W D'SOUZA, « Cognitive functioning in idiopathic generalised epilepsies : a systematic review and meta-analysis », in : *Neuroscience & Biobehavioral Reviews* 43 (2014), p. 20-34.

[83] Cheng LUO et al., « Altered functional and effective connectivity in anticorrelated intrinsic networks in children with benign childhood epilepsy with centrotemporal spikes », in : *Medicine* 95.*24* (2016).

[84] Cheng LUO et al., « Altered functional connectivity in default mode network in absence epilepsy : a resting-state fMRI study », in : *Human brain mapping* 32.*3* (2011), p. 438-449.

[85] Cheng LUO et al., « Altered structural and functional feature of striato-cortical circuit in benign epilepsy with centrotemporal spikes », in : *International journal of neural systems* 25.*06* (2015), p. 1550027.

[86] Stephane MALLAT et al., « A Wavelet Tour of Signal Processing : The Sparce Way », in : *AP Professional, Third Edition, London* (2009).

[87] Dante MANTINI et al., « Electrophysiological signatures of resting state networks in the human brain », in : *Proceedings of the National Academy of Sciences* 104.*32* (2007), p. 13170-13175.

[88] R MASSA et al., « EEG criteria predictive of complicated evolution in idiopathic rolandic epilepsy », in : *Neurology* 57.*6* (2001), p. 1071-1079.

[89] Colm J MCGINNITY et al., « Decreased functional connectivity within a language subnetwork in benign epilepsy with centrotemporal spikes », in : *Epilepsia open* 2.*2* (2017), p. 214-225.

[90] Francesco Carlo MORABITO et al., « Multivariate multi-scale permutation entropy for complexity analysis of Alzheimer's disease EEG », in : *Entropy* 14.*7* (2012), p. 1186-1202.

[91] Tateki MORIKAWA, Masakazu SEINO, Masako WATANABE et al., « Long-term outcome of CSWS syndrome », in : *Continuous spikes and waves during slow sleep* (1995), p. 27-36.

[92] Jukka-Pekka ONNELA et al., « Intensity and coherence of motifs in weighted complex networks », in : *Physical Review E* 71.*6* (2005), p. 065103.

[93] Nadine OSER et al., « Default mode network alterations during language task performance in children with benign epilepsy with centrotemporal spikes (BECTS) », in : *Epilepsy & Behavior* 33 (2014), p. 12-17.

[94] CP PANAYIOTOPOULOS, *A Clinical Guide to Epileptic Syndromes and their Treatment*, Springer Science & Business Media, 2007.

[95] Roberto Domingo PASCUAL-MARQUI et al., « Standardized low-resolution brain electromagnetic tomography (sLORETA) : technical details », in : *Methods Find Exp Clin Pharmacol* 24.*Suppl D* (2002), p. 5-12.

[96] Steven M PINCUS, « Approximate entropy as a measure of system complexity. », in : *Proceedings of the National Academy of Sciences* 88.*6* (1991), p. 2297-2301.

[97] K Vala RAGNARSDOTTIR, « Environmental fate and toxicology of organophosphate pesticides », in : *Journal of the Geological Society* 157.*4* (2000), p. 859-876.

[98] Alfréd RÉNYI et al., « On measures of entropy and information », in : *Proceedings of the Fourth Berkeley Symposium on Mathematical Statistics and Probability, Volume 1 : Contributions to the Theory of Statistics*, The Regents of the University of California, 1961.

[99] Joshua S RICHMAN et J Randall MOORMAN, « Physiological time-series analysis using approximate entropy and sample entropy », in : *American Journal of Physiology-Heart and Circulatory Physiology* 278.*6* (2000), H2039-H2049.

[100] Fabio ROTONDI et al., « Altered EEG resting-state effective connectivity in drug-naïve childhood absence epilepsy », in : *Clinical Neurophysiology* 127.*2* (2016), p. 1130-1137.

[101] Mikail RUBINOV et Olaf SPORNS, « Complex network measures of brain connectivity : uses and interpretations », in : *Neuroimage* 52.*3* (2010), p. 1059-1069.

[102] Luis A SANCHEZ, « Convergence to equilibria in the Lorenz system via monotone methods », in : *Journal of Differential Equations* 217.*2* (2005), p. 341-362.

[103] Nicoletta SAULIG et al., « Instantaneous counting of components in nonstationary signals », in : *21st European Signal Processing Conference (EUSIPCO 2013)*, IEEE, 2013, p. 1-5.

[104] Claude Elwood SHANNON, « A mathematical theory of communication. ACM SIGMOBILE Mob », in : *Comput. Commun. Rev* 5.*1* (2001), p. 3-55.

[105] FH Lopes da SILVA et A VAN ROTTERDAM, « Biophysical aspects of EEG and magnetoencephalographic generation », in : *Electroencephalography : basic principles, clinical applications and related fields, 5th edn. Lippincott, Williams & Wilkins, New York* (2005).

[106] GW STEWART, « Fredholm, Hilbert, Schmidt : three fundamental papers on integral equations », in : *See www. cs. umd. edu/˜ stewart/FHS. pdf* (2011).

[107] Victor SUCIC, Nicoletta SAULIG et Boualem BOASHASH, « Estimating the number of components of a multicomponent nonstationary signal using the short-term time-frequency Rényi entropy », in : *EURASIP Journal on Advances in Signal Processing* 2011.*1* (2011), p. 125.

[108] François TADEL et al., « Brainstorm : a user-friendly application for MEG/EEG analysis », in : *Computational intelligence and neuroscience* 2011 (2011), p. 8.

[109] Ye-Lei TANG et al., « Altered regional homogeneity in rolandic epilepsy : a resting-state FMRI study », in : *BioMed research international* 2014 (2014).

[110] Carlo Alberto TASSINARI et al., « Electrical status epilepticus during slow sleep (ESES or CSWS) including acquired epileptic aphasia (Landau-Kleffner syndrome) », in : *Epileptic syndromes in infancy, childhood and adolescence* 4 (2005), p. 295-314.

[111] Joana TEIXEIRA et Maria Emília SANTOS, « Language skills in children with benign childhood epilepsy with centrotemporal spikes : a systematic review », in : *Epilepsy & Behavior* 84 (2018), p. 15-21.

[112] Patrick VAN BOGAERT, « Physiopathology of atypical evolutions of idiopathic focal epilepsies in childhood », in : *Journal of Pediatric Epilepsy* 5.*03* (2016), p. 133-138.

[113] Patrick VAN BOGAERT et al., « The epileptic syndromes with continuous spikes and waves during slow sleep : definition and management guidelines. », in : *Acta neurologica belgica* 106.*2* (2006), p. 52-60.

[114] Michele VAN HIRTUM-DAS et al., « Children with ESES : variability in the syndrome », in : *Epilepsy Research* 70 (2006), p. 248-258.

[115] Jennifer VANNEST et al., « Changes in functional organization and functional connectivity during story listening in children with benign childhood epilepsy with centro-temporal spikes », in : *Brain and language* (2017).

[116] Alberto VERROTTI et al., « Memory impairment and benign epilepsy with centrotemporal spike (BECTS) : a growing suspicion », in : *Brain and cognition* 84.*1* (2014), p. 123-131.

[117] Danny JJ WANG et al., « Neurophysiological basis of multi-scale entropy of brain complexity and its relationship with functional connectivity », in : *Frontiers in neuroscience* 12 (2018), p. 352.

[118] Duncan J WATTS et Steven H STROGATZ, « Collective dynamics of 'small-world'networks », in : *nature* 393.*6684* (1998), p. 440.

[119] Josef WEGLAGE et al., « Neuropsychological, intellectual, and behavioral findings in patients with centrotemporal spikes with and without seizures », in : *Developmental Medicine & Child Neurology* 39.*10* (1997), p. 646-651.

[120] Vincent WENS et al., « A geometric correction scheme for spatial leakage effects in MEG/EEG seed-based functional connectivity mapping », in : *Human brain mapping* 36.*11* (2015), p. 4604-4621.

[121] Vincent WENS et al., « Inter-and intra-subject variability of neuromagnetic resting state networks », in : *Brain topography* 27.*5* (2014), p. 620-634.

[122] *What is an action potential ?*, `https://www.moleculardevices.com/applications/patch-clamp-electrophysiology/what-action-potential`, Accessed : 2019-07-10.

[123] Caiyun WU et al., « Altered effective connectivity network in childhood absence epilepsy : a multi-frequency MEG study », in : *Brain topography* 30.*5* (2017), p. 673-684.

[124] Hau-Tieng WU et al., « Using synchrosqueezing transform to discover breathing dynamics from ECG signals », in : *Applied and Computational Harmonic Analysis* 36.*2* (2014), p. 354-359.

[125] Yun WU et al., « Interhemispheric connectivity in drug-naive benign childhood epilepsy with centrotemporal spikes : combining function and diffusion MRI », in : *Medicine* 94.*37* (2015).

[126] Fenglai XIAO et al., « Altered attention networks in benign childhood epilepsy with centrotemporal spikes (BECTS) : a resting-state fMRI study », in : *Epilepsy & Behavior* 45 (2015), p. 234-241.

[127] Fenglai XIAO et al., « Real-time effects of centrotemporal spikes on cognition in rolandic epilepsy : an EEG-fMRI study », in : *Neurology* 86.*6* (2016), p. 544-551.

[128] Tianhua YANG et al., « Altered resting-state connectivity during interictal generalized spike-wave discharges in drug-naïve childhood absence epilepsy », in : *Human brain mapping* 34.*8* (2013), p. 1761-1767.

[129] Hongwu ZENG et al., « Regional homogeneity (ReHo) changes in new onset versus chronic benign epilepsy of childhood with centrotemporal spikes (BECTS) : A resting state fMRI study », in : *Epilepsy research* 116 (2015), p. 79-85.

[130] X-S ZHANG, Rob J ROY et Erik W JENSEN, « EEG complexity as a measure of depth of anesthesia for patients », in : *IEEE transactions on biomedical engineering* 48.*12* (2001), p. 1424-1433.

[131] Xun ZHANG, Kin Keung LAI et Shou-Yang WANG, « A new approach for crude oil price analysis based on empirical mode decomposition », in : *Energy economics* 30.*3* (2008), p. 905-918.

[132] Zhiqiang ZHANG et al., « Epileptic discharges specifically affect intrinsic connectivity networks during absence seizures », in : *Journal of the neurological sciences* 336.*1-2* (2014), p. 138-145.

Titre : Traitement des signaux d'électro-encéphalogrammes à 256 capteurs chez l'enfant épileptique

Mot clés : Entropie, Épilepsie, Complexité, Électroencéphalographie, Information Mutuelle, Connectivité Fonctionnelle

Resumé : Dans cette thèse, nous proposons des méthodes de traitement du signal et les appliquons à des signaux d'électro-encéphalographie (EEG) enregistrés chez des patients épileptiques. L'objectif est de pouvoir quantifier l'état du patient et d'étudier l'évolution du trouble neurologique au cours du temps. Les méthodes que nous avons développées sont basées sur des mesures d'entropie. Ainsi, nous introduisons la « multivariate Improved Weighted Multi-scale Permutation Entropy » (mvIWMPE) que nous appliquons à des signaux EEG d'enfants sains et épileptiques. Elle donne des résultats prometteurs. Nous proposons également une approche multivariée pour la « Sample Entropy ». Les résultats montrent qu'elle permet de traiter correctement un plus grand nombre de canaux que la méthode existante. Nous présentons aussi une mesure de complexité temps-fréquence variable dans le temps, basée sur la « Singular Value Decomposition » et la « Rényi Entropy ». Ces mesures, appliquées sur l'EEG d'enfants épileptiques avant et 4-6 semaines après un traitement, conduisent à des résultats qui sont en accord avec le diagnostic clinique quant à l'évolution de la pathologie. La dernière partie de la thèse porte sur les mesures de connectivité fonctionnelle. Nous proposons une méthode de connectivité fonctionnelle basée sur la mvIWMPE et l'information mutuelle. Elle est appliquée sur des signaux EEG d'enfants sains au repos. A l'aide de mesures de réseau, nous pouvons identifier des régions cérébrales actives dans des réseaux précédemment découverts grâce à l'imagerie par résonance magnétique fonctionnelle. La méthode est également utilisée pour étudier les réseaux chez des enfants épileptiques.

Title : Signal processing of electroencephalograms with 256 sensors in epileptic children

Keywords : Entropy, Epilepsy, Complexity, Electroencephalography, Mutual Information, Functional Connectivty

Abstract : In this thesis, our focus is to develop signal processing methods to be used on electroencephalography (EEG) signals recorded from epileptic patients. The aim of these methods is to be able to quantify the state of the patient with epilepsy and to study the progress of the neurological disorder over time. The methods we developed are based on entropy. From previous permutation entropy methods we introduce the multivariate Improved Weighted Multi-scale Permutation Entropy (mvIWMPE). This method is applied on EEG signals of both healthy and epileptic children and gives promising results. We also introduce a new multivariate approach for sample entropy and, when tested and compared with the existing multivariate approach, we find that the introduced approach is much better in handling a larger numbers of channels. We also introduce a time-varying time-frequency complexity measure based on Singular Value Decomposition and Rényi Entropy. These measures are applied on EEG of epileptic children before and after 4-6 weeks of treatment. The results come in correspondence with the clinical diagnosis from the hospital on whether the patients improve or not. The final part of the thesis focuses on functional connectivity measures. We introduce a new functional connectivity method based on mvIWMPE and Mutual Information. The method is applied on EEG signals of healthy children at rest. Using network measures, we are able to identify regions in the brain that are active in networks previously found using functional magnetic resonance imaging. The method is also used to study the networks of epileptic children at several points throughout the treatment.